Spring 2012

Analysis of Sol-Gel Encapsulated Aggregate-Prone Peptides by Circular Dichroism

Nathan James Birtwhistle
San Jose State University

ANALYSIS OF SOL-GEL ENCAPSULATED AGGREGATE-PRONE PEPTIDES BY CIRCULAR DICHROISM

A Thesis

Presented to

The Faculty of the Department of Chemistry

San Jose State University

In Partial Fulfillment

of the Requirements for the Degree

Master of Science

By

Nathan James Birtwhistle

May 2012

The Designated Thesis Committee Approves the Thesis Titled

ANALYSIS OF SOL-GEL ENCAPSULATED AGGREGATE-PRONE PEPTIDES BY CIRCULAR DICHROISM

by

Nathan J. Birtwhistle

APPROVED FOR THE DEPARTMENT OF CHEMISTRY

SAN JOSÉ STATE UNIVERSITY

Dr. Daryl Eggers	Department of Chemistry
Dr. Elaine Collins	Department of Chemistry
Dr. Joseph Becker	Department of Physics and Astronomy

ABSTRACT

ANALYSIS OF SOL-GEL ENCAPSULATED AGGREGATE-PRONE PEPTIDES BY CIRCULAR DICHROISM

by Nathan Birtwhistle

Protein aggregation has been linked to many debilitating neurological diseases. In each case, a specific protein is thought to have a region of intrinsically disordered structure that seeds the aggregation. Highly cooperative in nature, protein aggregation is difficult to investigate. The current study aims to characterize two aggregation-prone peptides involved in Huntington's disease, polyglutamine (polyQ, $D_2Q_{15}K_2$), and Alzheimer's disease, amyloid-beta (Aβ). A protocol was developed to encapsulate the peptides by the sol-gel technique. Generated from a liquid state, the silica matrix is presumed to isolate the soluble peptide, preventing aggregation. In addition, the porosity of the glass allows the solvent conditions to be altered. The peptides were characterized by circular dichroism spectroscopy (CD). In solution, both peptides were most aggregation-prone when they contained the least amount of secondary structure. Encapsulated polyQ showed unique pH-dependent spectra not seen in solution. Aβ was able to take on both a random coil and an apparent beta structure in 5% hexafluoroisopropanol (HFIP), depending on the prior solvent, indicating two semi-stable states of similar energy. The results for both peptides show that (1) the encapsulated peptides can adopt a significant amount of helical secondary structure, (2) the secondary structure can be altered by varying the solution, temperature, and pH, and (3) most changes in structure appear to be reversible. These results are consistent with the absence of aggregation in the encapsulated samples.

ACKNOWLEDGEMENTS

I wish to thank Dr. Daryl Eggers, my research advisor, for all his support, guidance, and faith in my work. My gratitude goes to my graduate committee, Dr. Elaine Collins and Dr. Joseph Becker, for their much-valued feedback. I would also like to acknowledge the members of my family and my friends for their unceasing support and encouragement.

This work was funded by the NIH through an MBRS- SCORE grant to DKE (#S06 GM008192).

TABLE OF CONTENTS

LIST OF FIGURES

LIST OF TABLES

TABLE OF ABBREVIATIONS

3,3,3-Trifluoropropyl-trimethoxysilane	F_3-propyl TriMOS
Alzheimer's disease	AD
Amyloid beta	Aβ
Amyloid precursor protein	APP
Cesium (ion)	Cs^+
Cesium hydroxide	CsOH
Circular dichroism	CD
Dentatorubral-pallidoluysian atrophy	DRPLA
Differential scanning calorimetry	DCS
Hexafluoroisopropanol	HFIP
High performance liquid chromatography	HPLC
Huntington's disease	HD
Hydrochloric acid	HCl
Infrared spectroscopy	IR
Neurofibrillary tangles	NFT
Nuclear magnetic resonance	NMR
Phosphate (ion)	PO_4^{3+}
Phosphoric acid	H_3PO_4
Potassium (ion)	K^+
Potassium hydroxide	KOH
Potassium phosphate	KPhos

Polyacrylamide gel electrophoresis	PAGE
Polyglutamine	polyQ
Rate-limiting step	RLS
Reverse phase HPLC	RP-HPLC
Size exclusion HPLC	SEC-HPLC
Sodium dodecyl sulfate PAGE	SDS-PAGE
Spinobulbar muscular atrophy	SBMA
Spinocerebellar ataxis	SCA
Tetramethoxysilane	TMOS
Tetramethylammonium (ion)	$N(CH_3)_4^+$
Tetramethylammonium hydroxide	$N(CH_3)_4OH$
Trifluoroacetate	TFA
Trifluoroethanol	TFE
Ultraviolet-visible spectroscopy	UV–vis

1. INTRODUCTION

In 1892, one of the first known reports of the presence of protein aggregates, or plaques, in the brains of deceased patients was documented by Georges Marinesco and Paul Blocq [1]. At the time they did not know that these plaques were made up of aggregated proteins and simply reported them as "senile plaques." In 1907, Alois Alzheimer published the first paper on the correlation between these plaques and dementia, linking protein aggregation to neurological atrophy [2]. The presence of protein aggregates has been linked to many other neurodegenerative diseases, but until recently the nature of these diseases still remained a mystery. When Stanley Prusiner published his manuscript on prion disease in 1982, for which he won the Nobel Prize in 1997, he opened the door to the nature of protein aggregation diseases [3].

The nature of proteins, or polypeptides, is to fold into a structure with a functional purpose. A peptide, a general term that will also be used to refer to proteins in this paper, is manufactured as a linear molecule made up of amino acids that may have one of two properties determined by its side chain: hydrophobic (nonpolar) or hydrophilic (polar/uncharged, acidic, or basic) [4]. It is the consecutive makeup of the peptide that determines its structure and function and is known as its primary structure. Because of this structure, there are two classes of factors affecting the structural/functional content of a peptide, intrinsic and extrinsic. Intrinsic factors include those derived from its primary structure such as genetic mutations, hydrophobicity, and electrostatics. Extrinsic factors come from the surrounding environment and how it interacts with the peptide, such as solvent, temperature, and excluded volume effects. Both of these factors together have

influence on the peptide's structure and function, and they provide the driving force for aggregation [5].

A peptide's natural tendency to aggregate comes from its intrinsic factors, *i.e.*, from what amino acids it is made and how they are organized along the peptide's backbone. Generally, the more solvent-exposed hydrophobic amino acids a peptide contains, the more likely it is to aggregate; more specifically, the more ordered hydrophobic surface content and its concentration, the more aggregate-prone the peptide becomes [6-8]. As a consequence, proteins that form hydrophobic beta structures are more likely to aggregate, and those that remain soluble and/or form hydrophilic alpha helices are less likely [9, 10]. This tendency to aggregate may be due to the fact that beta structures are highly ordered sheet-like structures, making them complementary surfaces to each other. Soto, *et al*. (1995, 1996), showed by inducing point mutations that proteins were more disposed to aggregate when helical content was reduced or beta content was increased and vice versa [11, 12]. Typically a peptide buries its hydrophobic content within its interior, shielding it from interacting with the aqueous (hydrophilic) solvent. If a peptide is built such that it is unstable or natively disordered, then slight variations in solvent quality (temperature, hydrophobicity, *etc*.) may cause it to transition through different secondary structures and therefore become prone to aggregation.

There are three ways by which solvent quality, or other external factors, may influence aggregation rates; they may favor intermediate formation, destabilize the native folded state, or stabilize the unfolded state [13]. Specific factors include temperature, pH, peptide concentration, hydrophobicity, crowding and excluded volume. First,

fluctuations in temperature may destabilize the peptides, increasing intermediate concentration and diffusions rates. This change increases the concentration of the aggregate-prone hydrophobic conformation and its likeliness to interact with another molecule, leading to aggregation. Second, changes in pH affect the relative type and distribution of charges on the peptides' surfaces. Since the structures peptides can take on are directly linked to the way they interact with the solvent, these changes in pH will influence the peptide's stability and structure. Decreasing the number of charged/hydrophilic residues, those usually found on the surface, can destabilize the peptide and cause it to unfold, exposing the hydrophobic interior [14]. Third, since a small sub-population of peptides will be in the intermediate and unfolded states even at equilibrium, if a peptide's concentration is increased, then effectively the concentration of the intermediates will also be increased, again enhancing aggregation [5]. At this point it should be noted that a theme is developing; there are two prerequisites to aggregation: a destabilized peptide and exposure of ordered hydrophobic content. All other extrinsic factors causing protein aggregation meet these prerequisites and will be discussed more extensively below. In essence, if a protein's structure is changed, then so is its function; in this case the function is toxic in nature.

Structure and function are synonymous in the world of peptides. Slight energy variations in a peptide's environment can potentially cause it to loose its native (functional) structure and gain non-native (toxic) function. This work is a study of two peptides known to have a strong tendency to aggregate, and they are believed to be intrinsically disordered. As a consequence, they easily transition between their native

and unfolded sates. The purpose of this work is to isolate these peptides within a sol-gel matrix that prevents aggregation, to induce the aggregate-prone intermediate transition state, and to characterize the resulting structure to study an early step in protein/peptide aggregation.

1.1. Protein Aggregation and Neurodegenerative Diseases

As the average human life span increases, sporadic forms of neurological diseases associated with protein aggregation are becoming much more prevalent [15]. For most, these diseases become the lethal element in their life. There are different stages and anatomical locations of aggregation associated with each disease, but all are believed to begin with the transition of a properly folded native peptide to an aggregation-prone state. Alzheimer's and Huntington's diseases are two of many neurological diseases that are associated with protein aggregation. The respective polypeptides, amyloid beta (Aβ) and the polyglutamine mutation (polyQ), are thought to seed aggregation by the formation of oligomers directly from this aggregation-prone transition state. Both peptides are natively disordered, making them thermodynamically sensitive, and they are the major components of the larger inclusion bodies (large, insoluble, highly homogeneous aggregates) associated with each disease. After death, the identification of these inclusion bodies, or plaques, during autopsy gives the definitive diagnosis of each disease. Figure 1-1 depicts a cartoon to demonstrate the different possible ways in which the aggregates may affect cellular activities (left), and presents several real pictures of diseased tissues showing the different types of aggregates (right).

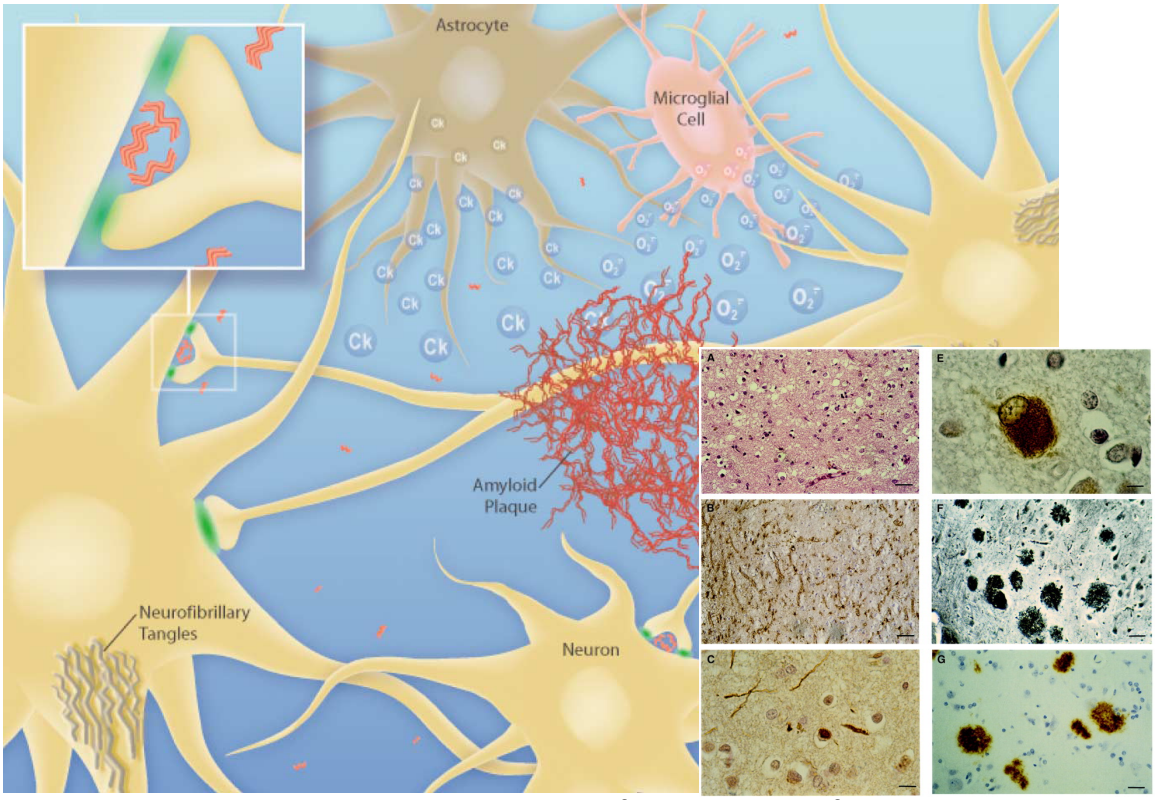

Figure 1-1. Artist's depiction and real images of aggregates. Left: A cartoon representation of the different aggregates that may form in Alzheimer's disease. Red W-shaped species are dimers and trimers of Aβ that may disrupt synaptic efficacy (enlarged portion). The larger amyloid plaques, also composed of Aβ, disrupt the cytoskeletal integrity of the astrocytes and microglial cell causing an immune response by the release of cytokines. These plaques also disrupt the axonal trajectories. The neurofibrillary tangles are composed of Tau protein and their formation may be protective against the damage caused by smaller oligomers, but this remains controversial. Right: Photomicrographs of several different types of inclusion bodies seen as the dark regions, due to staining. The plaques in each photomicrograph result from the aggregation of a different protein as in the other micrographs. Bars in the lower right hand corner represent the following distances: (A) 40 μm, (B) 80 μm, (C) 12 μm, (E) 8 μm, (F) 80 μm, (G) 40 μm. Reprinted with permission from (left) [16] with permission from Elsevier, and (right) reprinted from Rossor, et al. *Semantic dementia with ubiquitin-positive tau-negative inclusion bodies*. Brain. 2000. 123. p 267-276. by permission of Oxford University Press [17].

1.2. Aggregate-Prone Peptides: Structure and Function

Repeated studies have shown that both Aβ and polyQ mutated huntingtin protein (the protein involved in Huntington's Disease) are involved with nerve cell function [18-24]. These studies have demonstrated that the prefibrillar form of Aβ is associated with nerve synapse and learning, while huntingtin protein is linked to striatal neuron health. Specifically, huntingtin's putative normal functions are vesicular transport, signaling, and transcription [24]. Therefore, these peptides are thought to have normal and necessary functions in their natively folded states, but may transition to an aggregation-prone state prior to aggregate formation. Furthermore, it has been demonstrated that it is the oligomeric forms of Aβ that inhibit long term potentiation and not the monomeric [16].

1.2.1. The Intermediate: Partial Unfolding as an Aggregation Prerequisite

In an aqueous environment a completely folded peptide has its hydrophobic residues mostly buried eliminating the driving force behind aggregation. On the other hand, a completely unfolded peptide is unordered in terms of hydrophobic and hydrophilic residues, this too reducing the tendency towards aggregation since hydrophilic residues would remain hydrated. In the unfolded state the hydration of the hydrophobic residues is unfavorable and raises the free energy of the local water. To reduce this unfavorable hydration effect, the peptide is driven to form intramolecular hydrophobic interactions, releasing water to the bulk (Figure 1-2). These intramolecular interactions could result in a number of partially folded intermediates along the folding pathway (Figure 1-3). An ordering of the hydrophobic residues results in a highly

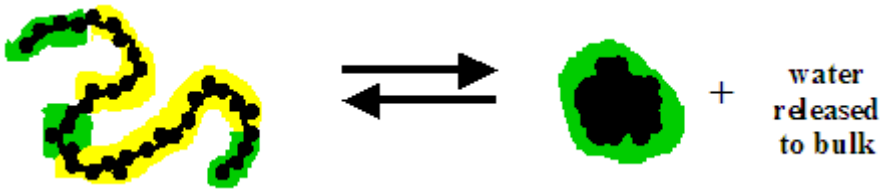

Figure 1-2. Hydration effects of water. Here it can be seen that the availability of the solvent to form hydrogen bonds with the backbone plays a crucial role in intramolecular backbone bond formation. Green shows favorable hydration and yellow unfavorable. Left shows an unfolded peptide with unfavorable hydration. Right shows a folded protein with the release of water into the bulk. Free energy of the system decreases from left to right in water but the direction may be reversed by addition of certain solvents and cosolvents that increase the free energy of bulk water.

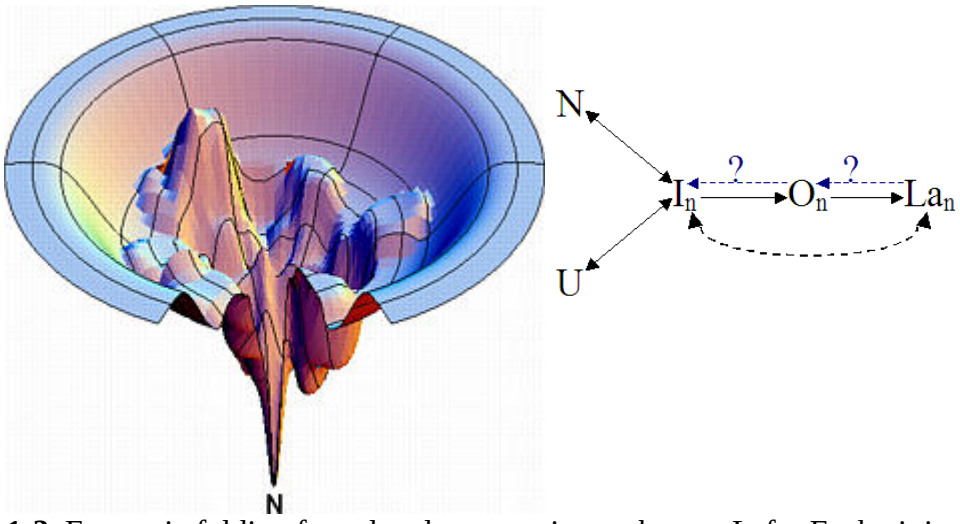

Figure 1-3. Energetic folding funnel and aggregation pathway. Left: Each pit in the folding landscape, above the native (**N**), represents a local energetic minimum where an intermediate is found. Some of these pits may be aggregation-prone while others are not. Identifying those that are aggregation-prone may allow us to introduce a small solute or molecule that influences the peptide to follow a pathway that is not aggregation-prone or destabilizes those forms that are aggregation-prone, guiding them safely along the folding pathway. Right: A simplified model of the 3-dimensional folding landscape where many different aggregation-prone intermediates may exist. N = Native, U = Unfolded, I_n = Multiple Intermediates that may exist, O_n = Multiple Oligomers that may exist, La_n = Multiple Large Aggregates that may exist (the subscript n represents the many different forms that may exist). Each intermediate could take separate routes to the larger aggregates and some may never form oligomers or the larger aggregates. It is possible that aggregation has a similarly complicated 3 dimensional landscape with pathways to many different aggregate forms, some of which are stable and some that are not. Energetic Folding Landscape (left) reprinted with permission from Macmillan Publishers Ltd: Nature Structural and Molecular Biology [25], copyright 1997.

hydrophobic core that may be transiently exposed to the solvent. These contiguous hydrophobic residues provide the strong driving force behind aggregation, as every intermolecular hydrophobic contact reduces the free energy. Small aggregates can form and go through further rearrangements to increase hydrophobic contacts and reduce unfavorable hydration. As a result, soluble aggregates (oligomers) are produced that become the building blocks for the more highly ordered and stable beta structures of the different orders of aggregates [26]. Though oligomers and larger aggregates are bulky, the partially folded monomeric intermediates are not. Intermediates and unfolded peptides can diffuse through the complex environment of the cell, and, since either unfolding or folding may form the intermediate, aggregation is further facilitated [13]. As a consequence, peptides with higher native folding energies are more likely to be aggregation-prone because they are less stable and more likely to transition back and forth between the folded and unfolded states at physiological conditions.

1.2.2. Nucleation, Aggregation, and Toxicity

As stated above, the intermediate may form from either the folded or fully unfolded peptide. As a consequence there may be multiple forms of intermediates that exist along both the folding and unfolding landscape. The existence of multiple intermediates increases the chances that other destabilized peptides nearby may provide a complementary hydrophobic surface, driving aggregation and stabilizing the aggregate-prone contiguous hydrophobic structure. Once the aggregate-prone state has formed, it is thought to seed oligomer formation, or prefibrillar aggregates, by inducing other

destabilized proteins into a complementary aggregation-prone state [8]. Because these aggregation-prone peptides are natively disordered, after nucleation the aggregation process is thermodynamically favored to minimize the unfavorable hydrophobic protein-solvent interactions [7].

Several different paths of aggregation have been demonstrated and are under debate [9, 27-31]. The path by which aggregation proceeds is of little consequence to this research, but it is important to note that each peptide may have different characteristic aggregation kinetics. As a consequence, the rate-limiting step (RLS) may occur in many different places: intermediate formation, dimer formation, nucleation/condensation/growth, *etc*. No matter, if the RLS is not the formation of the intermediate, then it must be down stream from it [32]. As a consequence, each neurodegenerative disease may be able to form different types of aggregates, some that may be benign and some that may be toxic. There may be several soluble forms that are each uniquely stable and toxic and some that are unstable and disaggregate. No matter the case, there is a strong correlation between neurodegenerative diseases and protein aggregation [16, 22, 26, 33].

It has been proposed that the formation of these soluble aggregates mark the onset of the associated disease and may also be most toxic in nature [34, 35]. A soluble aggregate may range in size from an oligomer, made up of just a few peptides and globular in structure, to the protofibrils that are larger and highly ordered. Protofibrils are the immediate precursors to the full-fledged fibrils that are linear and extend up to 400 nm in length [33, 36]. These fibrils make up the larger aggregates, plaques and

neurofibrillary tangles (NFT) that are hallmark of each disease. It has been demonstrated that intracellular protofibrils may be 100,000 times as toxic as their extracellular counterparts [37] and that they are able to embed into membranes creating permeable-pores [36] that could depolarize the cell membrane. Because of this toxicity, some researchers are asking if fiber formation is nature's way to reduce the toxic effects of soluble aggregates [38-43]. If soluble aggregates are toxic and the toxicity is an intracellular event, then understanding this transition state becomes even more important, in a therapeutic sense, since the goal becomes the prevention of their formation instead of their removal before mature fibril formation. It therefore becomes necessary to stop the formation of these aggregates at the source. Whether soluble aggregates are the toxic species or not, they are still the precursor to the larger fibers and plaques that are hallmark to these diseases. Most researchers do acknowledge that, as these fibers and plaques grow and amyloidosis sets in, there is irreversible damage to the nervous system as connections between nerve cells are disrupted and the cytoskeletal integrity is destroyed [39, 44, 45].

1.2.3. Polyglutamine Diseases

The polyglutamine diseases relevant to protein aggregation are caused by expanded repeat mutations in the coding region of the DNA sequence. The trinucleotide (CAG) codon that encodes for glutamine is repeated within the DNA sequence. Once the expansion exceeds a critical length of 35-45 repeats, the affected peptide is prone to forming stable, irreversible aggregates believed to be the toxic element [33, 46, 47].

Table 1-1. Details of polyglutamine diseases

Disease	Gene	Protein	Localization	Putative normal function	Most affected regions	Common Symptoms
SCA1	*ATXN1*	ataxin-1	Nucleus	Transcription (interaction with corepressor SMRT)	Cerebellar cortex, dentate nucleus, brainstem, cerebral cortex	Incoordination (hands, balance, swallowing, dysarthria)
SCA2	*ATXN2*	ataxin-2	Nucleus	RNA metabolism	Cerebellar cortex, brainstem, cerebral cortex	Incoordination (hands, balance), Neuropathy (loss of feeling and reflexes)
SCA3	*ATXN3*	ataxin-3	Nucleus	Deubiquitylating enzyme	Cerebellum, basal ganglia, brainstem, spinal cord	Incoordination (hands, dysarthria, spasticity, rigidity, muscular atrophy, slowness)
SCA6	*CACNA1A*	α1A voltage-dependent calcium channel subunit	Cytoplasm	P/Q type α1A calcium channel subunit	Cerebellum	Incoordination (limbs, tremors, dysarthria, dysphagia)
SCA7	*ATXN7*	ataxin-7	Nucleus	Subunit of TFTC/STAGA coactivator complexes	Cerebellum, retina, brainstem, visual cortex	Visual Problems (color, acuity), Incoordination (eye movement, dysarthria, dysphagia)
SCA17	*TBP*	TATA box binding protein	Nucleus	General transcription factor	Cerebellum, striatum	Incoordination, Dementia
HD	*HD*	huntingtin	Cytoplasm and nucleus	Vesicular transport, signaling, transcription	Striatum, cerebral cortex	Personality Changes, Cognitive Decline, Inccordination (balance, limbs, face)
SBMA	*AR*	androgen receptor	Cytoplasm and nucleus	Nuclear receptor	Spinal cord, brainstem	Muscle Weakness, Abnormal Processing of Androgens
DRPLA	*ATN1*	atrophin-1	Nucleus	Nuclear receptor corepressor	Cerebellum, cerebral cortex, basal ganglia, subthalamic nuclei	Incoordination, Dementia

SCA (spinocerebellar ataxis), HD (huntington's disease), SBMA (spinobulbar muscular atrophy), DRPLA (dentatorubral-pallidoluysian atrophy)
Adapted from [24].

Each susceptible peptide (Table 1-1) has a different critical length [48]. In addition, a single mutation in the flanking sequence could affect the stability of the susceptible peptide. Though in general, the translated peptides become more destabilized and aggregation-prone with the increasing number of repeats. Several studies have shown an inverse correlation between expansion length and age of onset, and an increasing aggregate stability with expansion length [21, 24, 46]. Table 1-1, that gives anextensive list of polyQ aggregation diseases, lists two common functions that are emerging among proteins associated with polyQ diseases: transcriptional dysregulation and organelle dysfunction [23, 24, 48, 49].

1.2.4. Aβ and Alzheimer's Disease

Alzheimer's disease (AD) is defined by the formation of neuritic plaques (amyloid deposits in the gray matter of the brain), and NFTs in the cerebral neuropil and vasculature [39]. Aβ peptides are a small fragment of a larger protein known as amyloid precursor protein (APP). APP is a Type I transmembrane protein with its N-terminus in the lumen and C-terminus in the cytosol. The N-terminus contains several sections that can be degraded into separate fragments, most of which are thought to have biological functions including neurite outgrowth, dendritic arborization, and synaptogenesis [22]. Aβ is believed to be a functional component in many of these processes, specifically the following: surface reception, cell/substratum adhesion, neurite outgrowth, calcium homeostasis regulation, and neurotoxic regulation [50]. Whether Aβ itself has any

function remains controversial, though more and more researchers are providing evidence as to its biological significance [18-20, 22, 34, 50].

Aβ is produced by the successive cleavage of APP by β-secretase at the N-terminus and γ-secretase at the C-terminus [51]. Cleavage by β-secretase releases soluble APP leaving Aβ partially anchored in the lipid membrane. Upon γ-secretase cleavage, Aβ is released into the lumen, and the APP intracellular domain is released into the cytosol. Together these two peptides make up the component that traverses the lipid membrane, anchoring APP to the endoplasmic reticulum. Aβ may be 39-43 amino acids in length, for which the C-terminus is the variable end except in certain familial versions of the disease [52]. The most common unmutated form, involved in sporadic Alzheimer's, is 40 amino acids in length (Aβ40), but since the γ-secretase cleavage site is not definite, Aβ42 makes up a small population. Each additional amino acid increases the hydrophobicity of the peptide, therefore influencing the aggregation kinetics. In some familial forms, certain mutations within Aβ40 also increase the propensity to aggregate [38, 52, 53].

A third enzyme, α-secretase, cleaves APP within the Aβ sequence preventing Aβ production and competes with β-secretase [54]. A mutation within α-secretase, inhibiting its enzymatic action, results in an over abundance of Aβ40, increasing its intracellular concentration. Following the same reasoning, mutations within any one of the secretase enzymes result in improper Aβ processing. This provides a rationale for three primary causes of aggregate formation. (1) The peptides themselves are

destabilized and more aggregate prone due to a mutation(s) within the Aβ sequence. (2) A mutation(s) with either Aβ or one of the secretases interferes with the normal processing of the peptide, producing a more aggregate-prone peptide. (3) A mutation(s) within either Aβ or one of the secretases interferes with the processing of the peptide and produces an overabundance, increasing the Aβ concentration [22].

To reiterate, AD cannot be reduced to a single pathological cause but instead has several that can be categorized as familial, those that facilitate Aβ assembly into aggregates, or sporadic, where an increase in Aβ concentration leads to aggregation [38]. The pathology may be rooted in the genetic coding sequence for APP itself or within that for an external regulatory system involved with APP processing, such as the Wnt signaling pathway or presenilin-1 (PS) proteins [13, 26, 55]. This research investigates the unmutated Aβ40, and so is applicable to the more common sporadic versions of the disease, those due to the extended human life span.

1.3. Review of Current Techniques in Peptide Aggregation Studies

This study is focused on detecting the aggregation-prone intermediate state(s), which exists prior to aggregation, and on the folding pathway between the native and unfolded states. Currently, no techniques have been successful at detecting and characterizing this (these) state(s). In most of the current techniques the peptides are in solution, and since the intermediate states are able to quickly diffuse through even a crowded environment, the intermediates quickly aggregate before detection [13]. Because most research has been focused on the aggregation process and its kinetics to try

and understand why these neurodegenerative diseases can vary from person to person in pathology, no technique for trapping intermediates has been developed. A brief review of current techniques is given below with focus on those that may be capable of detecting the intermediate state.

1.3.1. Analytical Techniques

Current research on protein aggregation utilizes a multitude of techniques that is too vast to cover in this paper. Table 1-2 in Section 1.3.1.1 was given in a review by Wang [13] and summarizes some of the more practiced techniques.

1.3.1.1. Detection of the Intermediate

Several of the analytical techniques listed in Table 1-2 have the potential of detecting the intermediate state if aggregation could be prevented. Differential Scanning Calorimetry (DSC) in conjunction with light scattering and/or spectroscopy has the potential to provide valuable information about the intermediate state. DSC gathers information about the energetics of the folding/unfolding pathways, light scattering gives information about size and shape, and spectroscopy can provide information about the structural content and changes [13, 76].

The thermal folding and unfolding of a peptide is well understood. DSC is capable of measuring the heat absorbed by a peptide by measuring the difference between the sample cell and a reference cell containing the same buffer. The cell temperatures are changed at the same rate and the difference in heat absorbed is reported. The enthalpy

Table 1-2. Analytical techniques in characterizing protein aggregation

Categories	Individual techniques	Applications	Protein examples	References
Calorimetry	DSC	Thermal protein unfolding/aggregation	FVIII SQ	[56]
Centrifugation	Analytical centrifugation	Size and shape estimation	Insulin	[57]
Chromatography	SEC-HPLC	Size estimation and quantitation	Factor IX	[58]
			hGH	[59]
	RP-HPLC	Isoforms of aggregates	bFGF	[60, 61]
Electrophoresis	SDS-PAGE	Size estimation and mechanistic probing	aFGF	[62]
	Native PAGE	Aggregation process and mechanistic probing	IL-2	[63]
Light scattering	Static light scattering	Size and shape estimation	β-Amyloid peptide, β1–40	[64]
			Insulin	[65]
	Dynamic light scattering	Size distribution of soluble aggregates	Deoxy hemoglobin	[66]
	Light scattering/obscuration	Size estimation and relative distribution	Deoxy hemoglobin	[66]
Rheology	Dynamic shear rheometry	Gelation characterization	BSA	[67]
Spectroscopy	CD	Aggregation process	Interferon-γ	[68, 69]
	Fluorescence	Aggregation process	α_1-Antitrypsin	[70]
	IR	Aggregation process	β-Lactoglobulin, *etc*.	[71]
	NMR	Aggregation process	CspA	[72]
	UV–vis	Soluble and insoluble aggregates	aFGF	[73]
Microscopy	Light microscopy	Shape and size determination	Immunoglobulin mutants	[74]
	Electron microscopy	Shape and size determination	β-Amyloid peptide	[12]
	Atomic force microscopy	Shape and size determination	β-Amyloid peptide	[75]

Table reprinted from [13] with permission from Elsevier.

landscape is capable of providing valuable information about the changes in the intramolecular contacts as the peptides transition through the intermediate(s) state(s). The intermediate states could be identified by changes in the absorption landscape indicating semi-stable folding states. One shortcoming of DSC is that it is not capable of providing information about the secondary structural content or even the general size and shape of the peptide [13, 76].

As the peptides transition from the tight globule form of the native fold to the long linear molecule of the unfolded state, the radius of gyration changes. Light scattering is able to monitor this structural transition. In this technique, collimated light is shown through a sample. When the light comes into contact with the large peptides, as compared to the wavelength, the light is scattered and the angle can be measured. By measuring the intensity and angle of the scattered light, information about the size and shape of the peptides may be calculated. The limit to this method is that only information about the size and shape is obtained and not the secondary structural content [13, 76].

Several spectroscopic techniques are capable of providing unique secondary structural information. Nuclear magnetic resonance (NMR) provides information about specific bonds made along the peptide backbone. The spectra returned gives signals that are correlated to each other, providing information about which residues are involved in hydrogen bonds with each other or the solvent, and that may be protected from interacting with the solvent. Any element with a non-zero total nuclear spin will feel a force from an external magnetic field, and whether that field is made by a neighboring element or an external man made electromagnet does not matter. It is the neighboring atoms' fields that correlate the signals, and it is the external field that induces the atoms to first align, and then flip, creating the spectra. Infrared spectroscopy (IR) is an absorption technique where the spectra signals' sizes, positions, and shapes are characteristic of specific bond types. The light absorbed is changed into vibrational energy. Each bond type can vibrate or rotate in three dimensions, each with a

precise/quantitated energy that is original and characteristic to the type of bond and the elements involved [13, 76].

In summary, DSC can identify semi-stable intermediate states, light scattering provides information as to the size and shape, and spectroscopic techniques allow one to estimate the secondary structural content. Still, all of these methods suffer from the tendency of the peptides to aggregate out of solution before the intermediate state can be detected. As a consequence, these analytical techniques are capable of detecting the intermediate only if an experimental technique that prevents aggregate formation is available.

1.3.2. Experimental Techniques Used in Protein Studies

1.3.2.1. Solution Methods

In solution experiments, peptides are usually brought up in 1 – 10 mg/ml concentrations in aqueous buffer. The solubilized peptides are stabilized by favorable peptide-water interactions that keep the hydrophobic portions of the peptide buried in the interior. The advantage of this method is the intrinsically low free energy and strong hydrophobic effect of water properties in a solution environment on the structure of the soluble peptide. Evolutionary pressure should have ensured that the cellular environment was at or lower than the free energy of neat water, thus stabilizing cellular membranes and other hydrophobically driven interactions vital to a living organism [13, 77]. Once the peptides in solutions are destabilized, either thermally or chemically, the hydrophobic core is exposed, providing the driving force for aggregation. Because of the exposed

core, the peptides quickly aggregate out of solution, and the intermediate cannot be detected. Because a small sub-population of the peptide is always in an intermediate state, aggregation still occurs on a larger timescale. So, even in solutions where the peptides are thought to be stable, aggregation is a major concern.

One way to overcome aggregation is to use fusion proteins. In this technique, the aggregation-prone peptide's sequence is inserted into a larger soluble protein's sequence. By performing the same experiments on both the fusion protein and the larger soluble protein, absent of the aggregation-prone peptide, data from the latter can be treated as background. Two such studies were preformed by Otzen *et al*. 2004 [78] and Konno 2000 [79] who both were investigating Aβ and its ability to induce aggregation in a soluble protein. A third by Masino 2002 [80] investigated the structures of different expansions of polyQ repeats. Unfortunately, there is no way to rule out that these two fused polypeptides affect each other's stability and structure, and they most likely do. Therefore, both peptides may have context-dependent structures, so that the background spectra is not representative of the structure in the fusion peptide, and so that the aggregation-prone portion may be different structurally, making interpretation difficult.

1.3.2.2. Crowding Agents and Excluded Volume

To mimic the peptides' natural environment, crowding agents are added to solutions that are treated in a similar way to the solution experiments. Crowding agents add effects absent in solution experiments. These are excluded volume effects and a variable hydrophobic effect due to the influence of the crowding agents' surface

chemistries and their interaction with water [81]. These effects create several competing biophysical effects: (1) The rate of diffusion is decreased because two molecules cannot occupy the same space and pass through each other. (2) The peptides' entropy is decreased because there are fewer ways for the molecules to be arranged, which in turn increases the total conformational free energy. (3) The effective concentration is increased due to the excluded volume [81]. These three conditions compete with each other. The decreased diffusion rate slows peptide interaction and therefore slows aggregation. The decrease in entropy induces a driving force to reduce the total excluded volume and increase the ways the molecules can be arranged. As a result, both the collapsed globular native fold and the aggregated states are favored, competing to increase and reduce aggregation. Therefore, the state that excludes the least total volume to surrounding macromolecules is favored. And the increase in concentration increases the likeliness of interaction and therefore increases the rate of aggregation. Factoring in the additional influence of the crowding agent's surface chemistry on the structure/free energy of the bulk water, a very complex thermodynamic environment is created that should be much closer to the environment *in vivo*. As a consequence, the choice of the wrong concentration and type of crowding agent could accelerate aggregation [40, 41]. Regardless of whether these effects work to increase or decrease the peptides' stability, the intermediates are still able to diffuse easily through the medium and may aggregate before they can be detected.

1.3.2.3. Experiments *In Vivo*

The natural environment of a living system is the only way to truly reproduce the intermediate structures responsible for the aggregation involved in neurodegenerative diseases. Unfortunately, current methods of study, such as in-cell NMR or fluorescence, are only able to detect large populations. Since the aggregation-prone state exists only transiently and in small populations during aggregation, these methods are limited to detection of either the aggregation-resistant folded peptide or the larger aggregates. The obvious consequence of these limitations is that detection of the intermediate is nearly impossible.

1.4. Project Goals and Rationale

The purpose of this work is to successfully encapsulate two aggregation-prone peptides, Aβ and polyQ, in a sol-gel matrix so that they are isolated and prevented from aggregating, to characterize this novel system by comparing the samples to solution experiments, and to identify the aggregation-prone intermediate/transition states along the folding/unfolding pathway and the environmental factors that lead to it. Additionally, we hope to introduce a particle small enough to penetrate the sol-gel matrix that can either stabilize or bypass the intermediate, avoiding aggregation.

Numerous studies have shown that the partial unfolding of proteins, which are not normally amyloidogenic, can lead to aggregation, making partial unfolding an aggregation prerequisite [82]. Both Aβ and polyQ are believed to be natively unstructured peptides and, therefore, characterized by a narrow free energy range along

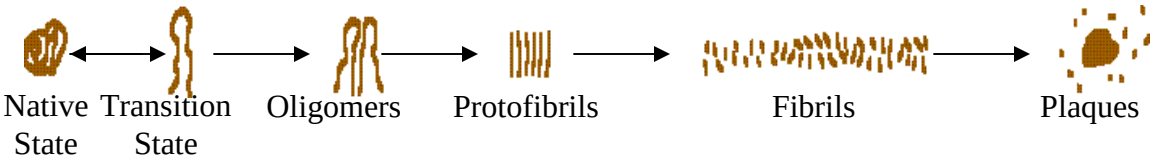

Figure 1-4. Protein aggregation from native state to disease-associated plaques. Aggregation-prone peptides are thought to have a useful purpose in a living organism and therefore must have a native state. These peptides may be destabilized by an unknown influence and transition into an aggregation-prone state known as the transition state. If these transition state peptides come into contact with another destabilized peptide, aggregation may proceed, and an oligomer is produced. These oligomers grow by contacting other oligomers or destabilized peptides, eventually becoming a protofibril. Protofibrils are large soluble aggregates and continue to grow into the insoluble fibrils, which eventually become the plaques associated with disease. This research focuses on identifying the transition state with the intent on discovering the conditions that cause it and prevent it. We focus our work on the change represented by the double-headed arrow above, so to stop aggregation all together.

their folding/unfolding transition. As a result, slight thermodynamic variation can cause these peptides to partially unfold, exposing their hydrophobic core to the solvent, and aggregation to occur at physiological conditions [83]. To study this transition the peptides will be encapsulated in a sol-gel matrix to prevent them from interacting and subsequently aggregating. To ensure peptide solubility during gelation a 10% 3,3,3-trifluoropropyl-trimethoxysilane (F_3-propyl TriMOS)/90% Tetramethoxysilane (TMOS) glass will be prepared. The F_3-Propyl TriMOS is known to increase the peptides' helical content, therefore increasing solubility [84].

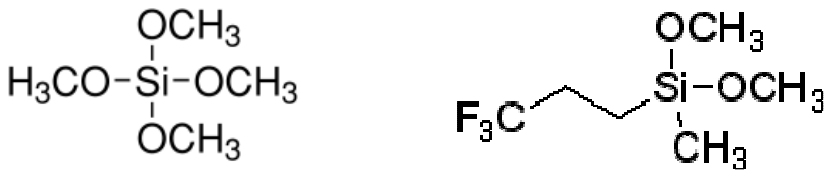

Figure 1-5. Tetramethoxysilane (left) and 3,3,3-trifluoropropyl-trimethoxysilane (right).

One of the major benefits of this method is that the glass sample can be reused and reversibility can be tested. Because both phases of the sol-gel environment are continuous, a sample can be equilibrated in one solution, the spectra can be taken, the sample can be removed, rinsed and placed into a new solution. This technique gives the obvious advantage of testing for intermediates along both the folding and unfolding landscape, determining if they are the same intermediates, and observing how these peptides are affected by the initial conditions.

To test the folding landscape, the solvent conditions can be controlled by adjusting the pH, potassium phosphate (KPhos) concentration, fluorinated alcohols concentration, and temperature. It has become widely accepted that peptide solubility is a function of its surface charge, hydrophilic content, and secondary structural arrangement. The surface charge content is a function of the pH. By altering the pH, the net ionic charge of the solution is adjusted and the peptide's net charge is altered, causing it to change structure and affecting its solubility. Salt concentration affects a peptide's solubility in a similar way. Fluorinated alcohols are known to induce helical structure, increasing a peptide's solubility with increasing alcohol concentration. Increasing temperature can increase peptide solubility to a certain point where the peptide begins to unfold. If the temperature is raised slowly enough, aggregation may occur but is more likely to occur during the refolding step when the temperature is reduced and smaller aggregates survive the thermal refolding threshold. As the temperature is increased, even the small aggregates are destabilized. By controlling these factors, one can explore the

peptides' structures and test the widely used hypothesis that these peptides partially unfold, losing secondary structure, and form a semi-stable intermediate [14].

Understanding the intermediates' structures and the pathways between their formations has many potential benefits, one of which would be the development or discovery of a solute that could interact with the intermediate preventing aggregation. Another outcome could be the development of a method of detection to determine the concentration of certain types of aggregation-prone peptides *in vivo* so a diagnosis of these diseases could be made before death. Understanding protein aggregation as applicable to neurodegenerative diseases may also lead to the understanding of other aggregation phenomena, both desirable and undesirable, *e.g.* drug development and storage (shelf life -- introduce a stabilizing agent), materials engineering [76, 83].

1.5. Introduction to Analytical and Experimental Techniques Used in this Study

1.5.1. Circular Dichroism Spectroscopy

Circular Dichroism (CD) Spectroscopy is a technique where equal amounts of left and right-handed circularly polarized light are independently passed through a chiral (asymmetric) sample. The absorptions are measured and a difference spectrum is reported. A chiral sample, such as a peptide, will absorb each handedness differently because it is not superimposable on its mirror image and can never be oriented in the same way to interact with both polarizations of light [76] (Figure 1-6).

A peptide is built as a linear arrangement of amino acids and is capable of taking on three basic arrangements, or secondary structures: α-helical, β-sheet, and random coil.

The first two, α-helical and β-sheet, are due to organized hydrogen bonds between the carbonyl oxygen and the amide hydrogen along the peptide backbone. An arrangement of these bonds, 3.6 residues apart, makes up the coiled structure of the α-helix. A β-sheet is formed when the peptide backbone passes by itself in a linear manner and forms these hydrogen bonds between two parallel or antiparallel chains. These two organized structures stress the bonds adjacent to alpha carbon (C_α, chiral center) in a specific way and determine the wavelength of light each bond can absorb (Figure 1-7). The third category, random coil, is characterized by a lack of repetitive secondary structure. Statistically, random coil is considered an ensemble of conformations of the same peptide and is not considered to be symmetric [4]. This asymmetry does not mean that the ϕ and

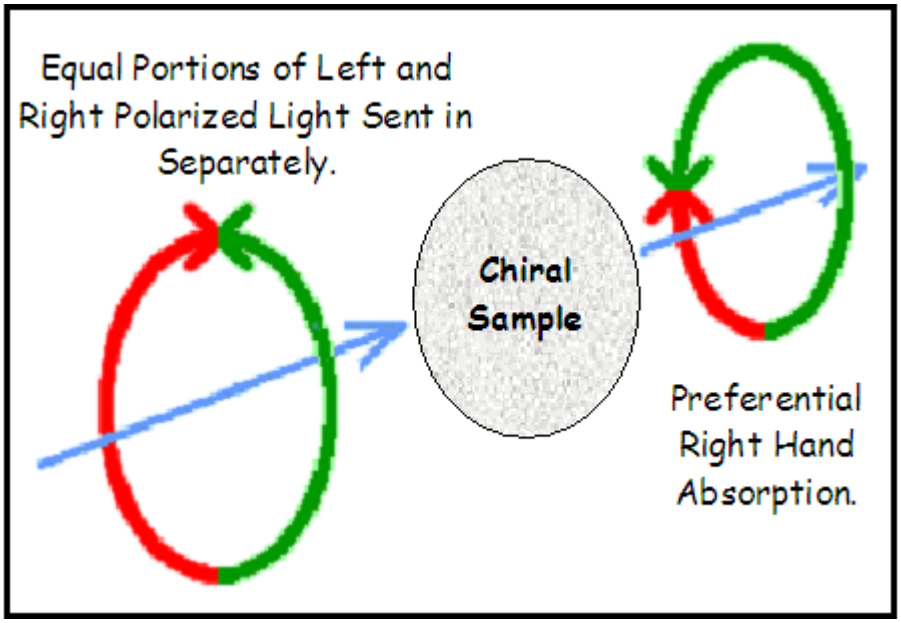

Figure 1-6. Circular dichroism. Left and right-handed circularly polarized light is transmitted through a chiral sample. The difference between the two absorptions (ΔA) is taken, and a unique profile is reported using: $\Delta A\ (\lambda) = A_L\ (\lambda) - A_R\ (\lambda)$, where $A = \varepsilon \bullet C \bullet l$

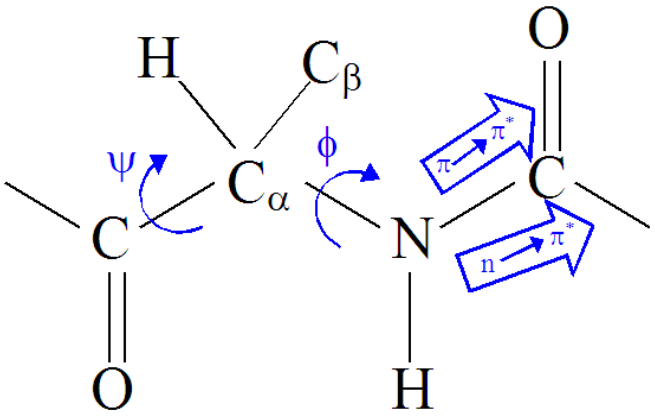

π -> π* ~ 190 nm & 210 nm
(π-electrons of the carbonyl)

n -> π* ~ 220 nm
(non-bonding electrons of the carbonyl O)

Figure 1-7. Peptide backbone transitions. The intensity and energy of the indicated transitions depends on ϕ and ψ angles (i.e., secondary structure). Transitions are centered around the indicated wavelengths and involve the indicated electrons.

ψ angles shown in Figure 1-7 are completely random, but are instead restricted by steric constraints and statistically take on one of three combinations, giving a distinct CD spectrum [76]. Figure 1-8 gives sample CD spectra for these three secondary structures, and Figure 1-9 shows the instrument used in this study.

In summary, CD provides a powerful tool for determining the average secondary structural content over a population of the same peptide. Even for a peptide that takes on combinations of these three structures, with a little knowledge of the nature of the peptide, a trained eye can interpret the composite spectrum. Additionally, by monitoring the changes in the spectra, as conditions are changed, much information about the structural changes can be gained. Even when interpretation is difficult, powerful deconvolution programs have been developed to calculate the percentage of each secondary structure present in each spectrum.

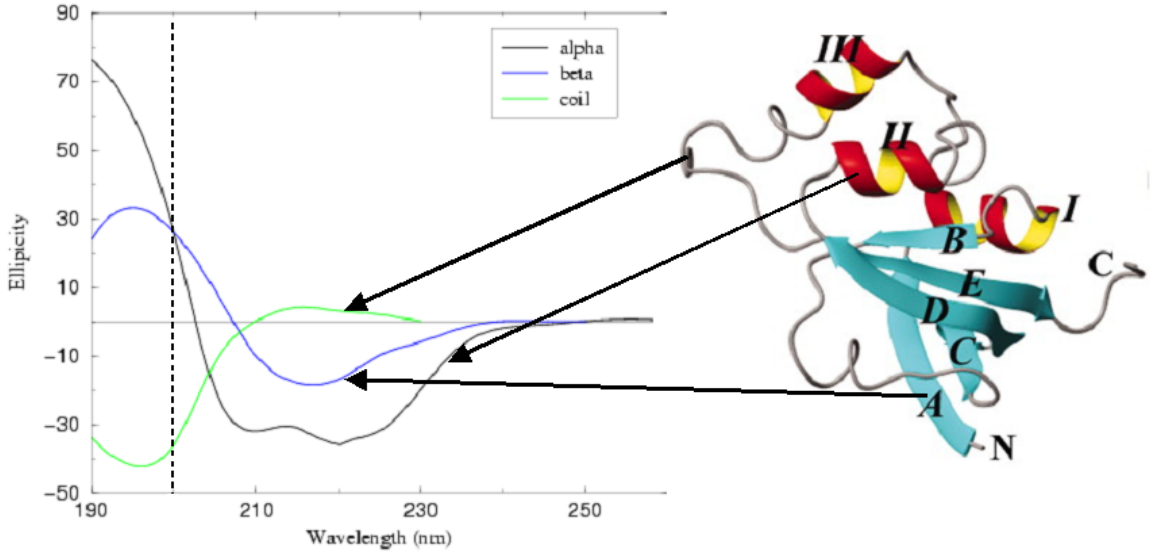

Figure 1-8. CD spectra of pure secondary structure. Alpha (α) helix is formed by repeated hydrogen bonds between the amide and carbonyl groups 3.6 residues from one another along the peptide backbone. Similarly, a beta sheet is formed by hydrogen bonds formed by parallel or antiparallel chains with the distance between residues being variable. Random coil possesses no structure except that inherent in the local interactions [85-87]. The dotted line at 200 nm indicates the minimum wavelength taken for the results presented within this thesis. The vertical axis reports ellipticity that results from the difference spectrum explained in Figure 1-6. Left: (CD Curves), reprinted with permission from [88]. Right: Arrows point from secondary structures found in an actual protein toward the corresponding CD spectrum.

Figure 1-9. Aviv model 215 circular dichroism instrument (New Jersey, USA) used in this study.

1.5.2. Sol-Gel Encapsulation

The name sol-gel combines two terms: “Sol” meaning solid particles in a liquid, and “Gel” meaning an agglomeration of sol particles extending throughout the solution. Both the solution and gel phases are continuous throughout. The glass phase is highly porous (Figure 1-10), trapping larger molecules within and allowing the smaller permeable solutes to be changed. Two reactions drive the formation of the glass phase, hydrolysis and condensation (equations 1, 2, and 3 below).

$$\equiv Si - OR + H_2O \underset{\text{← Dehydration}}{\overset{\text{Hydrolysis →}}{\leftrightarrow}} \equiv Si - OH + ROH \quad (1)$$

$$\equiv Si - OR + HO - Si\equiv \underset{\text{← Alcoholysis}}{\overset{\text{Alcohol Condensation →}}{\leftrightarrow}} \equiv Si - O - Si\equiv + ROH \quad (2)$$

$$\equiv Si - OH + HO - Si\equiv \underset{\text{← Hydrolysis}}{\overset{\text{Water Condensation →}}{\leftrightarrow}} \equiv Si - O - Si\equiv + H_2O \quad (3)$$

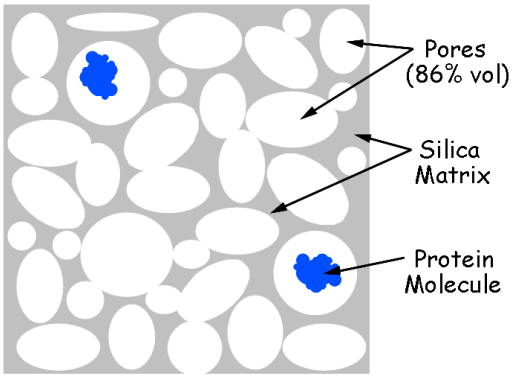

Figure 1-10. Sol-gel cross section. Sol-gel provides a porous environment that isolates the proteins. Both solid and liquid phases are continuous allowing the solution to be changed and the larger peptides to remain trapped.

These reactions allow for protein-compatible conditions during gelation, preserving peptide structure and function [81, 89, 90]. Because hydrolysis is the rate limiting step and must occur before either condensation step can proceed, the solution is made slightly acidic to catalyze the reaction, before the peptide solution is added. The peptide can be brought up in a wide variety of solutions in which it is soluble, usually a buffered solution near physiological pH that initiates the condensation reactions. There are two notable shortcomings to the encapsulation approach. (1) The glass matrix starts absorbing light below and around 200 nm, which means valuable structural information

is lost, making deconvolution of the CD spectra less reliable. (2) The peptide may be adsorbed to the silica surface and may alter the CD spectrum due to altered protein structure [91].

1.5.2.1. Thermodynamic Considerations in the Glass Matrix

Important and often neglected in peptide research are the effects of excluded volume, the peptides' interactions with surrounding surfaces, and the influence these surfaces have on the solutions [81]. As discussed in section 1.3.2.2, the excluded volume effect has important thermodynamic consequences on the peptide's structure, function, and interactions. A paper by Ellis [90] estimates the total protein and RNA concentration in *Escherichia coli* to be in the range of 300 – 400 g/l, making the total occupied volume 20 – 30% of the cell. In the sol-gel-derived environment it was shown that, after supercritical drying of the solvent, the silica's total volume was 14% of the total volume [89]. Though this is significantly less excluded volume then the cellular environment, it was shown that in the glass matrix the conformational sensitivity of apomyoglobin is increased to many solutes relative to soluble apomyoglobin behavior in the same solutions [92]. Further study showed that, even though there was no correlation between pore size and protein structure, the incorporation of 5% monosubstituted alkoxysilanes in the silica increased the helical content of apomyoglobin with increasing alkyl group chain length [89]. Therefore, the glass surface and choice of incorporated modifiers have a significant influence on peptide structure. This influence may be adjusted by changing the chemistry of the surface modifier and/or the solvents conditions [84].

1.6. Literature Review of Key Peptides

1.6.1. Recent Studies on PolyQ

Solution studies of polyQ structure suggest a two-state isodichroic helical-random coil transition while in monomeric form and a beta sheet secondary structure for small soluble aggregates [80, 93-97]. Altschuler and coworkers [95] solubilized two polyQ stretches of 9 and 17 residues by flanking them with alanine and lysine rich residues, a modification known to promote helical structure. These model peptides were 29% and 50% polyQ, respectively. The CD spectra showed increasing helicity with increasing TFE concentration and an isometric point near 203 nm for both peptides, indicating a two-state folding transition. Studies by Perutz and coworkers [96] and Sharma and coworkers [97] confirm that small soluble aggregates take on beta structure that Perutz had previously termed polar zippers [98]. Both of these studies also suggest that a hydrogen bonded hairpin turn exists within the soluble monomeric form. It should be noted that Perutz used the same peptide sequence tested in this thesis.

A study by Darnell *et al*., 2007 [93], demonstrates that the length of the repeat is also a factor in oligomer formation. Figure 1-11 shows the CD spectra and size exclusion chromatography (SEC) spectra from this study, demonstrating that the shorter repeat lengths appear random coil in structure and elute with one peak at the monomer's estimated molecular weight, whereas the longer repeat lengths appear beta in structure and elute as larger multiple peaks, indicating the presence of oligomers. Furthermore, it can be seen that the flanking amino acids are a factor in the formation of oligomers. Therefore, each specific sequence may differ in the polyQ repeat length necessary to

form oligomers, and the structures these peptides take on are influenced by the flanking residues. This influence is seen in the lower CD spectra of Figure 1-11 were all the peptides that are flanked by 11 prolines taken on, what the authors have termed, a polyproline type II-*like* structure; an "open" helix lacking internal hydrogen bonds. What's notable is the similarity of this spectrum to that of a random coil spectrum, and that the longer polyQ repeat lengths still elute as a series of peaks indicating the presence of oligomers and the possible influence of the flanking sequences on the oligomer's structure.

Most studies, as in this thesis, utilized flanking sequences to increase solubility in solution. One study by Walters and Murphy [94] went a step further to incorporate an interrupting sequence within the polyQ repeats. This experiment was done to compare secondary structure, obtained by CD, with rates of aggregation, analyzed by SEC and sedimentation kinetics. The following polypeptide was used, $K_2WQ_{10}XXQ_{10}AK_2$, where XX is the interrupting sequence. The interrupting sequences were chosen because of their ability to induce specific structures, as described by the authors: Pro-Pro (PP) extended conformation, Ala-Ala (AA) lack of influence, and D-Pro-Gly (PG) beta inducing. These were to be compared with a control polypeptide where the interrupting sequence had been deleted, termed Q20. The CD spectra and aggregation kinetics for these samples can be seen in Figure 1-12. All samples returned spectra indicative of random coil/helical structure, and aggregation rates were inversely proportional to the 200 nm CD signal intensity. In addition, all samples were shown to develop soluble oligomers suggesting that a random coil spectrum is not definitively monomeric.

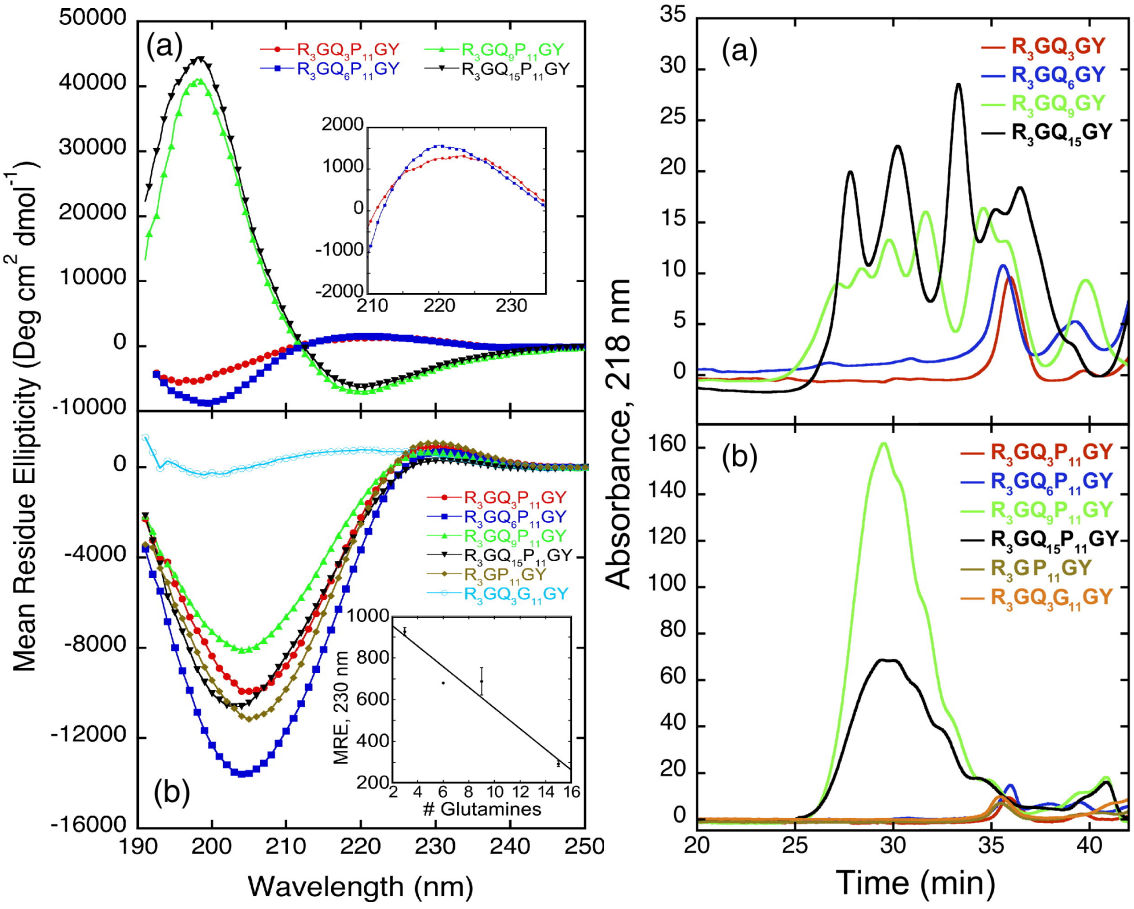

Figure 1-11. CD and SEC of flanked polyQ sequences. CD (left) and SEC (right). CD: (a) Displays data for the indicated polyQ repeat lengths, flanked by the indicated amino acids to increase solubility, without the proline repeats. (The same identification of peptide sequence in (a) and (b) may have been used to compare upper and lower figures, but (a) does not contain the proline repeats.) The short polyQ lengths of 3 (red) and 6 (blue) residues both return random coil spectra whereas the longer lengths of 9 (green) and 15 (black) give typical beta sheet spectra with a local minimum at 218nm. (b) Flanking proline repeats were added to the sequence. All return, what the authors term, polyproline type II like structure. SEC: (a) Demonstrates that the longer polyQ repeats, 9 and 15, both elute with multiple peaks, indicating the presents of oligomer, whereas the smaller two peptides have a single strong peak, indicating they are monomeric. All samples were brought up in 10 mM sodium phosphate ($NaPO_4$) (pH 7.0 – 7.3). Reprinted from [93] with permission from Elsevier.

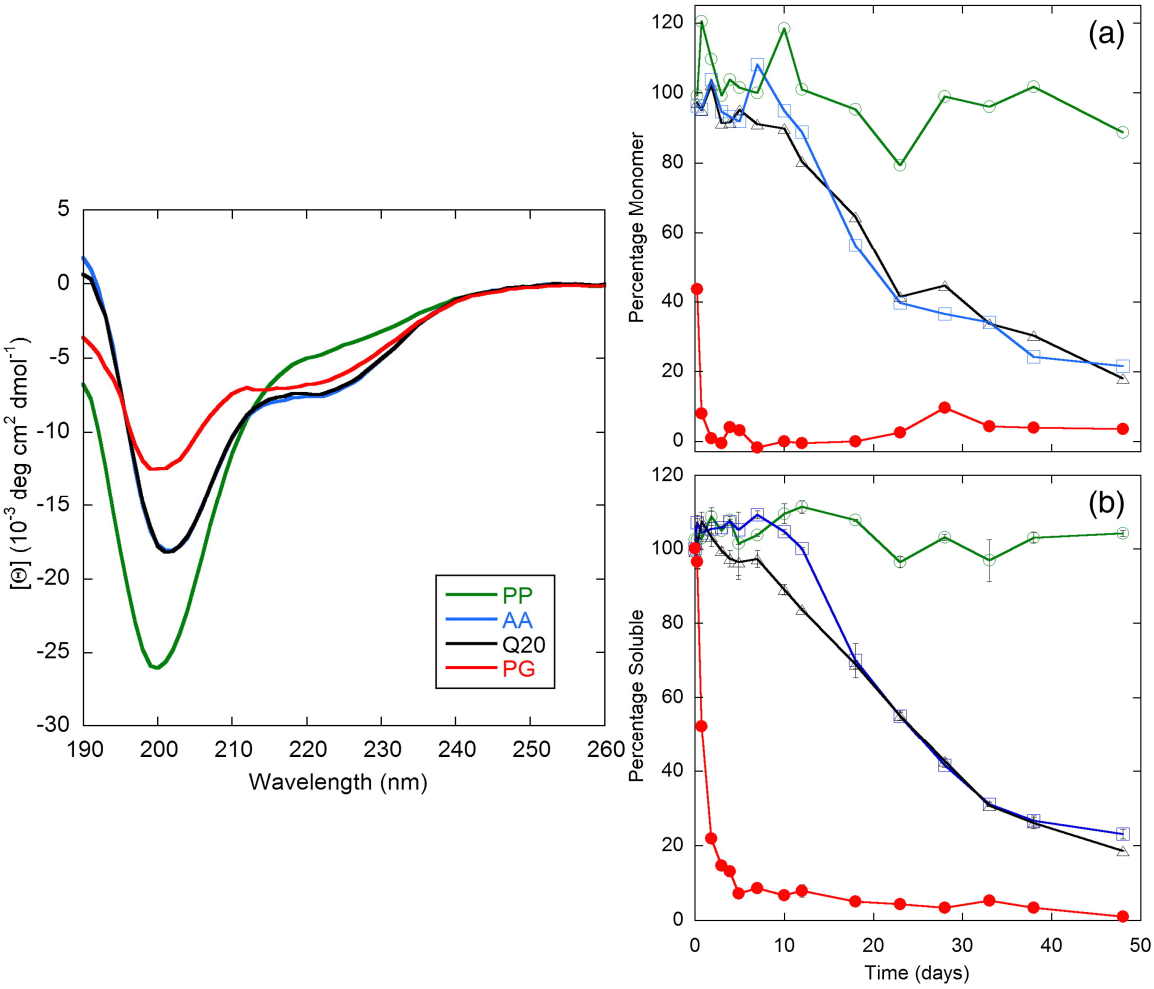

Figure 1-12. Comparison of interrupted polyQ CD spectra to aggregation kinetics. CD (left): All spectra appear primarily random coil. The PG sample was proposed to contain some beta structure by the authors and the PP was said to be extended. Aggregation kinetics (right): (a) After sedimentation, the supernatant was analyzed by SEC for the monomer. (b) After sedimentation, the total soluble peptide was determined by taking the ratio of the supernatant to an uncentrifuged sample using bicinichoninic acid assay. Reprinted from [94] with permission from Elsevier.

1.6.2. Recent Studies on Aβ

Like polyQ, several studies have proposed that Aβ is monomeric when in a random coil conformation and oligomeric when in a β-sheet conformation [99-101]. In

addition, these studies have shown a conformational dependence on pH, with all studies in agreement that the percent composition of beta structure and the rate of aggregation are highest around the isoelectric point of approximately pH 5.5 [102]. Figure 1-13 [101] shows the CD spectra for the pH dependence of three different lengths of Aβ: Aβ(1-28) the extracellular charged domain, Aβ(1-39) related to sporadic Alzheimer's, and Aβ(1-42) found in both sporadic and familial cases. In panels (a), (b), and (c), TFE was added to the indicated ratio to induce helical structure, enhance solubility, and to see if the peptide still took on the most beta structure around the isoelectric point. In panel (d), absent of TFE, it can be seen that the spectrum at pH 5.0 is weak, indicating insoluble aggregates have formed. Comparing the three panels with TFE, it is evident that helical structure is weakest near the isoelectric point, but the authors also propose that there is some beta structure in panels (a) – (c). The spectral shapes alone make this proposal debatable since panels (a) and (b) both have flattened regions between 220 and 210 nm and in panel (c) the minimum is red shifted away from 215 nm. Furthermore, how does a peptide interact with the solvent when 30 – 60% of it is not water, and do the pH values really represent proton concentrations? It is obvious the TFE has some stabilizing effect to the peptide's structure as compared to panel (d). Figure 1-14 [100] gives the pH curve for the extent of aggregation after 2 days of Aβ(1-40) in solution. Here the authors measured the amount of Congo red bound to the aggregate. This study shows that aggregation does occur to a greater extent near the isoelectric point.

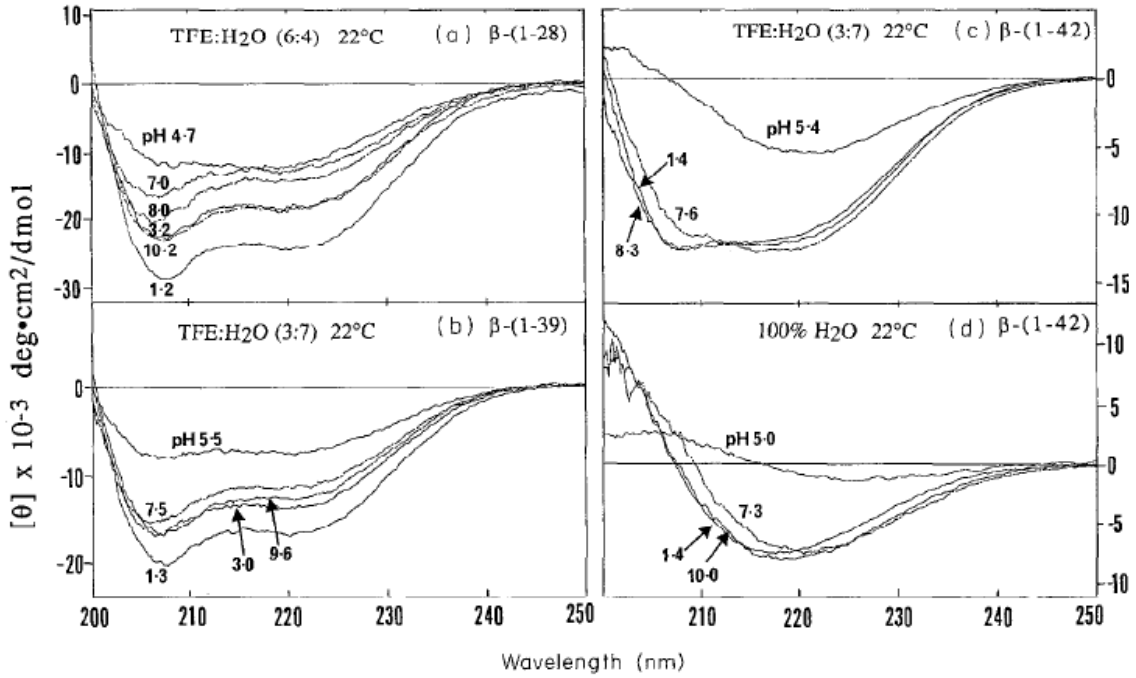

Figure 1-13. Effects of pH on various Aβ segments. (a) Aβ- (1-28), (b) Aβ- (1-39), and (c)/(d) Aβ- (1-42) in the indicated ratios of TFE:H_2O at the indicated pHs. All solutions were buffered with 5 μM KPhos and then adjusted as needed. Reprinted from [101] with permission from Elsevier.

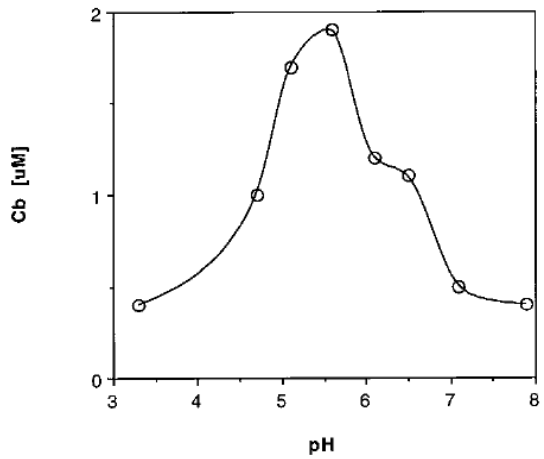

Figure 1-14. Quantification of pH dependent Aβ aggregation. Aβ(1-40) was allowed to sit in solution for two days after which the amount of aggregation was quantified by Congo red binding, ploted as Cb. Buffers used: (pH 3.3) 14 mM acetic acid, (pH 4.7 – 6.0) 100 mM Mes, and (pH 6.5 – 7.9) 100 mM KPhos. On the ordinate axis uM is μM. Reprinted from [100] with permission from Elsevier.

Aside from the structure being pH dependent, another study by Huo and coworkers [103], Figure 1-15, has shown that when Aβ(1–42) is brought up as a dilute concentration, it is initially random coil and shifts to the beta structure with time, which should be a natural transition for an aggregate-prone peptide. In addition, this study showed that, if methionine 35 were oxidized to methionine sulfoxide, the random coil to beta structure transition is slowed, along with aggregation. They also showed that methionine oxidation prevented protofibril formation and altered fibril morphology.

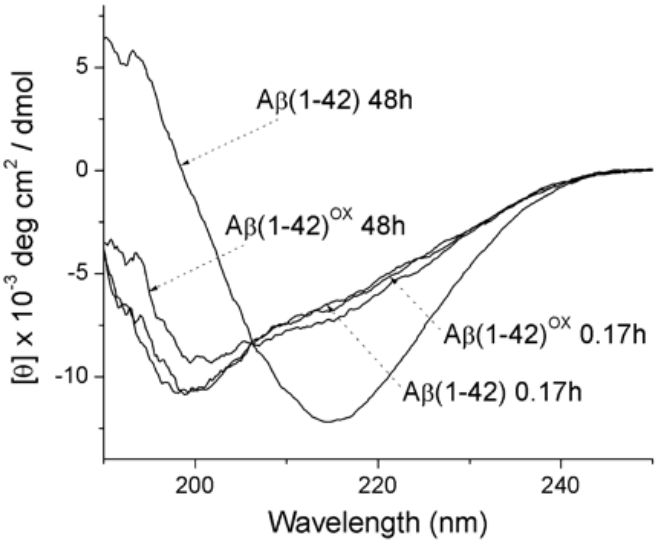

Figure 1-15. CD spectra of Aβ(1-42) at 0.17 and 48 h in 50 μM KPhos pH 7.3. The unoxidized peptide changes from random coil to beta where the oxidized remains stable. Figure source [103].

These changes in conformation transition and aggregation may be due to the fact that methionine sulfoxide is more hydrophilic than methionine, this promoting a stable disordered peptide structure that resists taking on the ordered aggregation-prone beta structure.

2. MATERIALS AND METHODS

2.1. Chemical Reagents

All reagents were diluted into Milli-Q purified H_2O. The Integral water purification systems is a Millipore™ product that filters tap water producing ultra-pure water meeting European Union (EU) and United States Pharmacopeia (USP) standards. The system uses their Elix technology, which is an electro deionization system. All references made to water or H_2O, unless otherwise noted, will refer to Milli-Q purified H_2O.

Table 2-1. List of Chemical Reagents Used in this Study.

Reagent	Abreviation	Company
3,3,3-Trifluoropropyl-trimethoxysilane	F_3-propyl triMOS	Gelest Inc.
Cesium Hydroxide	CsOH	ACROS
Hexafluoroisopropanol	HFIP	ACROS
Hydrochloric Acid	HCl	Fisher Chemicals
Phosphoric Acid	H_3PO_4	Mallinckrodt
Potassium Hydroxide	KOH	Fisher Chemicals
Tetramethylammonium Hydroxide	$N(CH_3)_4OH$	Fisher Chemicals
Tetramethylorthosilicate	TMOS	ACROS
Trifluoroacetate	TFA	ACROS/EM Science
Trifluoroethanol	TFE	ACROS

2.2. Peptides

Two model polypeptides, polyQ and Aβ, were obtained from AnaSpec and American Peptide, respectively. PolyQ was comprised of 15 glutamine repeats with two

aspartates attached to the N-terminus and two lysines to the C-terminus. The unmutated (but sporadic disease-associated) form of Aβ40 was used, having the following sequence: DAEFRHDSGYEVHHQKLVFFAEDVGSNKGAIIGLMVGGVV.

2.3. Solubilization of Peptides

A protocol from Chen and Wetzel was adapted for this research [104]. The peptides were brought up in 1.5 ml of 50:50 TFA:TFE, using approximately 3.5 – 4.0 mg for solution experiments and 1 – 1.5 mg for sol-gel experiments (per cassette, and for xerogel experiments below). The solutions were mixed by inverting several times and allowed to sit overnight in a 15 ml plastic centrifuge tube. To dry, nitrogen gas was bubbled through the sample using a small glass Pasteur pipette at a rate of a few bubbles per second, usually for 1 –3 days. The dried peptides were resuspended in 1.2 ml of 1.00 mM TFA (for sol-gel) or H_2O (for solution experiments), and repetitive pipetting was performed until the peptides no longer stuck to the bottom of the centrifuge tube. These solutions were allowed to sit until they clarified indicating the peptide was dissolved, approximately 1 h.

2.4. Sol-Gel Glass Encapsulation

Three 15 ml centrifuge tubes each had the following added in order: 895 μl TMOS, 105 μl F_3-propyl triMOS, 30 μl 0.04 N HCl, 214 μl H_2O. Each tube was sonicated in a Branson model 1510 sonicator in ice water for no less than 30 min. F_3-propyl triMOS was added to maintain peptide solubility during glass formation. A 1.17

ml volume of peptide solution (described above) was diluted to 4.65 ml with water. A 3.10 ml volume of the sol was combined with the diluted peptide solution making a final concentration of 0.129 – 0.194 mg/ml. The tubes were inverted three times, taking care not to produce any trapped air in the solution, and transferred to a disposable electrophoresis cassette with 1 mm spacing (Novex/Invitrogen). The cassette was covered with Parafilm and left at room temperature to solidify (~4-5 days), at which time approximately 1 ml of water was layered on top of the glass to prevent drying, and the cassette was moved to 4°C to age for no less than two weeks. Any sample analyzed after this step, with no further processing, will be referred to as a "wet-aged glass."

2.5. Xerogels

Wet-aged glasses were opened using a spatula to carefully break free the two sides of the electrophoresis cassette, and 1x2 cm samples were cut. Water was used as a lubricant to slide each piece to a 10x10 cm piece of Parafilm. The samples were patted down on each side with a tissue, and the Parafilm was also dried. The Parafilm, with the samples, was placed flat inside a plastic storage container. A second 10x10 cm piece of Parafilm was cut and stretched over the container making an air-tight seal. One or two small pinholes, equally spaced, were made above each sample. This container was then stored at 4°C for a minimum of two weeks or until the glass samples appeared to stop shrinking. Starting with a wet-aged glass with dimension 0.1cm x 1cm x 2cm (height x width x length), the final dimensions of the xerogel were approximately 0.06cm x 0.6cm x 1.2cm corresponding to about 22% of the original volume. Each piece was then

transferred to the bottom of a plastic Fisherbrand semicuvette that was tilted approximately 45° from the vertical, such that the sample lay flat against the lower side. To slowly rehydrate the sample, 30 μl of H_2O was added on the lip inside the cuvette just above the sample (direct contact with water may cause cracking). Samples were then covered with Parafilm with one small pinhole, and returned to 4°C for ~5 days before being analyzed. The final peptide concentration was estimated to be 0.614 – 0.924 mg/ml.

2.6. Solution Experiments

A 1:10 dilution of the solubilized peptide was preformed with different concentrations of HFIP, TFE, and phosphate buffers at various pH values. KPhos solution experiments were prepared by a 1:10 dilution of the peptide stock solution with 1.00 M, 50.0 mM, and 10.0 mM KPhos solutions at the desired pH. This dilution resulted in final phosphate concentrations being 0.900 M, 45.0 mM, and 9.00 mM. However, solution experiments were compared to xerogel experiments in the corresponding phosphate buffers (1.00 M, 50.0 mM, and 10.0 mM). Percent HFIP was calculated as volume per volume (v/v) and represents the true concentration for both solution and xerogel experiments. Solution samples were stored in 3 ml centrifuge tubes at an initial concentration of 0.30 mg/ml over the course of the time dependent data collection. Any specifics that differ from the above will be noted where appropriate.

2.7. Xerogel Experiments

Prior to analysis, xerogel samples were placed in 3 ml plastic cuvettes with 3 ml of solvent, covered with Parafilm, tilted, and incubated for 24 h at 25°C. For solvent exchange experiments, after the initial spectra were taken, the sample was allowed to equilibrate for 1 h in the new solvent and then drained and replaced with a fresh volume of the new solvent. This initial equilibration was done to reduce the amount of the previous solvent carried over in the xerogel matrix.

2.8. CD

An Aviv model 215 Circular Dichroism Instrument (New Jersey, USA) was used with 2 mm quartz cuvets (Starna Cells). All data were collected in the far-UV region. Wet-aged glass/xerogel samples were placed in the cells with the same solutions in which they had been equilibrated with. Prior to data collection, spectra of the cells containing only (fresh) solution were taken as background and were subtracted from the peptide-containing sample's spectra. Unless otherwise noted, peptide solution spectra were also collected using the same 2 mm quartz cells. In thermal stability experiments, the background was not subtracted from the single wavelength intensity but was subtracted from the complete wavelength scans that were taken at constant temperature. All spectra in time dependent experiments were taken at 1, 19, 168, 240, 336, 504, and 1008 h unless otherwise noted.

3. RESULTS AND DISCUSSION

3.1. Peptide Disaggregation and Solubilization

A protocol developed by Chen and Wetzel [104] was adapted where TFE was substituted for HFIP. Two steps were identified to be most crucial in the disaggregation and solubilization process. First, visual clarity of the suspended peptides in 1:1 TFA:TFE (v/v) after vortexing was not an adequate indicator of complete dissagregation. Peptides that sat at room temperature for only an hour after clarification in the TFA:TFE solution gave inconsistent results. However, when the clarified solution was allowed to sit overnight at room temperature (~14 h), consistent results were obtained. Second, when resuspending the dried peptide in TFA solution at pH 3, the peptide was not immediately soluble but the solution clarified if a period of repetitive pipetting was performed several times over the course of approximately 1 h. In addition, the clarified and resuspended peptide should be allowed to sit at room temperature for no less than 30 min prior to the experiment.

3.2. Sol-Gel Encapsulation

This work utilized the sol-gel process to isolate aggregation-prone peptides in the porous environment. Both the solid and liquid phases are continuous, allowing the solvent to be exchanged. A standard protocol [105] adapted by Eggers and Valentine [89] was modified to prevent peptide aggregation during gelation. Since fluorinated alcohols are known to induce helical structure in peptides, thereby increasing solubility, a fluorinated monosubstituted alkoxysilane precursor was used. Successful encapsulation

of the solubilized peptides was performed using glasses made from 10% F_3-propyl TriMOS and 90% TMOS precursors (v/v) (Figure 1-5). In addition, since both Aβ and polyQ promptly aggregated in buffered solutions, the addition of buffer prior to gelation was deleted and the volume was replaced by H_2O.

3.2.1. Development of Xerogels to Minimize Peptide Leaching

Initial experiments showed a uniform loss of signal with each successive analysis in time, during thermal experiments, and upon solvent exchange. Leaching of the peptides through the wet-aged glass matrix was suspected, so a protocol for the preparation of xerogels (a more condensed form of the wet-aged glass) was developed. PolyQ was used to test the xerogel environment. The peptide's small size of 19 residues makes it susceptible to leaching and, therefore, ideal for testing. Preliminary data indicated that there was little to no leaching of the peptide out of the xerogel matrix. Further study showed that leaching did occur, though to a lesser extent (details will be discussed below as appropriate to each result).

3.2.2. Analysis of Wet-Aged Glasses vs. Xerogel Spectral Data

As stated in section 2.5, the xerogel was estimated to be 22% of the wet-aged glass's original volume. This has two possible consequences that may affect the peptide's secondary structure. (1) The volume of the pore is decreased, possibly increasing excluded volume effects, or creating direct interactions between the glass and the peptide. (2) The surface density of the trifluoropropyl arm of the monosubstituted

alkoxysilane that interacts with the solvent was increased, further stabilizing the soluble peptide by increasing its helical content and/or altering peptide adsorption to the silica surface. To explore these possibilities, a series of identical experiments was performed on both wet-aged and xerogel glass samples. Though not all samples were prepared simultaneously, they were prepared with an identical protocol and with only slight variations in the total mass of the peptide. In addition, the peptide was always obtained from the same stock.

3.2.2.1. Spectral Intensities and Curve Shape

Preliminary analysis of wet-aged glass-encapsulated polyQ was performed using potassium (K^+), cesium (Cs^+), and tetramethylammonium ($N(CH_3)_4^+$) phosphate buffers at 10.0 mM, 50.0 mM, and 1.00 M concentrations at pH values near 7. The strongest and most stable signal was obtained when samples were equilibrated in 1.00 M KPhos at pH 6.8, so this buffer was chosen to test for any influences due to the increased density of the xerogel matrix. A comparison of wet-aged glass to xerogel encapsulated peptides shows an increase in CD signal intensity for the xerogel with no noticeable effect on spectral curve shape. This suggested that there were no additional effects on the peptide's secondary structure in the xerogel environment (Figure 3-1), and that there was an increase in peptide concentration. The blue curve gives the spectrum of the wet-aged glass encapsulated peptide, red the xerogel, and green an enhanced wet-aged glass. The green curve was obtained by multiplying the wet-aged glass spectrum by a factor of 4. The overlap of the red and green curves confirmed that there was little to no change in

secondary structure, and suggested that an increase in concentration was due to reduced leaching in the xerogel. This increase in concentration allowed for less peptide to be used in the preparation of all subsequent xerogels.

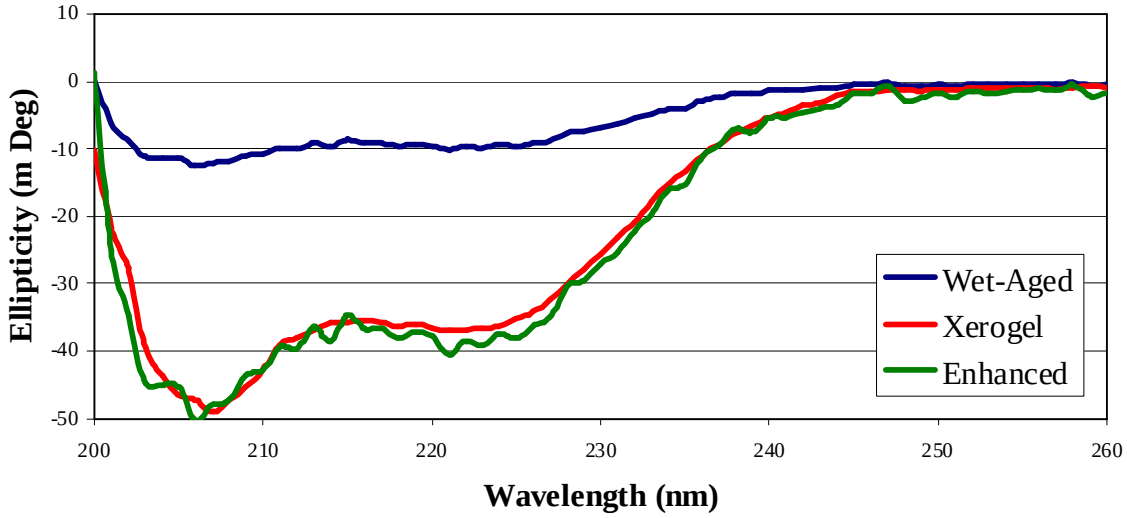

Figure 3-1. Comparison of wet-aged glass to xerogel encapsulated PolyQ. Both wet-aged glass (blue) and xerogel (red) samples were placed in 1.0 M KPhos pH 6.7. The enhanced wet-aged glass spectrum (green) is that of the wet-aged glass multiplied by 4. The overlap of the enhanced wet-aged glass spectrum on the xerogel indicates that there is an increase in concentration with little to no effect on the peptide's secondary structure.

The phosphate buffer cations were chosen because of their variable effects on peptide secondary structure, as predicted by the Hofmeister series [106]. In general, each cation should stabilize a peptide's secondary structure in the following order: $K^+ < Cs^+ < N(CH_3)_4^+$. The wet-aged glass spectra in Figure 3-2 (top) do not follow this trend. This failure to follow the trend was most likely due to enhanced leaching of the peptide. These ions have previously been observed, by the Eggers Lab, to induce leaching of other peptides out of the wet-aged glass matrix in the same order. Because polyQ in this study

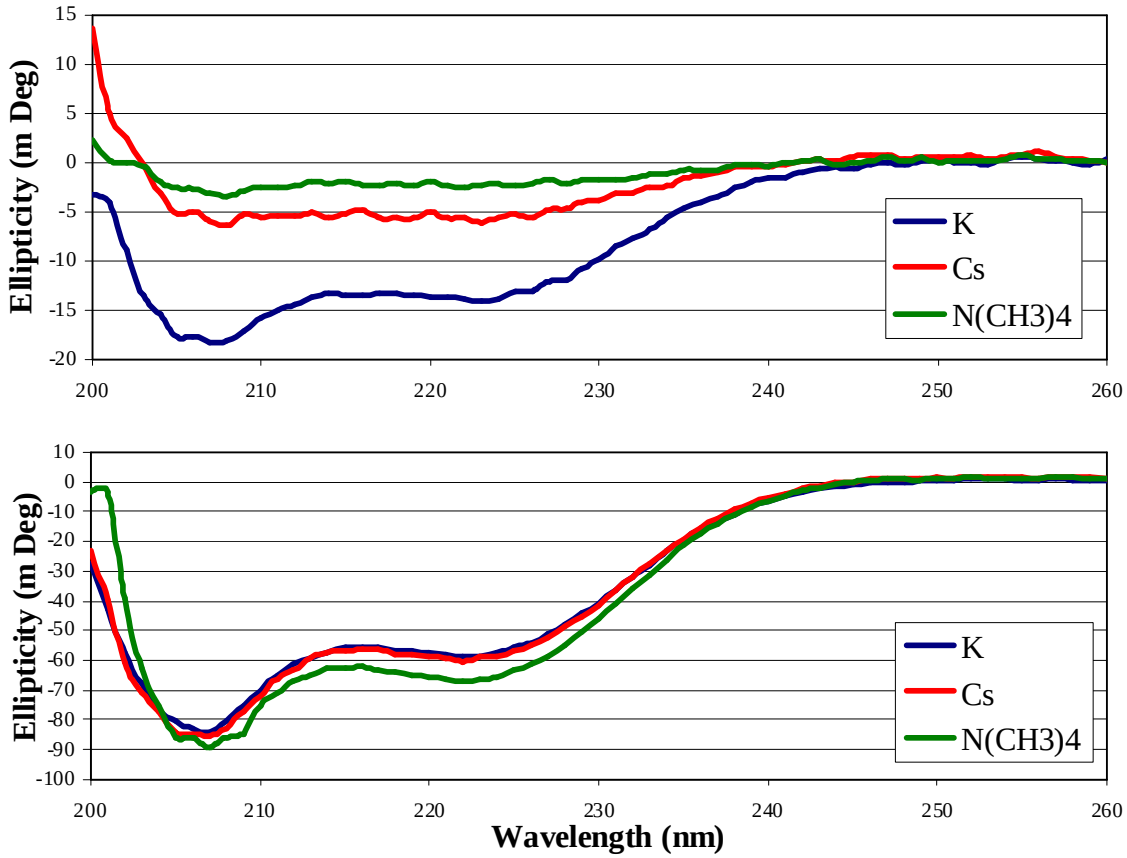

Figure 3-2. Comparison of encapsulated polyQ wet-aged glass vs. xerogel and the leaching effects of phosphate buffers. Top (wet-aged glass) and bottom (xerogel). PolyQ in 10.0 mM KPhos, CsPhos, and $N(CH_3)_4$Phos buffers all at pH 7. Both leaching and peptide stability increase as $K^+ < Cs^+ < N(CH_3)_4^+$. The wet-aged glass spectra decrease in this order indicating leaching. In the xerogel spectra there is a structural enhancement from $K^+ = Cs^+ < N(CH_3)_4^+$, which is in agreement with the Hofmeister series with $N(CH_3)_4^+$ being the weakest kosmotrope, and K^+ and Cs^+ having very similar chemical properties in solution. The overlap of the K^+ and Cs^+ spectra may indicate that leaching is still occurring but has been minimized.

was only 19 residues, and because the intensity of the wet-aged glass spectra followed this trend, the loss of signal was most likely due to leaching. The lower panel of Figure 3-2 is for the same experiment using xerogel samples. It can be seen that the spectra of the $N(CH_3)_4^+$ sample was slightly enhanced as compared to the other two, but that of the

Cs^+ was not when compared to the K^+. These spectra demonstrate that the xerogel environment was superior under all solvent conditions due to reduced leaching and the favorable effects of the F_3-propyl modifier on helical structure.

3.2.2.2. Spectral Intensities as a Function of Time

Spectra of the wet-aged glass encapsulated peptides demonstrated a uniform loss of intensity as a function of time in 1.00 M KPhos at pH 6.8 (as seen in Figure 3-3 left).

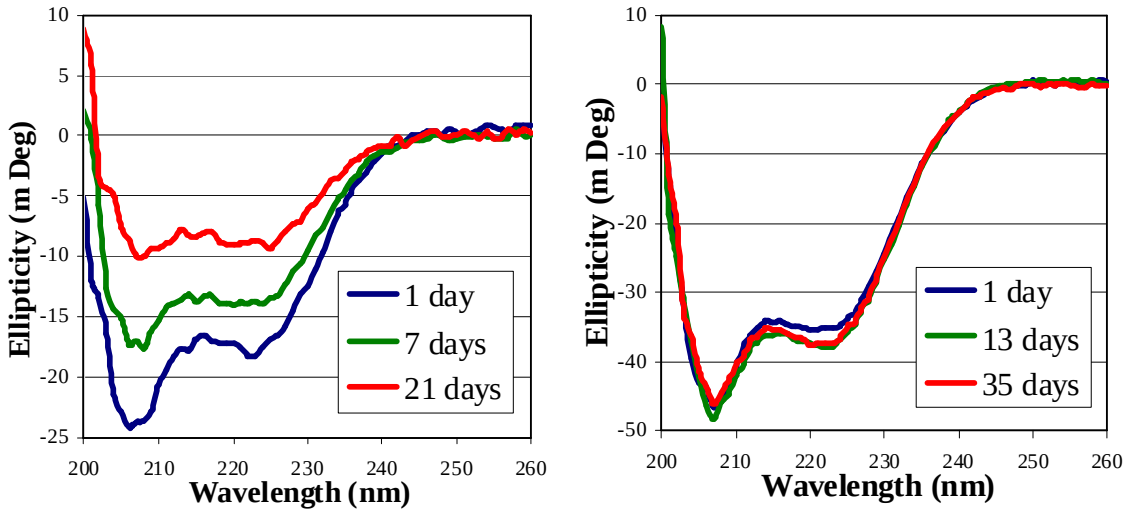

Figure 3-3. Spectral intensities as a function of time in the wet-aged glass vs. xerogel encapsulated peptides in 1.0 M KPhos, pH 6.7. Left (wet-aged glass) and right (xerogel). Wet-aged glass encapsulated peptides show a continuously weakening signal intensity over 1, 7, and 21 days. Relative signal intensities are constant with wavelength, indicating no change in secondary structure and probable leaching. Xerogel encapsulated peptides show a slight increase in the 222 nm signal intensity between 1 and 13 days, and no change between 13 and 35 days. The slight increase at 222 nm may be due to a gain in stable secondary structure in a small population of the isolated peptides.

Because the general shape of each spectrum retained the same character as the one before it, the encapsulated peptides likely retained the same percent of secondary structures, and

leaching was the cause of signal loss. Xerogels, Figure 3-3 right, returned spectra with stable signal intensities, indicating that leaching does not occur after more than a month.

3.2.2.3. Changes in Signal Intensities as a Function of Temperature

The thermal stability of polyQ is shown in Figures 3-4 and 3-5. The loss of signal intensity at the end of cooling was not recoverable for either sample, confirming that leaching did occur, but the xerogel sample had a much-reduced percent loss of peptide, as expected. Figure 3-5 shows the before and after CD spectra related to Figure 3-4 for the wet-aged glass (left) and the xerogel (right). Both show little change in curve shape but

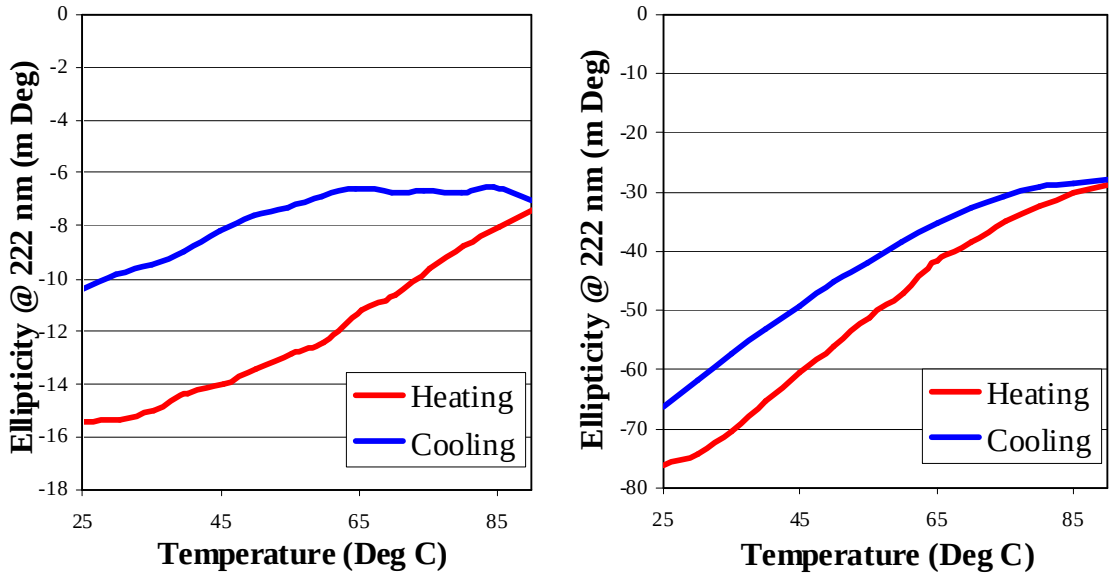

Figure 3-4. Comparison of wet-aged glass to xerogel encapsulated peptides at 222 nm as a function of temperature. Left (wet-aged glass) and right (xerogel). The wet-aged glass sample was stored in 10 mM KPhos for 2 days and a temperature step of 5°C was used between data points with an averaging time of 2 s. The temperature was held at 90°C for 1 min between heating and cooling. The xerogel sample was stored in H_2O for 10 days and a temperature step of 2°C was used between data points with an averaging time of 15 s. The temperature was held at 95°C for 5 min. The background has not been subtracted for either sample.

slightly weaker intensity, demonstrating that leaching took place with little change in secondary structure. Figure 3-5 shows that there is approximately a 33% loss of signal in the wet-aged glass whereas there is a less than 10% loss in the xerogel after heating to 90°C.

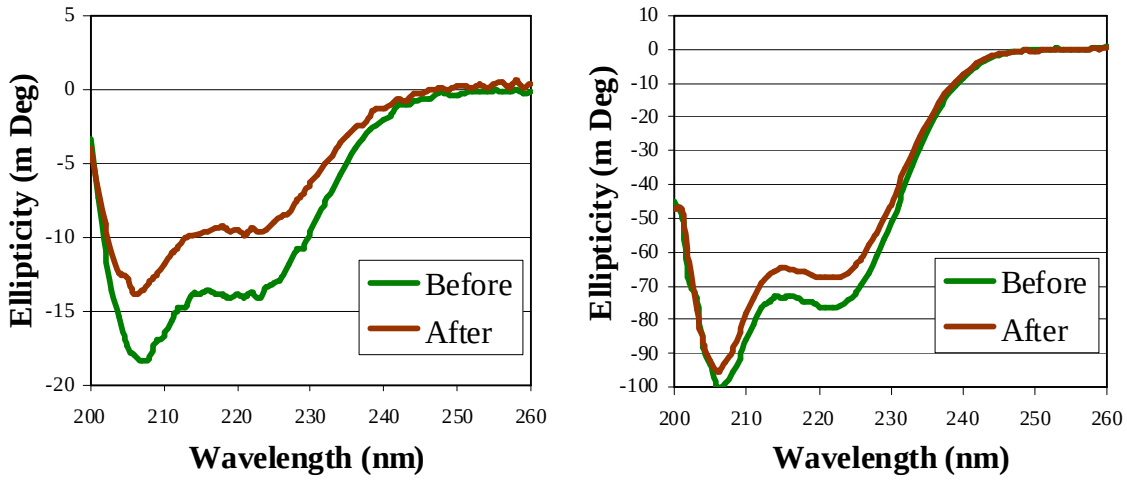

Figure 3-5. Comparison of wet-aged glass and xerogel spectra at 25°C before and after heating cycle. Left (wet-aged glass) and right (xerogel) (Figure 3-4).

3.2.2.4. Leaching of Encapsulated Peptides upon Solvent Exchange

During solvent exchange, a peptide's structure may be altered as it adjusts to the change in the environment, and this may also affect its interaction with the silica surface, thereby inducing leaching under the right conditions. To test the extent of leaching upon solvent exchange, not only must the sample be returned to the original solvent, but also the changes in secondary structure must be reversible so that changes in intensity can be related to changes in peptide concentration. All wet-aged glass samples showed a loss of signal with each successive solvent exchange. Xerogels demonstrated the ability to recover their original signal intensities in certain solvents, as will be seen in Section 3.8.

3.2.2.5. Leaching and the Internal Environment of Wet-Aged and Xerogel Samples

As stated in section 1.5.2.1, there is no obvious correlation between protein structure, average pore size, and surface area [92]. In addition, the fact that leaching still occured in the xerogel suggests that the extent to which the pore had been reduced did not drastically affect the internal environment where the peptides resided. This is further supported by the coincidence of the enhanced spectrum of the wet-aged glass and the xerogel spectrum (in Figure 3-1). As a consequence, one may conclude that the peptides populated the same states in the same ratios, indicating the same structure but different concentrations. One possible reason for the xerogel's resistance to leaching could be the increased density of the F_3-Propyl-triMOS modifier and its hydrophobic influence on the solvent. It is well known that fluorinated compounds are hydrophobic [107]. The hydrophobicity of the F_3-propyl group should alter nearby water's structure, raise the solvent free energy, and influence peptide adsorption to the surface [91]. Most likely, reductions in pore size and the channels between the pores restricted the motion of the peptides and minimized leaching.

3.3. Characterization of Xerogel Encapsulated Peptides

To characterize the influence of the xerogel matrix on the peptides' secondary structures, data were collected and compared for encapsulated peptides and peptides in solution. Due to aggregation during experiments in solution and because only very rough estimates of the peptides' concentrations after encapsulation could be made, only the shape of the spectra are compared. Pure water, TFE, HFIP, ethanol, KPhos, and HCl

were chosen as solvents because they are well understood and documented for their influence on peptide structure. Additionally, because the 10% F_3-propyl TriMOS was suspected to have some influence on peptide secondary structure, different concentrations of TFE and HFIP were used to determine the extent of this influence.

3.3.1. PolyQ

3.3.1.1. Percent HFIP Solutions

Figure 3-6 compares the spectra for soluble polyQ in water and encapsulated polyQ. It can be seen that there was a significant increase in helical content after

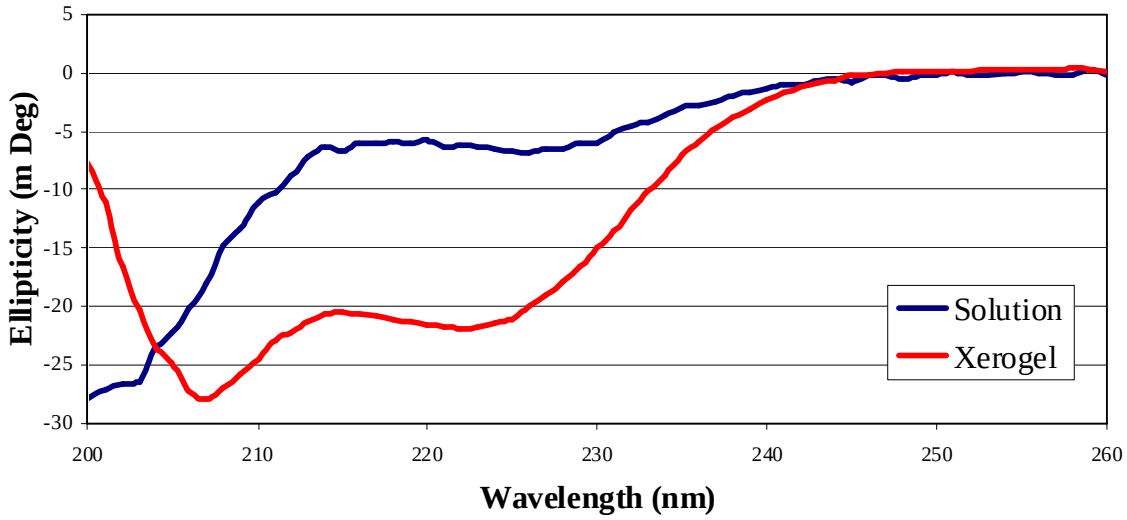

Figure 3-6. Comparison of xerogel encapsulated polyQ to solution CD spectra in H_2O. To compare shapes, the xerogel spectrum has been reduced by estimating the value of the most intense minimum in each spectrum and normalizing to that value

encapsulation. Figure 3-7 gives the spectra for solution (top) and xerogel encapsulated (bottom) polyQ at 1%, 5%, 10%, 25%, 35%, and 50% HFIP in H_2O (v/v). The xerogel spectra in 1 – 10% HFIP were greatly enhanced in secondary structure as compared to

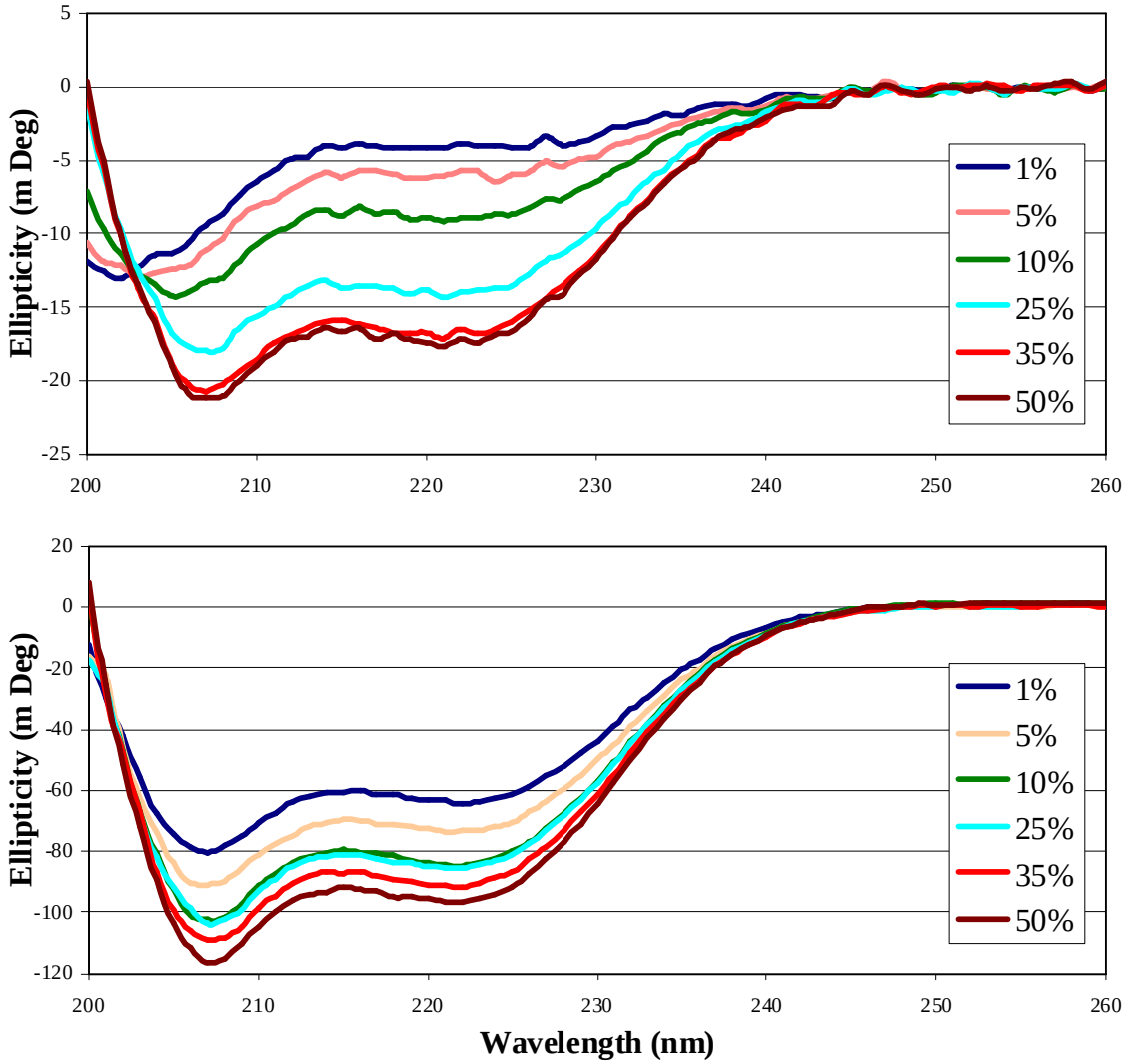

Figure 3-7. PolyQ in solution vs. xerogel encapsulated spectra in HFIP solutions. Top (solution) and bottom (xerogel). Percent HFIP in water (v/v) are indicated to the right. Xerogel sample at 1% - 10% HFIP show enhanced helicity as indicated by the ratio of intensities at 222 nm to 208 nm.

solution. This increase may be partially due to the 10% F_3-propyl triMOS glass and partially due to the crowded environment. The relative increase of the signal at 222 nm as compared to the signal below 210 nm is indicative of increased helical content, and the increase is even more pronounced when comparing pure water, or 0%, spectra (Figure 3-

6). A similar shape is seen when comparing the 10% solution spectrum to the xerogel spectrum in 0 – 1% HFIP, which suggests that the xerogel environment was similar to the 10% HFIP solution environment. Because the xerogel is made from the 10% F_3-propyl TriMOS precursors, this is a likely situation. Solution and xerogel spectra at higher percent HFIP are similar in shape, which is to be expected since HFIP is known to induce helical structure in peptides, and at these concentrations of HFIP, the influence of the F_3-propyl modifier on the spectral shape would be less pronounced. Both solution and xerogel samples show the same trend of increasing helical content with increasing HFIP concentration, but the solution spectrum appears to reach maximum helicity at 35% HFIP, whereas the encapsulated sample became slightly more helical in 50% HFIP.

3.3.1.2. Effects of KPhos Concentration

In Figure 3-8, xerogel encapsulated peptides show an increase in helical structure with increasing phosphate concentration compared to solution, as indicated by the more intense 222 nm signal when compared to the signal below 210 nm. In both cases, the samples at the two lower KPhos concentrations gave similar spectra, indicating that KPhos had little effect on the structure at low concentrations, and that the increased helical structure in the glass was likely due to the F_3-propyl modifier. The 1.00 M encapsulated sample gave a highly enhanced spectrum while the 0.90 M solution sample gave a negligible increase in the 222 nm signal. Because there was little change in the 0.90 M KPhos solution spectrum after 1 h (not shown) or after 24 h (shown in Figure 3-8), aggregation was not a factor (Figure 3-21 for time-dependent aggregation

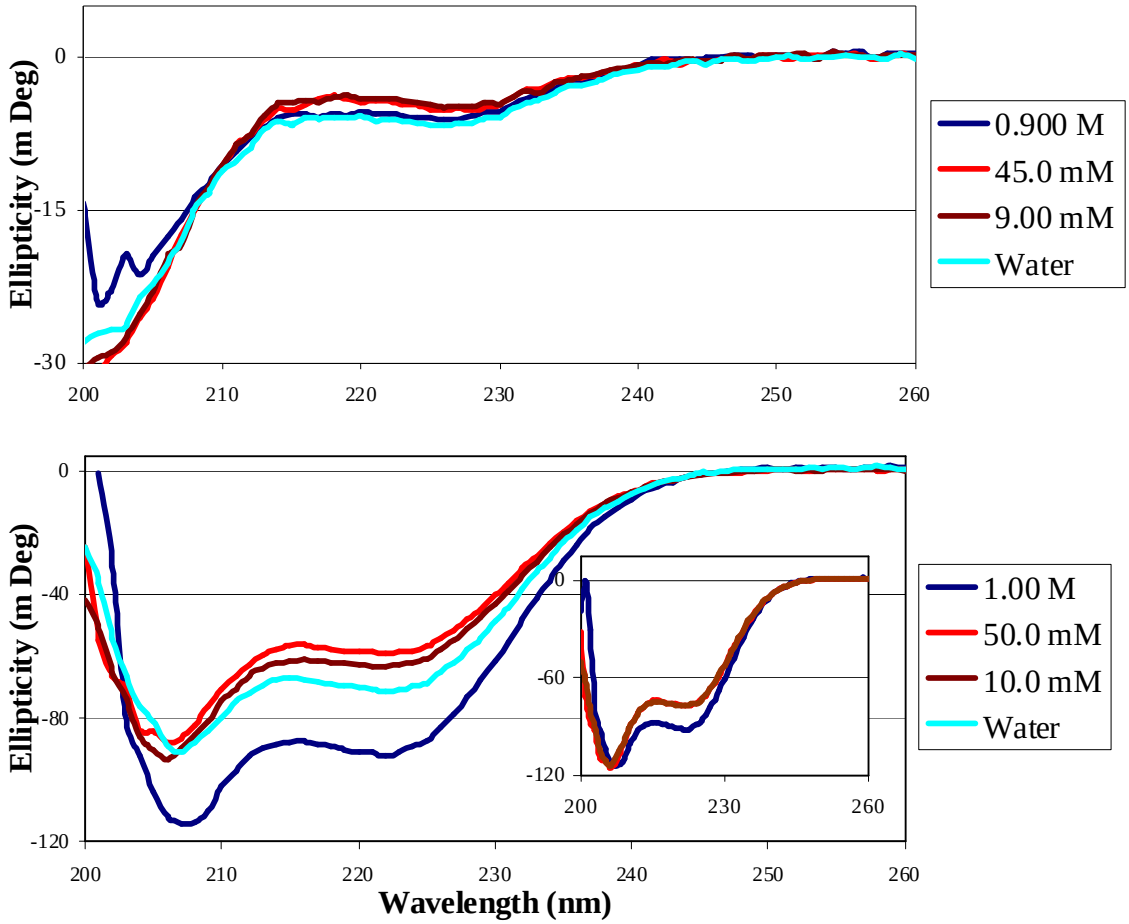

Figure 3-8. Xerogel encapsulated vs. solution polyQ in KPhos at several concentrations. Top: solution at the indicated concentrations. Bottom: xerogel encapsulated at the indicated concentrations. All buffers were at pH 6.9, except the 1.00 M and 0.90 M samples that were at pH 6.8. Both panels also contain the spectra of control samples incubated in water. Inset: Comparison of the minima intensities of the 50.0 mM and 10.0 mM xerogel samples to the 1.00 M sample. Signals were normalized to the minimum value near 207 nm.

data). Additionally, the encapsulated spectrum in 1.00 M KPhos shows a relative increase in the 222 nm signal over the signal below 210 nm as compared to the other KPhos samples (Figure 3-8 bottom inset). This was not observed for the solution spectra.

This data suggests that the encapsulated peptides were monomeric and do not form irreversible aggregates.

3.3.1.3. pH Dependence in KPhos Buffers

The pH-dependent structure of the samples shown in Figure 3-8 can be seen in Figures 3-9 to 3-11. Solution spectra give similar random coil profiles for all samples, except the 0.90 M KPhos sample at pH 11.4 that could not be interpreted because of noise below 215 nm most likely due to the high concentration of PO_4^{3-} (Figure 3-9). This sample appears to have a slightly stronger signal at 222 nm, as compared to the others, which may also be due to the PO_4^{3-} concentration and its strong kosmotropic affect. Xerogel samples show enhanced secondary structures compared to solution data in all cases and separate into 3 distinct pH dependent spectra (Figures 3-10 and 3-11).

At 1.00 M KPhos (Figure 3-9), the signal intensities gave the following pH dependence: 6.8 > 11.4 > 4.1. The sample with the strongest signal (pH 6.8) may be the result of the peptide having no net charge with its termini equally and oppositely charged. This should increase favorable hydration of the peptide and, with the high KPhos concentration, increase secondary structure. It is also possible that the oppositely-charged termini form a hairpin, as discussed in Section 1.6.1, and that there was a tight coiling induced by the KPhos. Following the same reasoning, at pH 11.4 the peptide would have a net negative charge due to the aspartates (pK_a 3.86), and at pH 4.1 a significant population of the aspartates were still protonated, giving the peptide a net positive charge due to the lysines (pK_a 10.53), thus reducing the favorable hydration on

the peptides at pH 4.1 and 11.4 and decreasing the influence of the KPhos, as compared to the pH 6.8 sample. The increased intensity of the pH 11.4 over the pH 4.1 sample can be explained by the difference in the phosphate ion. At pH 11.4 the phosphate ion is in the PO_4^{3-} state, a strong structure enhancing kosmotrope, and at pH 4.1 it was in the $H_2PO_4^{1-}$ state, a weak kosmotrope.

At the lower KPhos concentrations of 50.0 mM (Figure 4-10) and 10.0 mM (Figure 3-11) the acidic pH values were raised to 4.5 and 4.7, respectively. At these pH

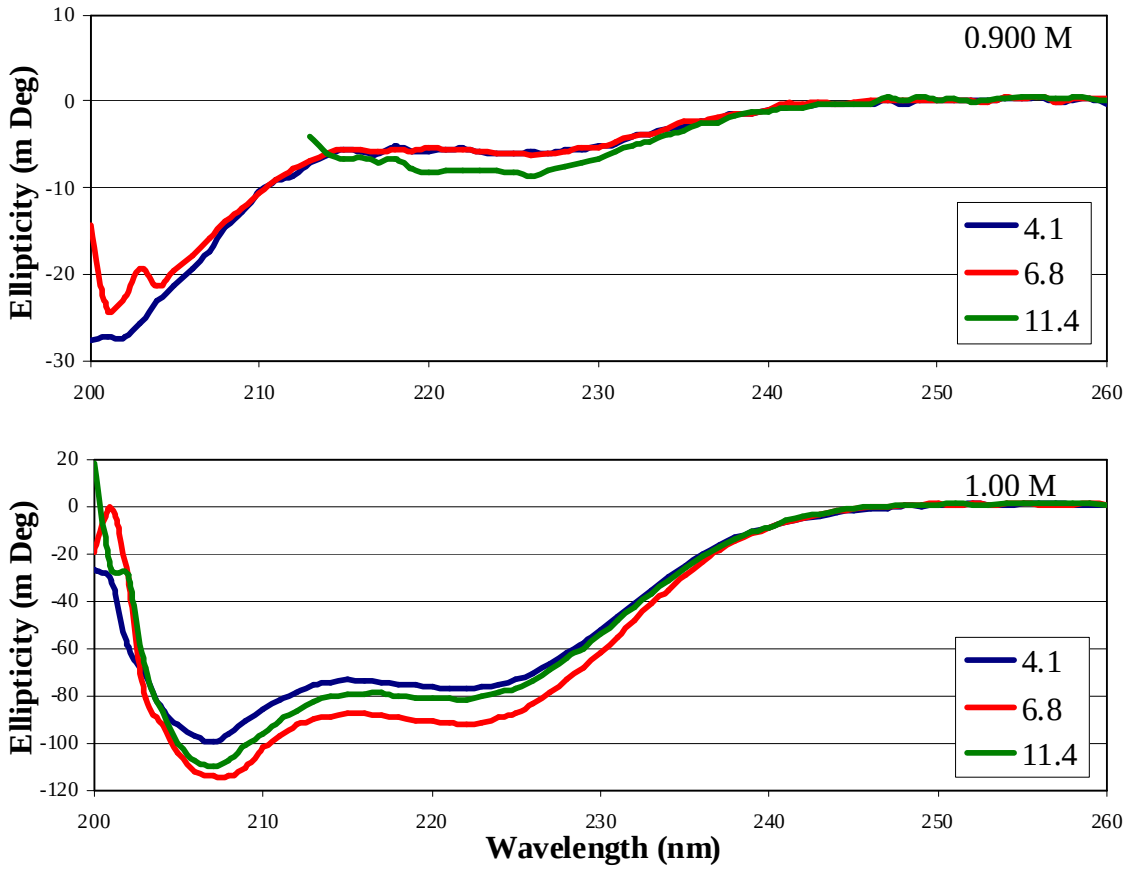

Figure 3-9. Comparison of pH dependence of solution to xerogel encapsulated for polyQ in 0.90 M and 1.00 M KPhos solution, respectively. Top (solution) and bottom (xerogel). Solution sample at pH 11.4 became extremely noisy below 212 nm so data was not taken below 210 nm.

values the aspartates should have been mostly deprotonated, and so the peptide should have been more strongly hydrated. The fact that these acidic samples showed the most secondary structure may be related to changes in the silica surface. Under acidic conditions, the surface may have been protonated (more Si-OH groups relative to $Si-O^-$ groups), making it more hydrophobic as compared to at neutral pH samples. Looking at the 10.0 mM KPhos samples in Figure 3-11, it can be seen that the sample at pH 6.9 had less secondary structure than that at pH 4.7. It has been shown previously that increasing

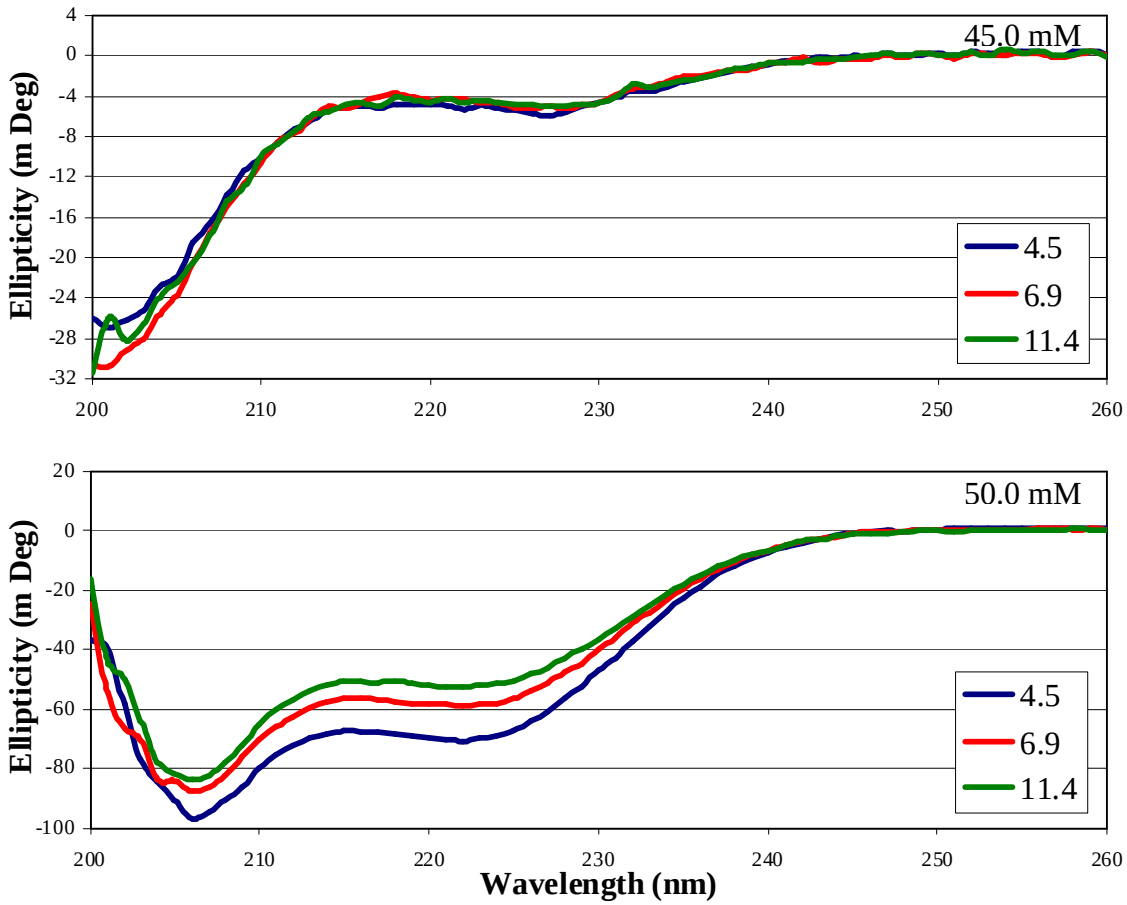

Figure 3-10. Comparison of pH dependence of solution to xerogel encapsulated for polyQ in 45.0 mM and 50.0 mM KPhos, respectively. Top (solution) and bottom (xerogel).

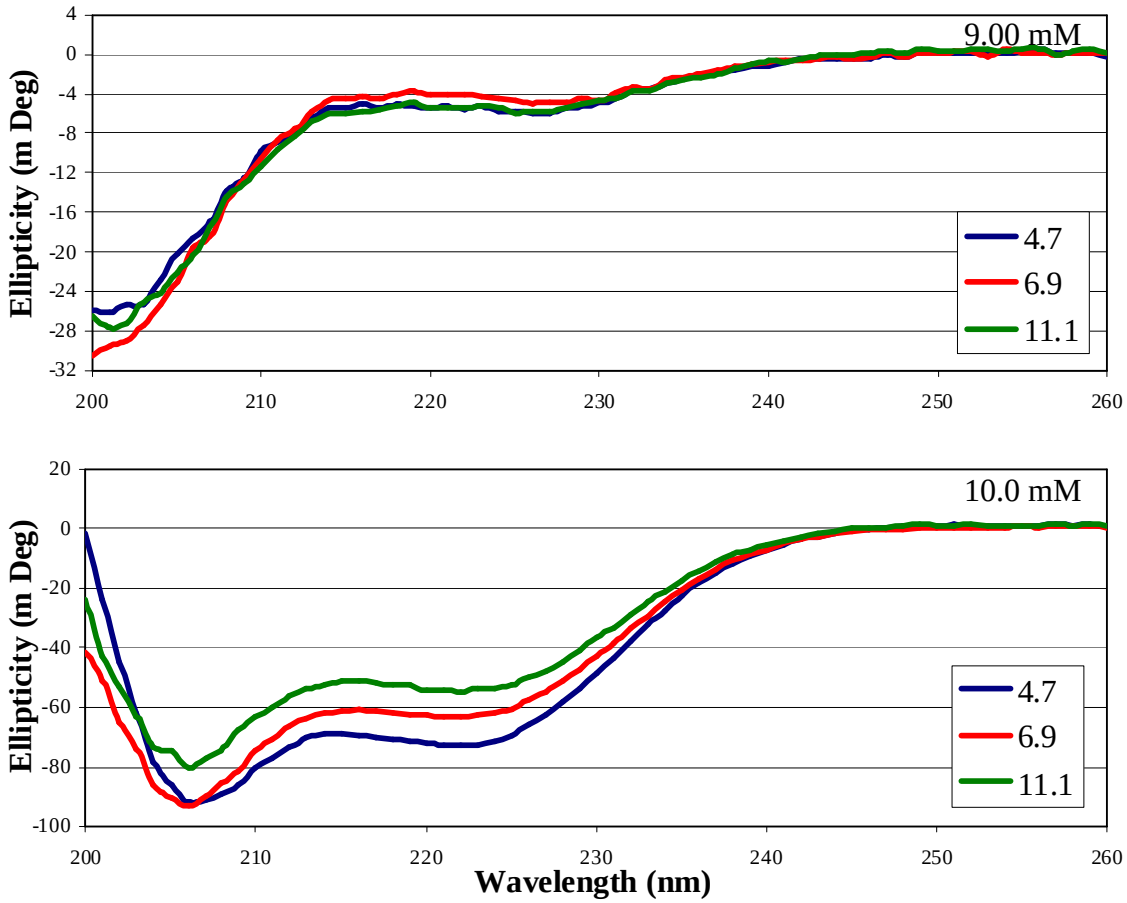

Figure 3-11. Comparison of pH dependence of solution to xerogel encapsulated for polyQ in 9.0 mM and 10.0 mM KPhos solution, respectively. Top (solution) and bottom (xerogel).

the hydrophobicity of the glass surface leads to an increase in the secondary structure of peptides [84]. This observation may explain why the acidic samples showed the most secondary structure relative to other pH values at lower KPhos concentrations. At these same KPhos concentrations, the basic samples (pH ~11) may display the least amount of secondary structure due to changes in the overall charge of the peptide. A pH of 11 is

well above lysine's pK_a, and so the peptide should have had a net negative charge, decreasing favorable hydration.

The failure of the solution samples to show any pH dependence, and the fact that they all return similar spectra at each concentration, may indicate that the peptide had formed stable soluble oligomers in solution. Alternatively, one may attribute the more-structured peptide in the glass to be the result of crowding and the chemistry of the silica surface. Peptides appear to be more sensitive to solvent conditions when confined in this environment. This observation is significant because information not seen by standard solution methods is obtained by sol-gel encapsulation.

3.3.2. Aβ

3.3.2.1. Percent HFIP Solutions

A comparison of the pure water spectra for both solution and xerogel samples are presented in Figure 3-12. The encapsulated peptide had a weakly enhanced secondary structure as indicated by the increased intensity between 210 nm and 225 nm. Though there was an increase in secondary structure, the signal below 210 nm indicates that the sample was still largely random coil. This increase in secondary structure may have been due to excluded volume, the modifier, or both.

The spectra for Aβ peptide in solution and xerogel for different percent HFIP/H_2O solutions (v/v) are given in Figure 3-13. In solution, the Aβ 1% HFIP spectrum is still indicative of a random coil structure. At 5%, Aβ began to take on secondary structure, as seen in the inset of Figure 3-13 (top). The 5% HFIP spectrum in solution is similar to the

xerogel spectrum in H_2O (Figure 4-12). Deconvolution of this spectrum by CDNN software [108] can be seen in Table 3-1. Later, in Section 3.4.2.1, it will be shown that

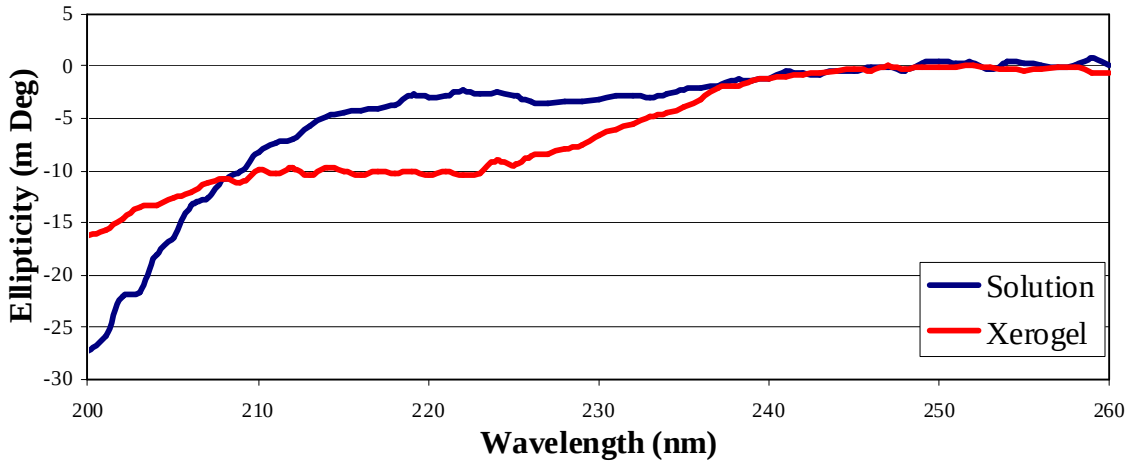

Figure 3-12. Comparison of xerogel encapsulated Aβ to solution CD spectra. The increased intensity at 222 nm and the decreased intensity at 200 nm indicate that in the xerogel Aβ peptide sample has increased secondary structure.

this spectrum was highly stable with time, indicating that it did not form large insoluble aggregates. In either case, the peptide had taken on increased secondary structure, which is even more apparent in the spectra at 10% and above where significant helical structure can be seen. It is also notable that at 50% HFIP there was a drop in intensity as compared to the 25% and 35% HFIP spectra.

Xerogel encapsulated Aβ showed a general increase in secondary structure with added HFIP up to 10% HFIP, as compared to that seen in solution (Figure 3-13). The xerogel encapsulated spectra at 1% and 5% HFIP take on increased secondary structure relative to water. As the HFIP concentration was increased, some beta character appeared to develop at 10% HFIP but this was hard to verify due to noise at the shorter

wavelengths. At 25% HFIP, the spectra began to flatten out between 210 nm and 225 nm indicating an increase in helical content up to 50%. The inset in the bottom panel of

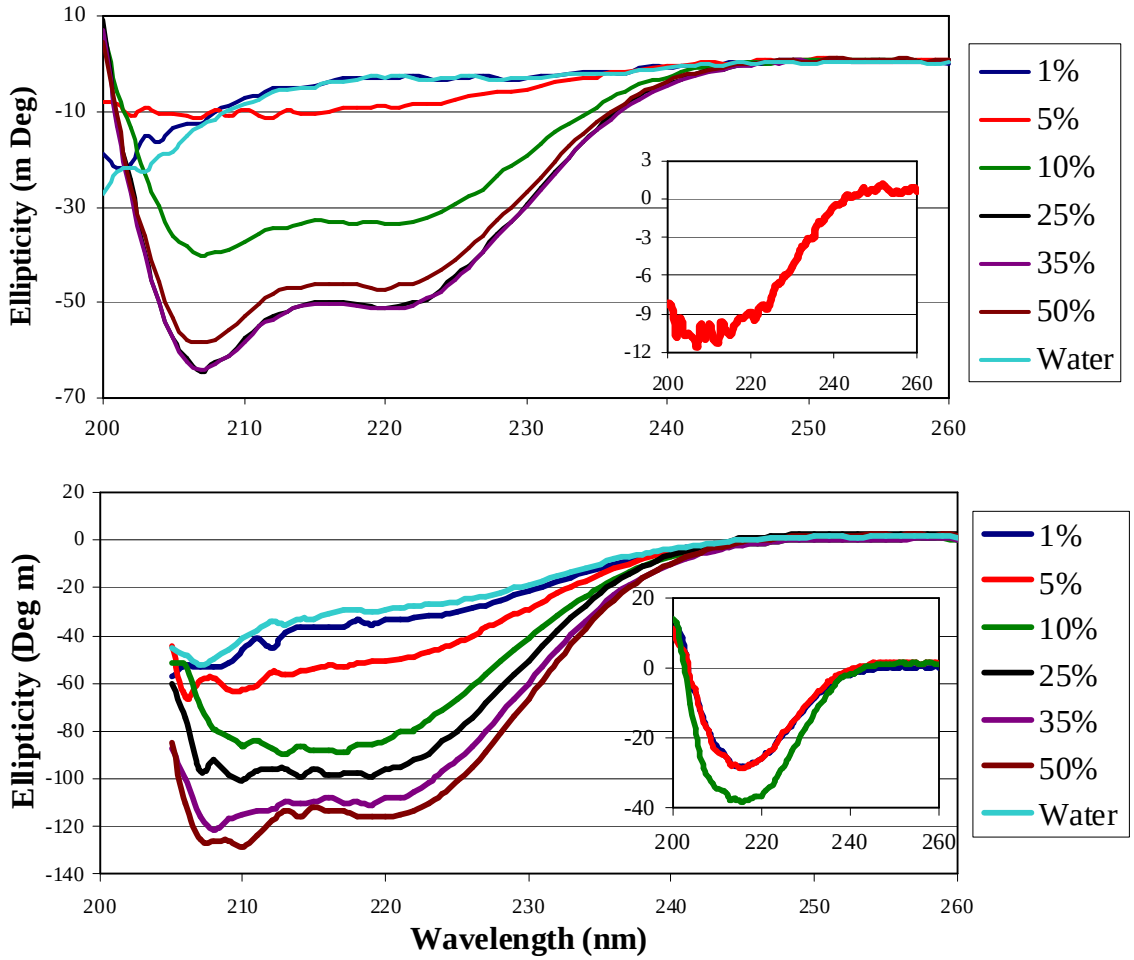

Figure 3-13. Aβ spectra in solution vs. xerogel. Top (solution) and bottom (xerogel). Percent HFIP in water (v/v) are indicated to the right. Inset (top): Aβ in 5% HFIP solution. Inset (bottom): xerogel encapsulated Aβ in 1%, 5%, and 10% HFIP left temperature over night during an approximate 10°C change in room temperature.

Figure 3-13 shows a similar experiment when the samples were left at room temperature during a summer night and there was an approximate 10°C fluctuation in temperature. While other samples cut from the same glass gave consistent result with previous

findings, these samples showed significant beta structure at the lower HFIP concentrations. It can be seen in the inset that there was a slight increase in secondary structure at 10% HFIP. By comparing the panel to the inset, this increase is most likely due to an increase in helical structure. Furthermore, the similarity between both 10% spectra (panel and inset) suggested that beta structure in the 10% HFIP spectrum was probable.

Table 3-1. Deconvolution of soluble Aβ peptide in 5% HFIP solution.

	200-260 nm	205-260 nm	210-260 nm
Helix	28.00%	33.80%	31.80%
Antiparallel	10.70%	7.80%	8.70%
Parallel	9.50%	8.90%	9.10%
Beta-Turn	18.30%	16.70%	17.20%
Rndm. Coil	32.60%	32.80%	34.10%
Total Sum	99.20%	100.00%	100.80%

Top column gives the wavelength range over which the program used to fit the secondary structural content to.

The changes in secondary structure of the encapsulated samples in 1 – 10% HFIP cannot be attributed to the F_3-propyl modifier alone because of the significant differences in the glass spectra as compared to the solutions. Aβ was about twice the size of the polyQ peptide but still small compared to an average globular protein. Nevertheless, excluded volume effects might have had more of an influence on Aβ's secondary structure. The different amino acid composition of Aβ relative to polyQ might also have changed the silica adsorption properties of the peptide. For a peptide that is naturally prone to aggregation, it would be sensible to reason that the beta fold was

favored in a crowded environment. This would have not only reduce the peptide's hydrodynamic radius but also increase its tendency to aggregate upon partial unfolding. As discussed in Section 1.3.2.2, both the folded and aggregated states are favored in a crowded environment. In time, the solution sample in 10% HFIP gave a single minimum near 217 nm, indicating a beta fold and a local energetic minimum in the folding landscape (to be discussed later in Sections 3.4.2.1 and 3.5).

Within the xerogel environment, the excluded volume effects driving the peptide to a more compact state and the helix-inducing effects of HFIP would compete, whereas in solution the excluded volume effects were absent. This absence would indicate that the helical structure seen in solution is most likely not a compact stable intermediate but was instead a peptide with a large hydrodynamic radius consisting of helices and random coil secondary structures, with little stable tertiary structure.

The probable beta structure observed for some samples in Figure 3-13 (bottom) was not expected. Since Aβ should have been isolated in the pores of the silica matrix as a monomer, the peptide must have been able to form intramolecular β-strands not seen in solution. Barrow and coworkers [101] found a similar spectrum in 25% TFE solution but demonstrated that the peptides had formed oligomers by centrifugation. Here it appears that Aβ maked a structural transition from random coil to beta to α-helical in a monomeric form with increasing HFIP concentration.

3.3.2.2. Effects of KPhos Concentration

The effects of KPhos concentration for solution/xerogel encapsulated Aβ in 0.90/1.00 M, 45.0 mM/50 mM, and 9.0/10.0 mM KPhos are shown in Figure 3-14. The

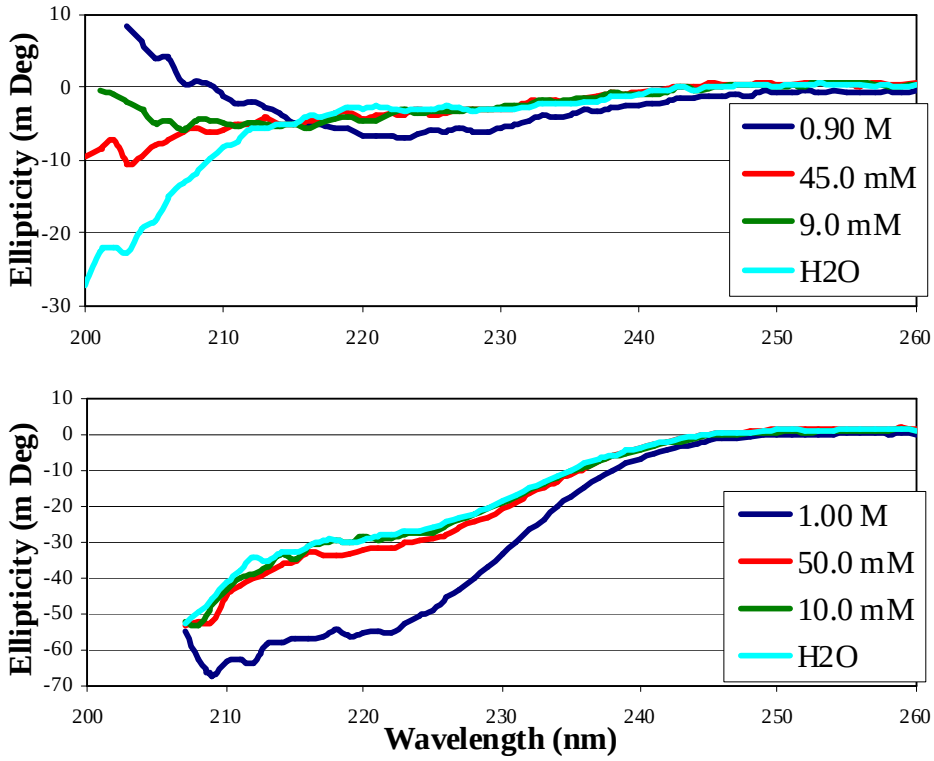

Figure 3-14. Xerogel encapsulated vs. soluble Aβ in KPhos at several concentrations. Top: solution at the indicated concentrations. Bottom: xerogel encapsulated at the indicated concentrations. Xerogel samples were too noisy below 207 nm to be interpreted. All buffers were at pH 6.9, except the 1.00 M and 0.90 M samples that were at pH 6.8. Both panels also contain the spectra of control samples incubated in H_2O.

xerogel spectra are reminiscent of some combination of random coil and α-helical structure, while the solution spectra are so weak that no conclusions may be drawn. It can be seen that there was no notable difference in the encapsulated peptide's spectra at 50.0 mM and 10.0 mM KPhos as compared to water, but in 1.00 M KPhos there was a

significant increase in helical structure. A similar trend was seen for encapsulated polyQ (Figure 3-8).

3.3.2.3. pH Dependence in KPhos Buffers

Figure 3-15 shows spectra for Aβ in 0.90 M KPhos solution and 1.00 M KPhos xerogel encapsulated peptides at pH 4.1, 6.8, and 11.4. The xerogel spectra in Figure 3-15 were taken after 19 h in solution and show increasing secondary structure with increasing pH, but, due to noise caused by high absorbance of the [PO_4^{3-}] at the shorter wavelengths, the secondary structure was difficult to evaluate. The solution spectra were taken after 1 h in solution, and, due to [PO_4^{3-}] absorbance below 212 nm, the pH 11.4 sample could not be evaluated. At the lower pH values of 6.8 and 4.1, a single minimum in ellipticity was observed in each sample above 220 nm. Because these minima did not occur at the same wavelength, it was difficult to conclude anything about the secondary structural content. Aβ has an isoelectric point near pH 5.5 that falls just between two of the pH measurements [102]. Figure 3-16 shows these solution spectra at 19 h. Both pH 4.1 and 6.8 samples returned flat profiles indicating that aggregation might have occurred. Upon visual inspection at this time point, the 3 ml centrifuge tubes contained white fuzz, reminiscent of loose cotton fibers, providing further evidence of aggregated peptide. Because of this aggregation, comparison of the solution and xerogel spectra was complicated; diffraction has altered minima intensities, and aggregation rates may be a factor for the samples in Figure 3-15 top. All that is certain is that the spectrum at pH

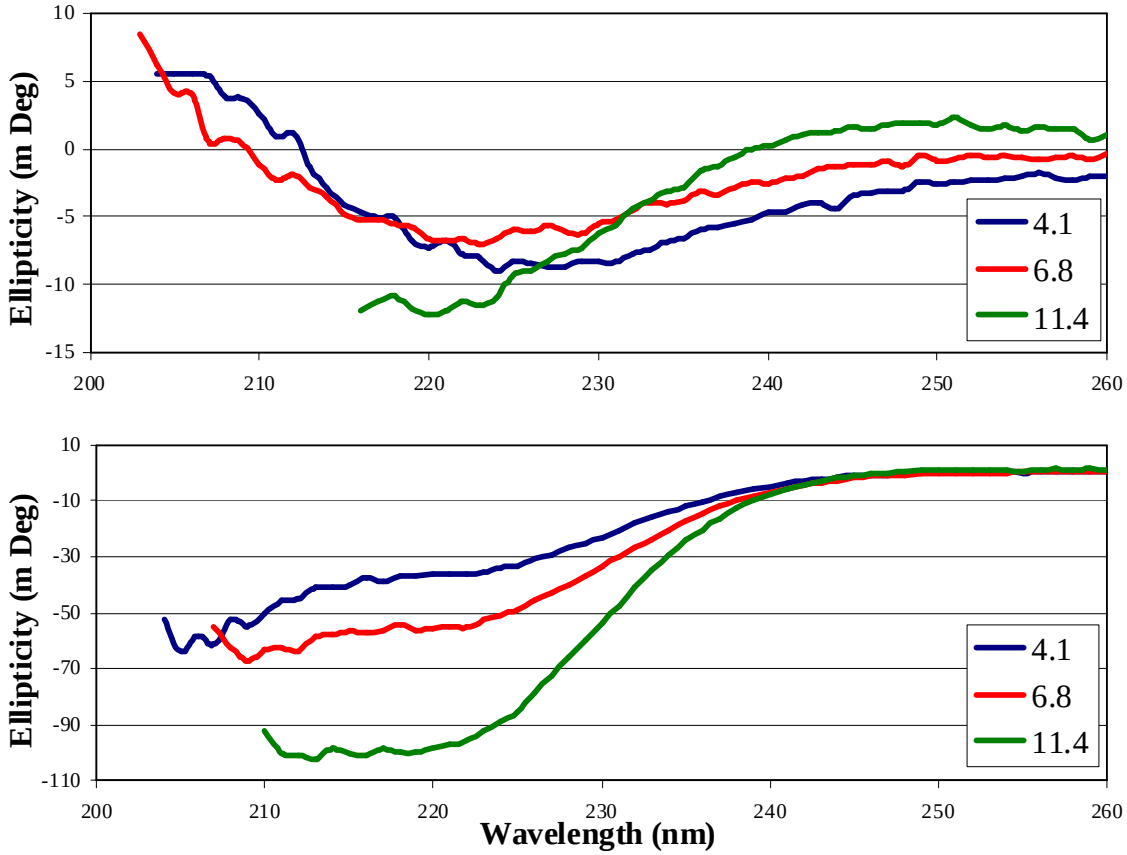

Figure 3-15. Comparison of pH dependence of soluble to xerogel encapsulated Aβ in 1.00 M and 0.90 M KPhos solution, respectively. Top (soluble) and bottom (xerogel).

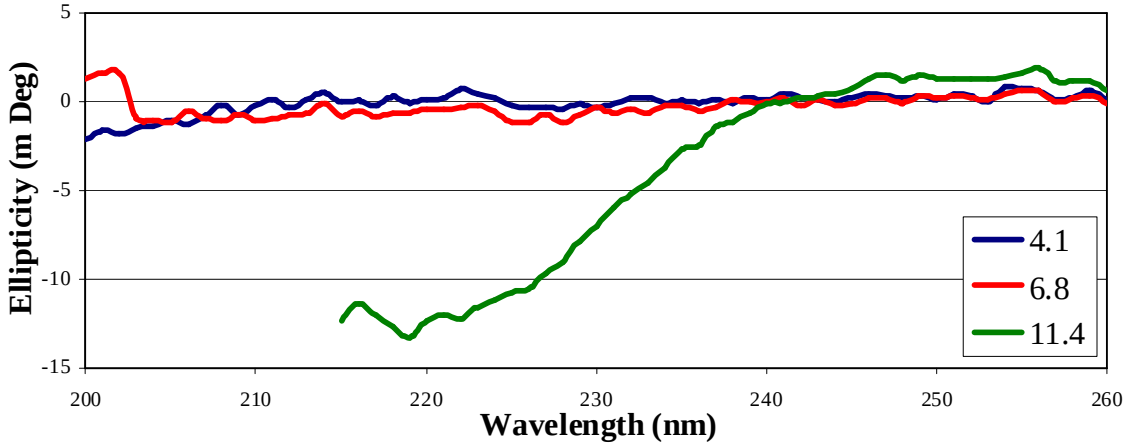

Figure 3-16. Soluble Aβ in 0.90 KPhos at the indicated pH for 19 h. Samples at pH 11.4 became extremely noisy below 212 nm so data was not taken. The flat zero spectra of the pH 4.1 and 6.8 samples indicate that no significant amount of protein remains in the solutions and that aggregation had occurred.

11.4 was stable over a 19 h period, which is consistent with previous findings [102] and indicated that the peptide remained soluble under basic conditions.

Aβ in 45.0 mM (solution) and 50.0 mM (xerogel) KPhos at pH 4.5, 6.9, and 11.4 can be seen in Figure 3-17. In solution, the pH 4.5 sample shows a single minimum around 217 nm, which is a hallmark of beta structure, but difficult to interpret due to the weak intensity and noise at the shorter wavelengths. The samples at pH 6.9 and 11.4

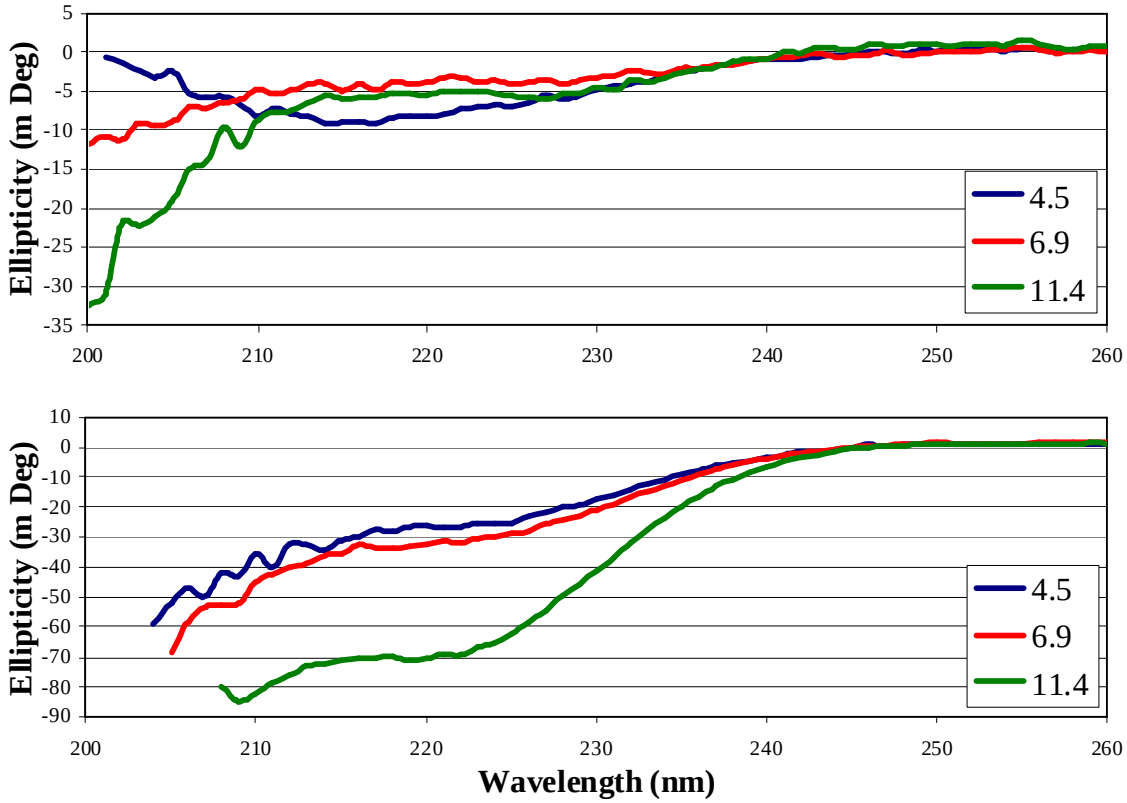

Figure 3-17. Comparison of pH dependence of solution to xerogel encapsulated Aβ in 45.0 mM and 50.0 mM KPhos solutions, respectively. Xerogel samples became noisy below 205 nm.

both returned random coil spectra with the pH 11.4 sample returning the strongest intensity below 210 nm. This was consistent with the results above in Figure 3-16 where

the sample at higher pH was found to be less likely to aggregate. Similar to the 1.00 M KPhos samples, the xerogel-encapsulated samples appeared to be mostly random coil/helical with an enhanced intensity with increasing pH (Figure 3-17 bottom).

Figure 3-18 for 9.0 mM (solution) and 10.0 mM (xerogel) KPhos shows similar results as Figure 3-17 except that, in solution, the sample at pH 6.9 now had a single minimum near 217 nm and the pH 4.7 sample was random coil. A complete loss of signal occured at pH 6.9 after 168 h, which may indicate that the spectrum in Figure 3-18 was compromised by diffraction. The soluble spectra were hard to interpret because of their weak signal intensity, which further suggests diffraction problems due to aggregation. Xerogel samples at low KPhos concentrations again showed an increase in secondary structure with pH, as indicated by the minimum near 222 nm. The pH dependence of these samples was only apparent in the pH 11.1 sample, whereas the 4.7 and 6.9 samples returned almost identical spectra.

Below Figure 3-18, the Aβ peptide sequence is given with the residues that would be ionized under the specific conditions of this work: red (anion), and blue (cation). The N- and C-terminals are given but because they cancel, they are neglected in the total charge calculation for all but the basic condition. The residue number is indicated above each 10^{th} residue. Note that in acidic conditions at pH 4.1, glutamic acid (E) and aspartic acid (D) were near their pK_a values where they are only half ionized. This was the condition for the 1.0 M and 0.9 M samples, but not the others, and is indicated in the acidic sequence by underlining the residues. The pK_a values for each residue and the change in charge taking place as the pH is raised above the pK_a are shown in Table 3-2.

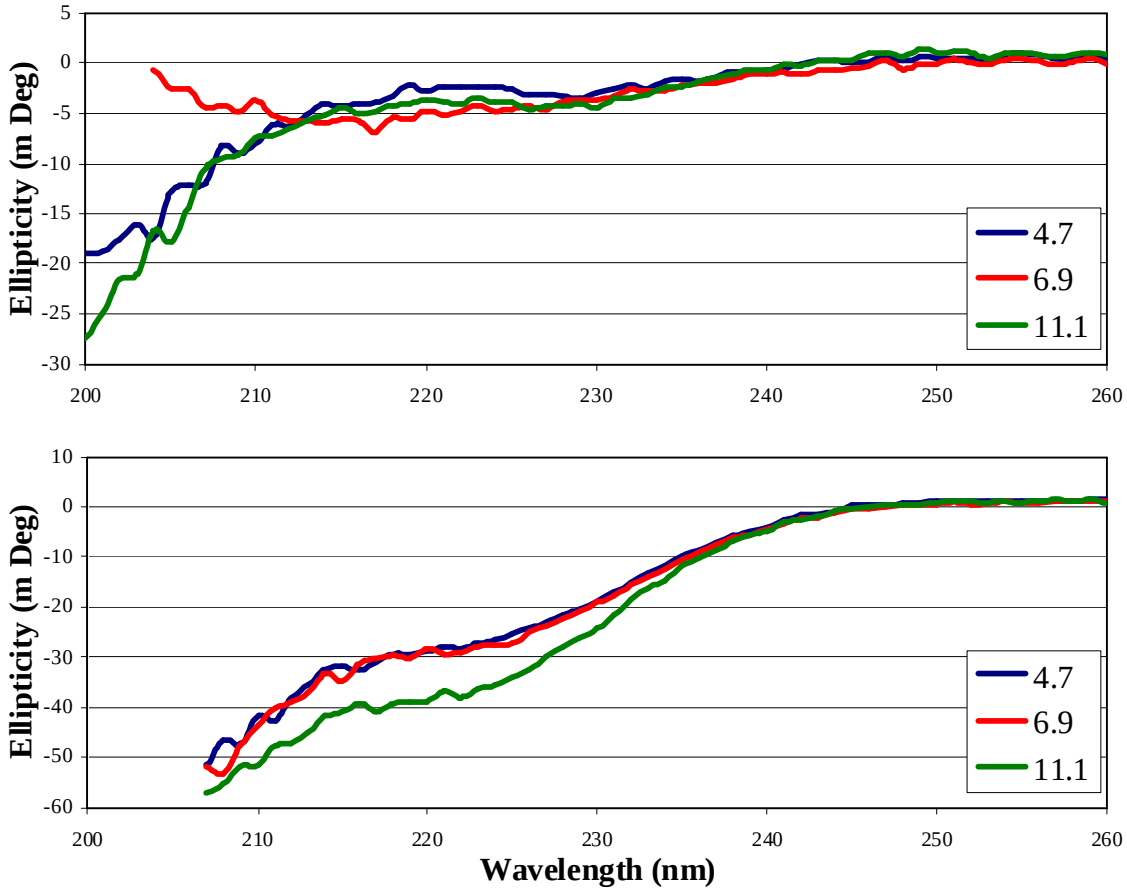

Figure 3-18. Comparison of pH dependence of solution to xerogel encapsulated Aβ in 9.0 mM and 10.0 mM KPhos solution, respectively. Xerogel samples became noisy below 205 nm.

Acid (Total Charges = -6+6 = 0)

1 10 20 30 40

+ D^- A E^- F R^+ H^+ D^- S G Y E^- V H^+ H^+ Q K^+ L V F F A E^- D^- V G S N K^+ G A I I G L M V G G V V -

Neutral (Total Charges = -6+3 = -3)

1 10 20 30 40

+ D^- A E^- F R^+ H D^- S G Y E^- V H H Q K^+ L V F F A E^- D^- V G S N K^+ G A I I G L M V G G V V -

Basic (Total Charges = -7+1-1 = -7)

1 10 20 30 40

D^- A E^- F R^+ H D^- S G Y^- E^- V H H Q K L V F F A E^- D^- V G S N K G A I I G L M V G G V V -

Table 3-2. Aβ Side Chain pK_a Values and Number of Corresponding Residues.

Amino Acid	Side chain pK_a	Number of Residues	Change in Charge
Asp	3.9	3	0 --> -1
Glu	4.3	3	0 --> -1
His	6.0	3	+1 --> 0
Tyr	10.1	1	0 --> -1
Lys	10.5	2	+1 --> 0
Arg	12.5	1	+1 --> 0

Change in Charge indicates the change taking place as the pH is increased above the pK_a value. pK_a values from [4].

The change in overall charge may explain why the samples at the higher pH showed increased solubility. The total charge of the peptide would create a repulsive effect, preventing aggregation. In addition, the peptide itself would have felt an intramolecular net repulsion between residues 1 to 23, since all the charged residues exist within this region. Therefore, any secondary structure formation should be driven by the high concentration of PO_4^{3-}.

At neutral and acidic pH values, it can be seen that the positive and negative charges are interspersed along the peptide's backbone, reducing any repulsive effect. This would have favored aggregation, as was seen in the 0.9 M sample, by allowing for more random intramolecular, and possibly intermolecular, electrostatic interactions. In addition, at these pH values the number of uncharged residues was reduced, thereby reducing the hydrophobic driving force behind folding. Therefore, it is highly probable that the diffraction-related spectrum was the result of large aggregated peptides, and the random coil spectrum is that of monomers and possibly small oligomers.

Following encapsulation, all samples except the 1.00 M KPhos and all pH 11 samples, showed mainly random coil character similar to the non-aggregated samples in solution, but with slightly more helical structure. Neutral and acidic samples were essentially the same in all cases, with the basic samples returning stronger signals. This similarity to the solution spectra could indicate that the peptide had not been adsorbed to the silica surface and that the structures of the monomeric peptides were similar in both cases. Furthermore, since none of the samples had a net positive charge, attracting the peptide to the negatively charged SiO^-, adsorption was not likely. The increased helical structure can be explained by excluded volume effects, favoring a more collapsed fold. This increase in helical structure was most pronounced in the basic pH samples where folding was driven by the hydrophobic effect, and it may be that the hydrophobic regions were forming a tight coil.

3.3.3. Comparison of PolyQ and Aβ Spectra

Solution and xerogel spectra for both polyQ and Aβ showed an increase in secondary structure as KPhos concentration was increased at near neutral pH, with the exception being that the 10.0 mM/9.0 mM → 50.0 mM/45.0 mM transition was negligible in some cases (Figures 3-8 and 3-14). This increase is in agreement with the Hofmeister Series and with the structure-stabilizing properties of the phosphate ion. At the high pH used in these experiments, the phosphate ion would have largely been in the PO_4^{3-} state, which is a strong kosmotrope that enhances peptide stability, while at low pH the phosphate ion would have largely been in the $H_2PO_4^{1-}$ state, which is a weak

kosmotrope. At high pH, both polyQ and Aβ had a net negative charge that would have caused a repulsive force, preventing intermolecular peptide aggregation (Section 3.3.2.3 for Aβ). Under the conditions of this work, polyglutamine with the flanking lysines and aspartates would have had no net charge until above pH 10.5 where it had a net negative charge at the N-terminus, due to the two aspartates. Therefore, at high pH both peptides had a net negative charge, but while Aβ contained hydrophobic residues to drive folding, polyQ contained only hydrophilic residues at this pH [109, 110]. As discussed in Section 3.3.2.3, Aβ took on more intermittent charge distributions and had more charged residues at the lower pH values that may have dominated the folding process. Since these residues should have interacted more favorably with the solvent, tight packing of the residues, or the hydrophobic effect, would not have been the dominant driving force for folding. On the contrary, polyQ's termini became oppositely charged, favoring both intermolecular and intramolecular attraction. Also, it was found by Sereda and coworkers [110] when studying protein binding as a function of the hydrophobicity of the environment that glutamine became less hydrophilic and more neutral as the pH was decreased. This neutrality should have allowed polyQ to fold into a monomeric coil, which could explain the increased helical structure upon encapsulation, or to have formed small soluble oligomers in solution, which may have remained largely unstructured since the glutamine side chain was both bulky and neutral. This bulkiness would have driven the coiling in the monomeric form due to the steric constraints of the alternating side chains that include nonpolar $–CH_2–CH_2–$ groups at the base, and this may have driven tighter coiling.

The difference in the amino acid content explains the difference in the two peptides' structural dependence on KPhos concentration and pH. Comparing each peptide only to itself, Aβ showed an increase in structure at high pH and an increased stability, while polyQ showed a decrease in structure. In addition, in all cases, save the Aβ 45/50 mM KPhos pH 4.5 spectra, there was an increase in secondary structure in xerogel samples. As previously stated, the glass added two factors that may cause this increase: excluded volume effects and the F_3-propyl glass modifier. These effects act independently of one another and so should be thermodynamically addressable by separate routes, meaning the use of different solutes or surface modifiers could be used to control these effects independently. As an example, overlapping effects are apparent at the higher HFIP concentrations where the influence of the F_3-propyl modifier became less obvious as compared to solution.

3.4. Stability of Solubilized Peptides in Solutions vs. Time

To check the solubilized peptides' resistance to aggregation in the various solvents, spectra were taken over a period of 504 h, or 21 days. Signal intensities at 205 nm, 217 nm, and 222 nm were plotted separately as a function of time. Plotting ellipticity at these wavelengths allows secondary structure to be evaluated, providing insight into which structures were resistant or most prone to aggregate: 205 nm is indicative of random structure, 217 nm of beta, and 222 nm of helical. A complete loss in all three signals would indicate aggregation and loss of protein (precipitation).

3.4.1. Soluble PolyQ Peptide

3.4.1.1. HFIP Solutions

All three wavelengths at each HFIP concentration can be seen for polyQ in Figure 3-19. The complete profile (full spectra) for these samples at 24 h can be seen in Figure 3-7 (top), and the 0% spectrum can be seen in Figure 4-6. Figure 3-20 (top) gives the full spectra for the 0% HFIP sample over a period of 1008 h, which was the only solution that returned a positive 205 nm ellipticity at 504 h. The bottom panel of Figure 3-20 gives the 1% sample over a period of 504 h. The only difference between the 1% and 5% samples in time was that the 5% had a more intense signal. The spectra taken at 1 h indicate random coil structures and all slowly lost intensity at 205 nm over time. The 0% spectra slowly folded to a curve indicating beta structure at 504 h, and it can be seen that there was a loss of intensity at 1008 h, indicating aggregation.

An isodichroic point can be seen in Figure 3-20, which indicates a two state folding transition between random coil and possibly beta sheet secondary structures. This isodichroic point suggests that both the 1% and 5% samples may have followed the same trend, though analysis at 1008 h returned a flat-zero spectrum for both low percents HFIP. It is possible that this weak beta spectrum was that of small soluble pre-fibril aggregates, consistent with the fact that the 504 and 1008 h spectra appear to be centered near 217 nm.

Comparing all three wavelengths, it can be seen that 10% and 25% HFIP solutions returned ellipticity values that parallel each other in terms of signal loss at each data point. This tendency would indicate a slow rate of aggregation, which is consistent

with theory since these samples had more helical structure than the others (seen in Figure 3-7). Therefore, polyQ became more aggregation resistant with increasing helical structure.

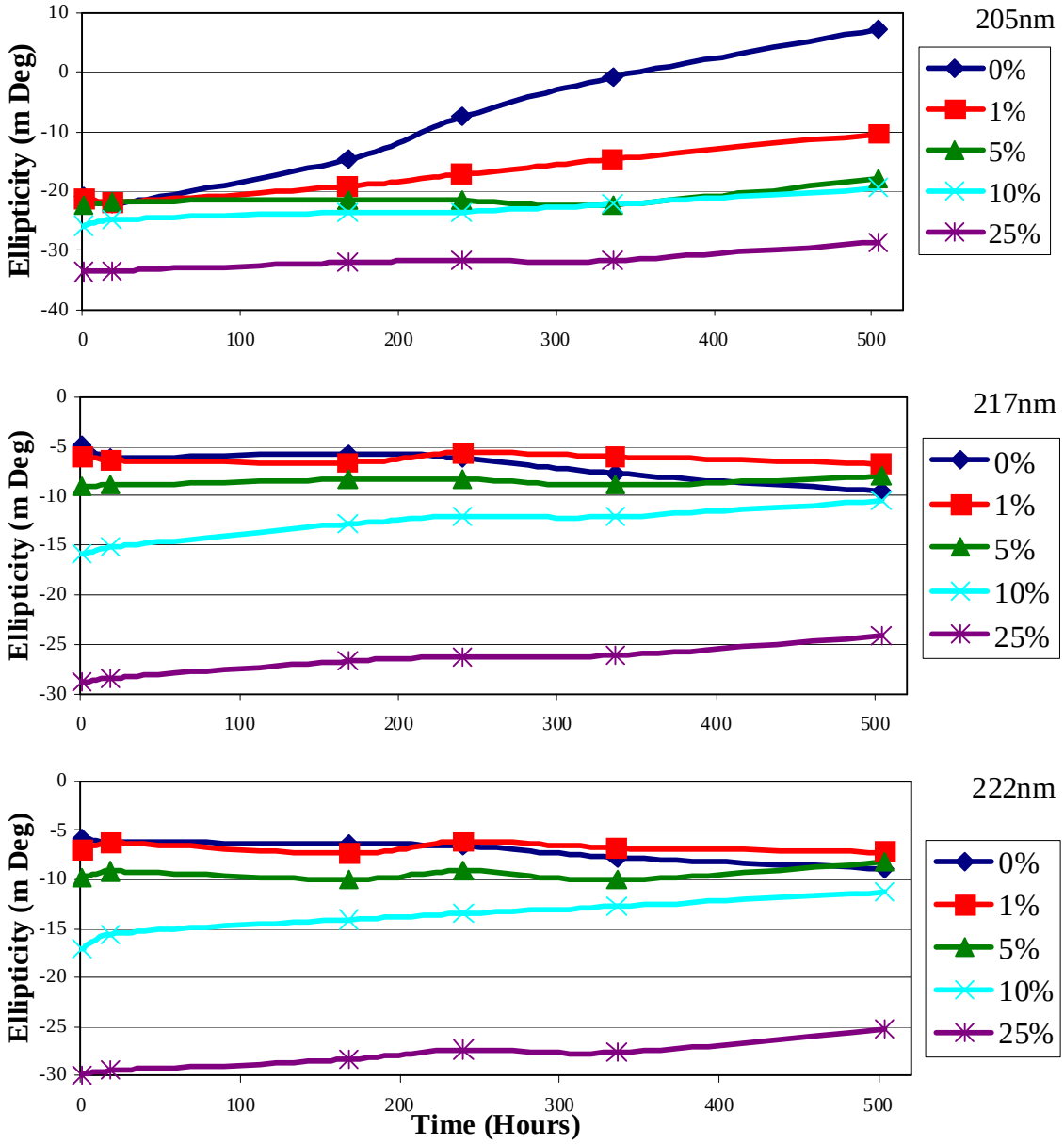

Figure 3-19. Stability of soluble polyQ in %HFIP H_2O at 205 nm, 217 nm, and 222 nm.

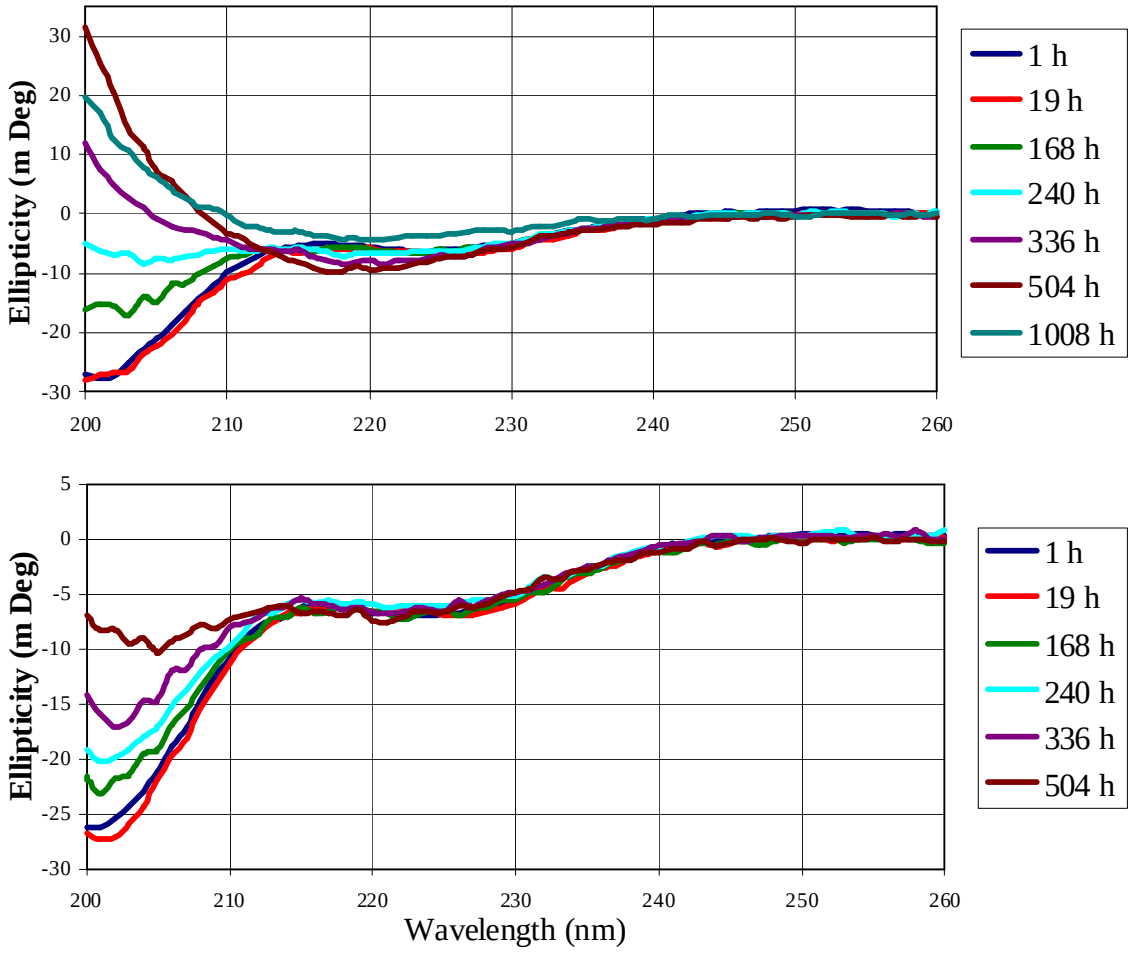

Figure 3-20. Structural stability of soluble polyQ in water and 1% HFIP. Top (water) and bottom (HFIP). Note the isodichroic point near 213 nm indicating a two-state folding transition between random coil and a possible beta sheet or aggregate structure.

3.4.1.2. Effects of KPhos Concentration

The time dependence for the structures analyzed at 205 nm for soluble polyQ in 0.90 M, 45.0 mM, and 9.0 mM KPhos can be seen in Figure 4-21 (Figure 3-8 for full spectra after 24 h in solution). All solutions gave random coil spectra with some helical content and retained their general shape as their signals weakened in time. All solutions had a visible precipitant at the time they gave a flat-zero spectrum. The 0.90 M solution

gave a weak, positive, and noisy signal at the 504 h data point, which was probably due to contamination; at 336 h very little of this sample was left, so the contents of the quartz cuvette was returned to the 3 ml centrifuge tube after the spectrum was taken. The sample contained a visible precipitant at 504 h that was similar to the other two samples and resembled loose cotton fibers.

The HFIP stability support the statement in Section 3.4.1.1 that polyQ became more aggregation resistant with increasing helical structure. Furthermore, this statement is in agreement with current theory on polyQ repeat diseases. The length of the repeat is associated with the extent of destabilization, or random structure, in the affected peptide and with the rate of aggregation. Here, and in the previous section, it has been shown that the more random the structure, the higher the rate of signal loss due to aggregation. Non-pathogenic huntingtin protein is an ordered peptide. In the pathogenic version, as the number of glutamine repeats increases, the protein becomes more destabilized and begins to take on more random coil structure, becoming more aggregate prone.

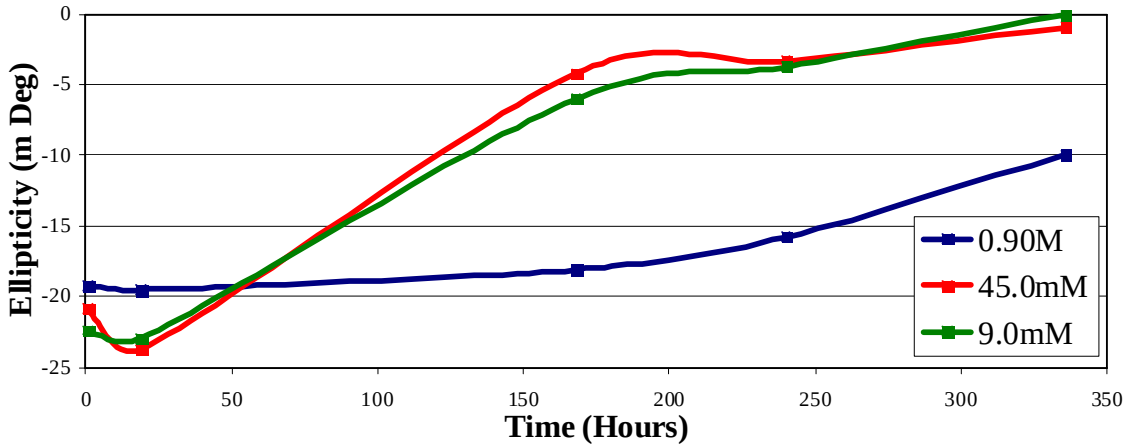

Figure 3-21. Stability of soluble polyQ in 0.90 M pH 6.8, 45.0 mM pH 6.9, and 9.0 mM pH 6.9 KPhos solutions, 205 nm signal intensity. Spectra were taken at 1, 19, 168, 240, and 336 h.

3.4.1.3. pH Dependence in KPhos Buffers

The pH dependence for polyQ in 0.90 M KPhos can be seen in Figure 3-22. The samples at pH 4.1 and 6.8 gave similar random coil spectra at the initial time point, as

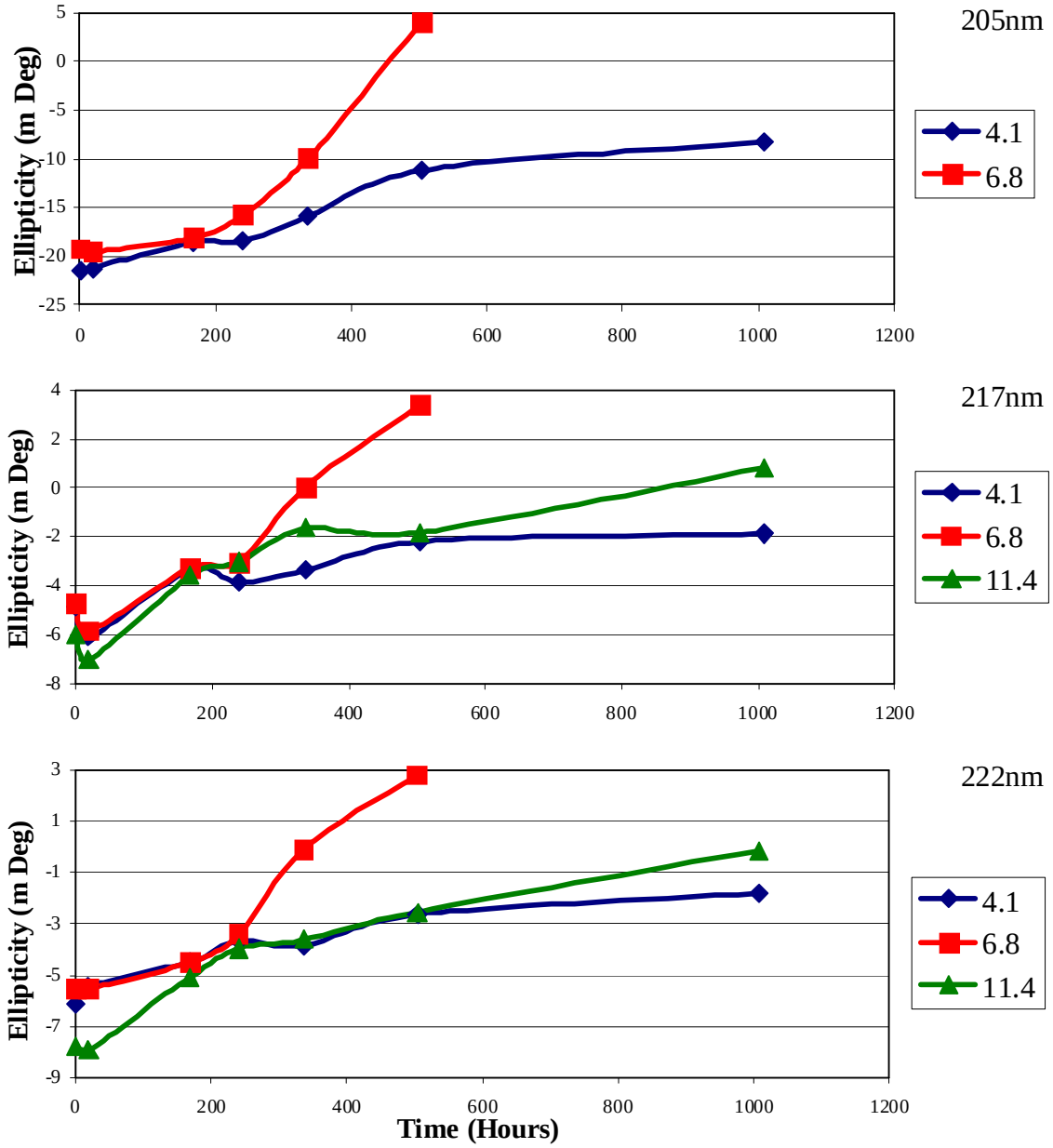

Figure 3-22. Stability of soluble polyQ in 0.90 M KPhos at pH 4.1, 6.8 and 11.4. Due to noise, the data for the 210 nm signal at pH 11.4 could not be obtained.

seen in Figure 3-9 (top). Signal loss occured fastest at pH 6.8 indicating that, of the samples, polyQ was most prone to aggregation at this pH. At 168 h, the samples at pH 4.1 contained aggregates upon visual inspection, but still had a weak minimum below 212 nm at 1008 h. A single minimum around 222 nm was seen in the pH 11.4 sample, but was too noisy below 212 nm to determine the structure. The signal slowly flattened to zero at 1008 h and upon visual inspection contained aggregates resembling a small amount of cotton fibers floating in the 3 ml tube. This pH extreme would have given the peptide a net negative charge due to the two aspartates, which might have created a repulsive force that slowed aggregation. At pH 4.1, as discussed in Section 3.3.3, the phosphate ion would have largely been in the $H_2PO_4^{1-}$ state, which is a weaker kosmotrope than HPO_4^{2-} or PO_4^{3-}. Previous studies, under different conditions as discussed in Section 1.6.1, had determined that the monomer had a random coil structure [93], and since there was a steady loss of signal at all wavelengths with no isodichroic point, interpretation under this condition was difficult.

Figure 3-23 shows similar data for polyQ in 45.0 mM KPhos. The spectra seen in Figure 3-10 (top) summarize the 24 h time point spectra for this KPhos concentration. All three pH values gave the same random coil spectra throughout the experiment without changing general shape, but flattening to zero in time. At this concentration the sample at pH 11.4 was the most resistant to aggregation, as seen by the intensity at 210 nm at 1008 h. At the lower concentration of 9.0 mM, the data again showed that the higher pH sample was the most aggregation resistant (Figure 3-24). As with the 45 mM samples, all three pH values gave the same random coil spectra (Figure 3-11 top)

throughout the experiment and slowly flattened to baseline. A slight difference was that the pH 4.5 sample flattened to zero at the last time point at this concentration, whereas it gave a weak signal in 0.9 M KPhos. Also, where the basic sample could not be

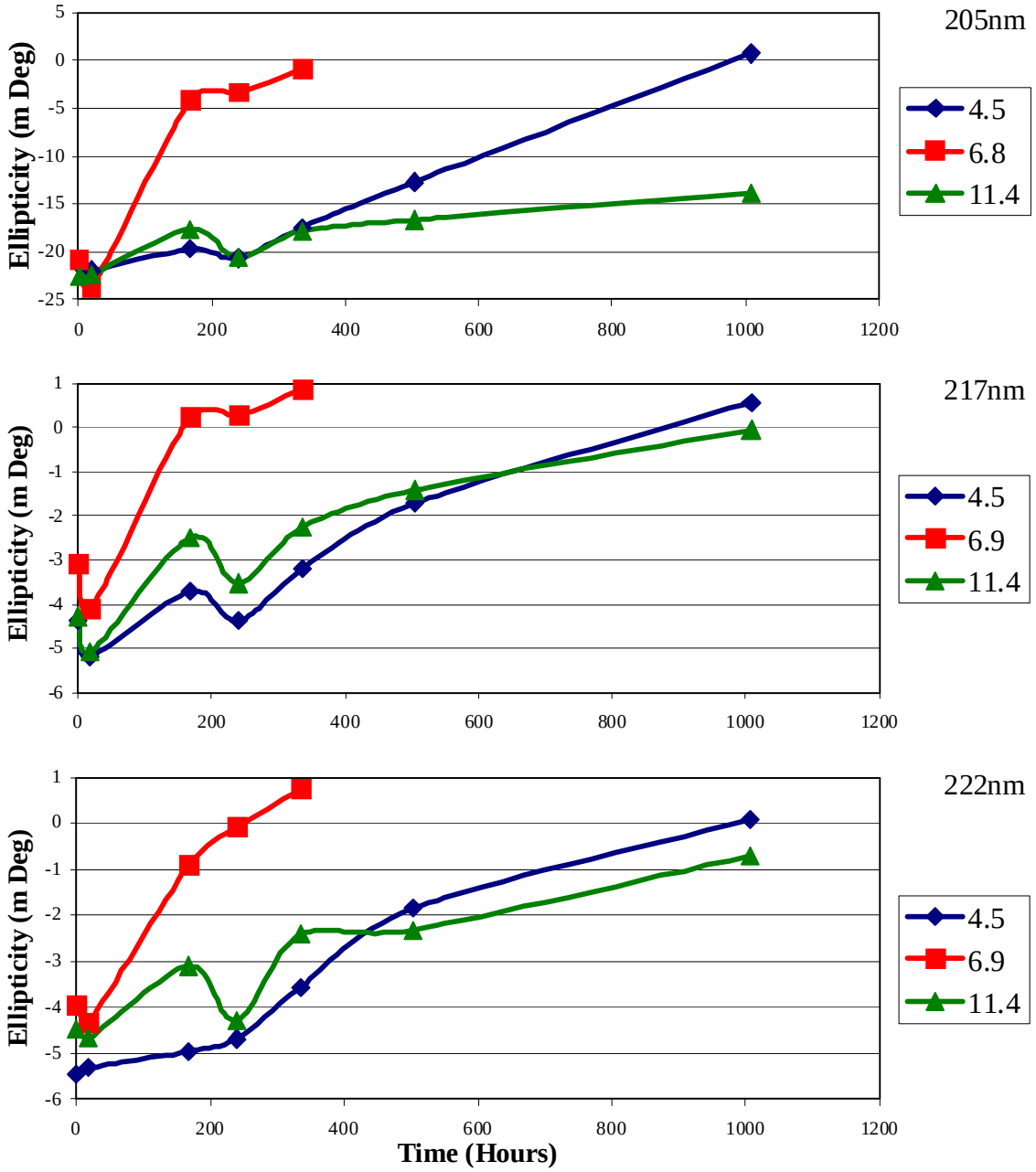

Figure 3-23. Stability of soluble polyQ in 45.0 mM KPhos at pH 4.5, 6.9 and 11.4.

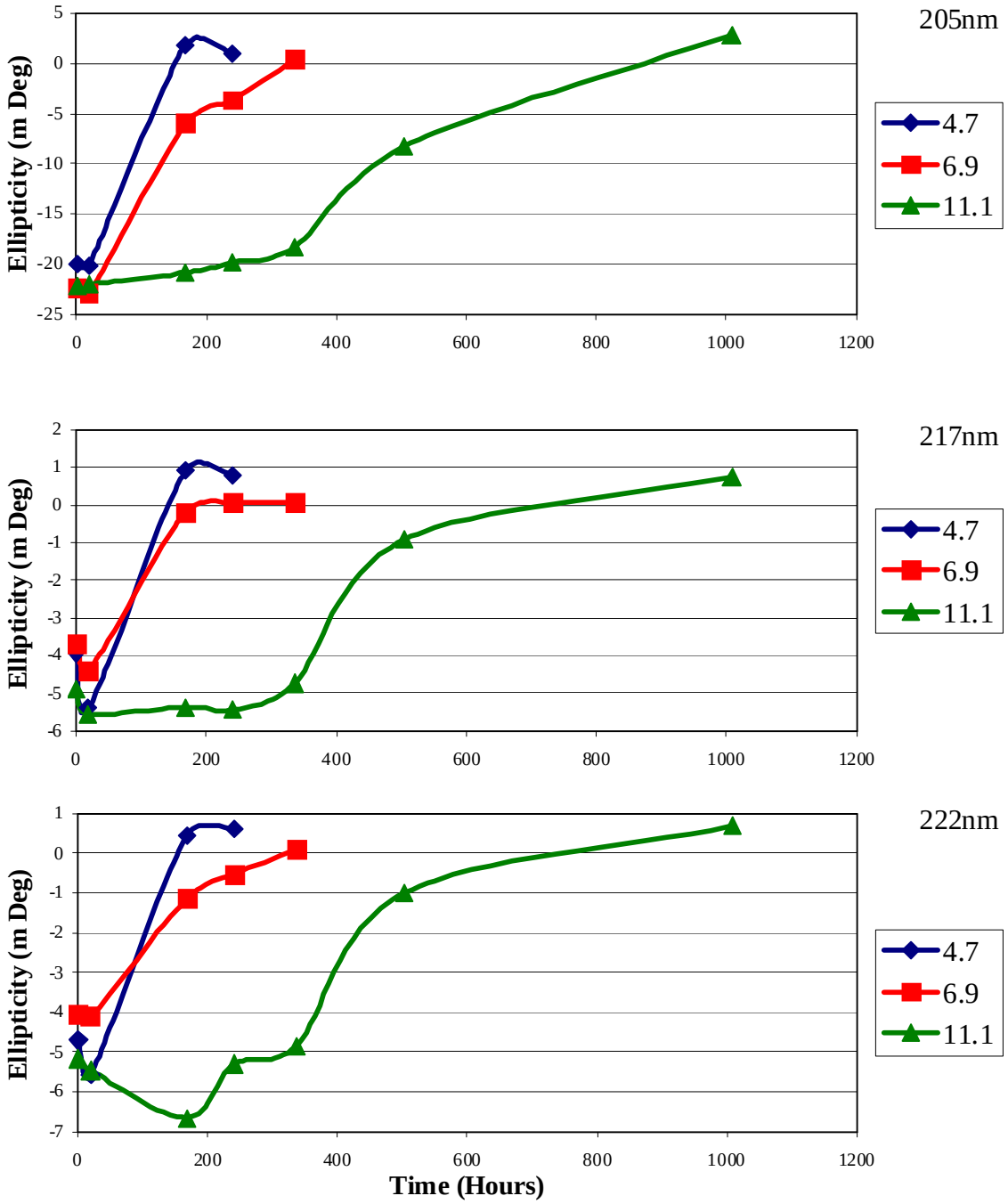

Figure 3-24. Stability of soluble polyQ in 9.0 mM KPhos at pH 4.1, 6.8 and 11.4.

interpreted at 205 nm, in 45.0 mM KPhos it gave the most stable signal intensity. Otherwise, these two samples, acidic and basic, closely paralleled each other's stability at 217 nm and 222 nm. As stated before, at high pH the [PO_4^{3-}] was prevalent, and it is expected to be a powerful kosmotrope that tends to increase peptide structural stability. This, with the fact that the peptide would have had a net repulsive charge, explains the increased time stability of polyQ at all KPhos concentrations when at high pH. What cannot be explained by this data was the increased stability in time of the acidic samples over the neutral pH, especially since at neutral pH the [$H_2PO_4^{1-}$] should have shifted towards the more kosmotropic [HPO_4^{2-}].

3.4.2. Soluble Aβ Peptide

3.4.2.1. HFIP Solutions

Figure 3-25 shows the time dependent data for Aβ in HFIP solutions over a period of 3 weeks. The 24 h full-wavelength spectra can be seen in Figure 3-13 (top). All spectra retained their general shape throughout the experiment except for the 10% HFIP sample. The 10% HFIP sample had no sign of aggregation upon visual inspection at 504 h but instead depicted a change in secondary structure from a helical spectrum to a stable beta spectrum. The 10% HFIP slope began with random coil, 210 nm and 222 nm being the stronger signals, but folded to a typical beta spectrum with the 217 nm signal being the strongest. The full spectra for 1 and 504 h can be seen in Figure 3-30 in Section 3.5 where they are discussed further. After the formation of this beta spectrum the signals stabilized. The 0% sample (Figure 3-26 also) portrayed the least amount of

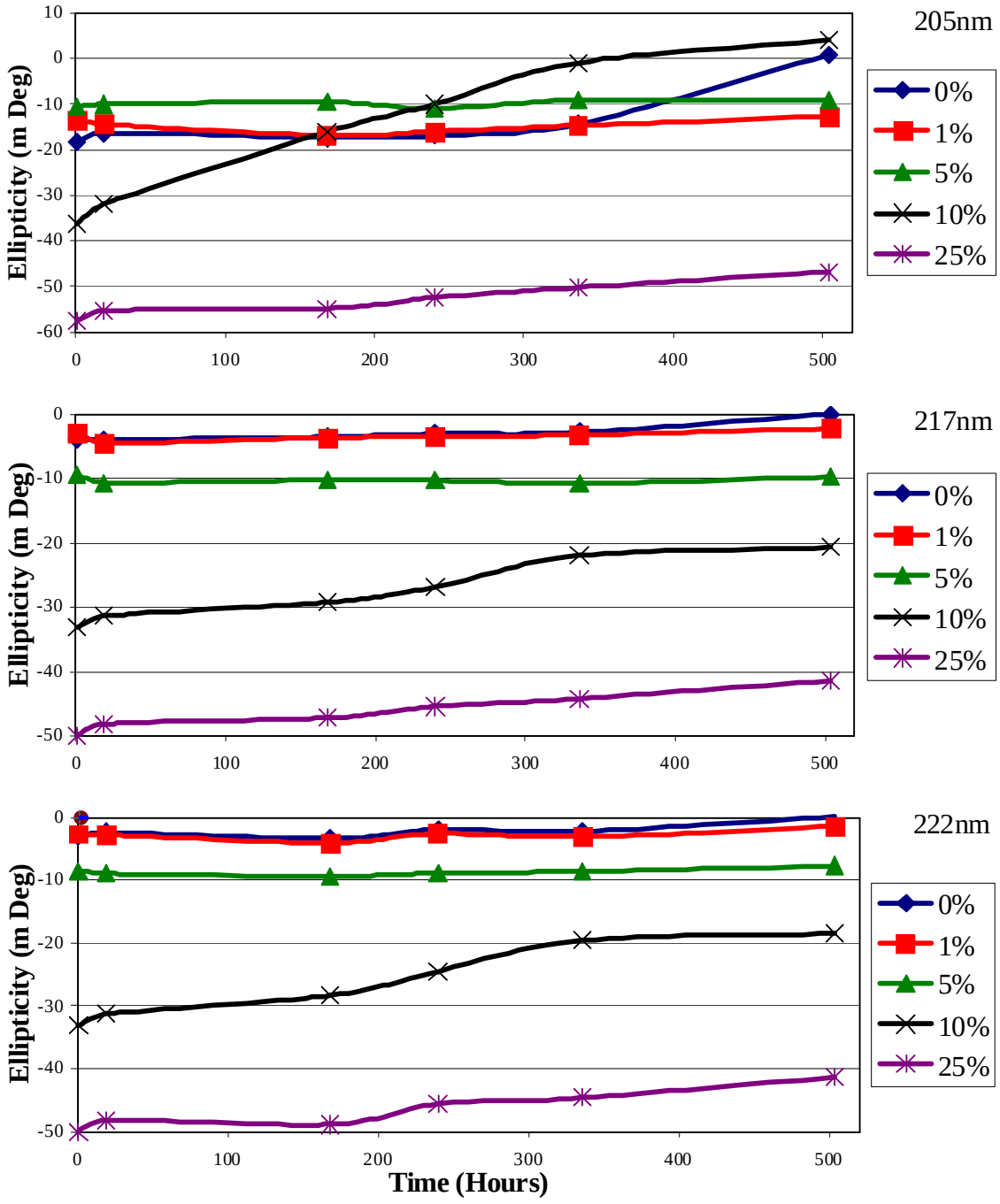

Figure 3-25. Stability of soluble Aβ in HFIP/water at 205 nm, 217 nm, and 222 nm.

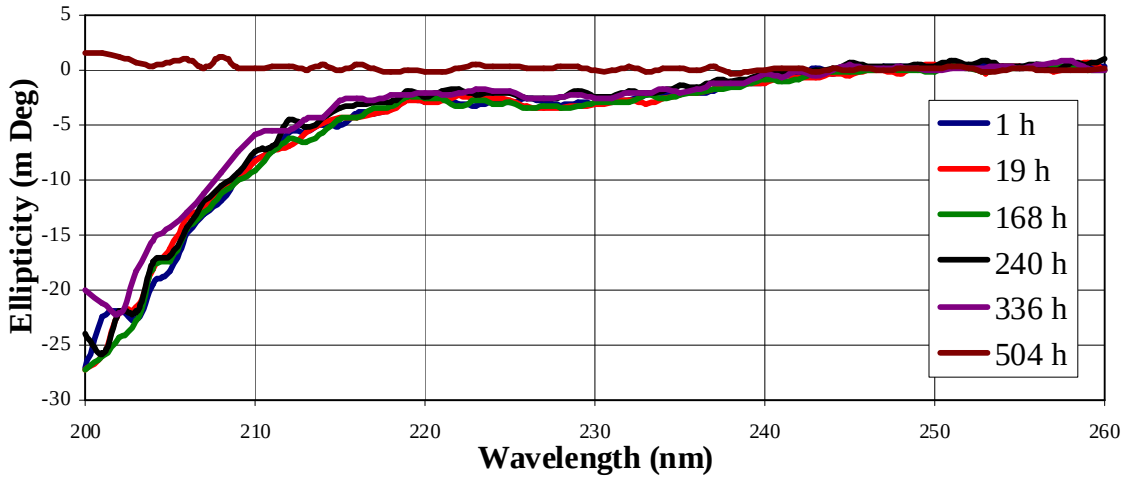

Figure 3-26. Aβ in pure water for 504 h (21 days).

secondary structure compared to the 1% sample, as indicated by the more intense 205 nm signal. This spectrum is typical for random coil and was the only sample to flatten to zero in the time of the experiment. The sudden loss of signal may be due to aggregation or proteolytic degradation. Except for the 10% HFIP sample, all other samples were stable with time.

3.4.2.2. Effects of KPhos Concentration

The Aβ peptide quickly aggregated out of solution in 0.90 M, 45.0 mM, and 9.0 mM KPhos solution at neutral pH. The ellipticity values at 205 nm, 217 nm, and 222 nm can be found in Figures 3-27 to 3-29 as a function of time. The 0.90 M signal reached the baseline in less than 19 h at pH 4.1 and 6.8 (Figure 3-27). The 45.0 mM and 9.0 mM samples gave flat-zero spectra in less than 7 days at similar pH values (Figures 3-28 and 3-29). The initial spectra obtained 1 h after diluting the resuspended peptide in buffer,

approximately 2 h after beginning the resuspension, can be seen in Figure 3-14. No changes in the general shapes of the spectra were observed.

3.4.2.3. pH Dependence in KPhos Buffers

Data for the pH dependence of soluble Aβ at each phosphate concentration is summarized in Figures 3-27, 3-28, and 3-29. The full spectra for the 0.90 M sample at 1 h can be seen in Figure 3-15, and the full spectra for the 24 h time point in 45.0 mM and 9.0 mM KPhos can be seen in Figures 3-17 and 3-18. In all cases, the samples near pH 4 and pH 7 aggregated out of solution well before the basic sample near pH 11.

The 0.90 M samples at pH 4.1 and 6.8 gave a single weak minimum above 220 nm with a positive signal below 210 nm at 1 h and contained aggregation upon visual inspection at 19 h. This rapid aggregation supports the previous proposal that these spectra are affected by diffraction of larger aggregates still in solution. The data here suggests that these red shifted spectra originate from samples containing these larger aggregates that are still forming. At the same concentration, the pH 11.4 sample gave a week minimum near 222 nm but was too noisy below 212 nm to gain any structural information. The shape of the discernible region of the spectrum did not change in the time period of the experiment. The stability of the sample at pH 11.4 indicated that it was least prone to aggregation, whereas the other two that started with a single weak signal above 220 nm were the most prone to aggregation (Figure 3-15).

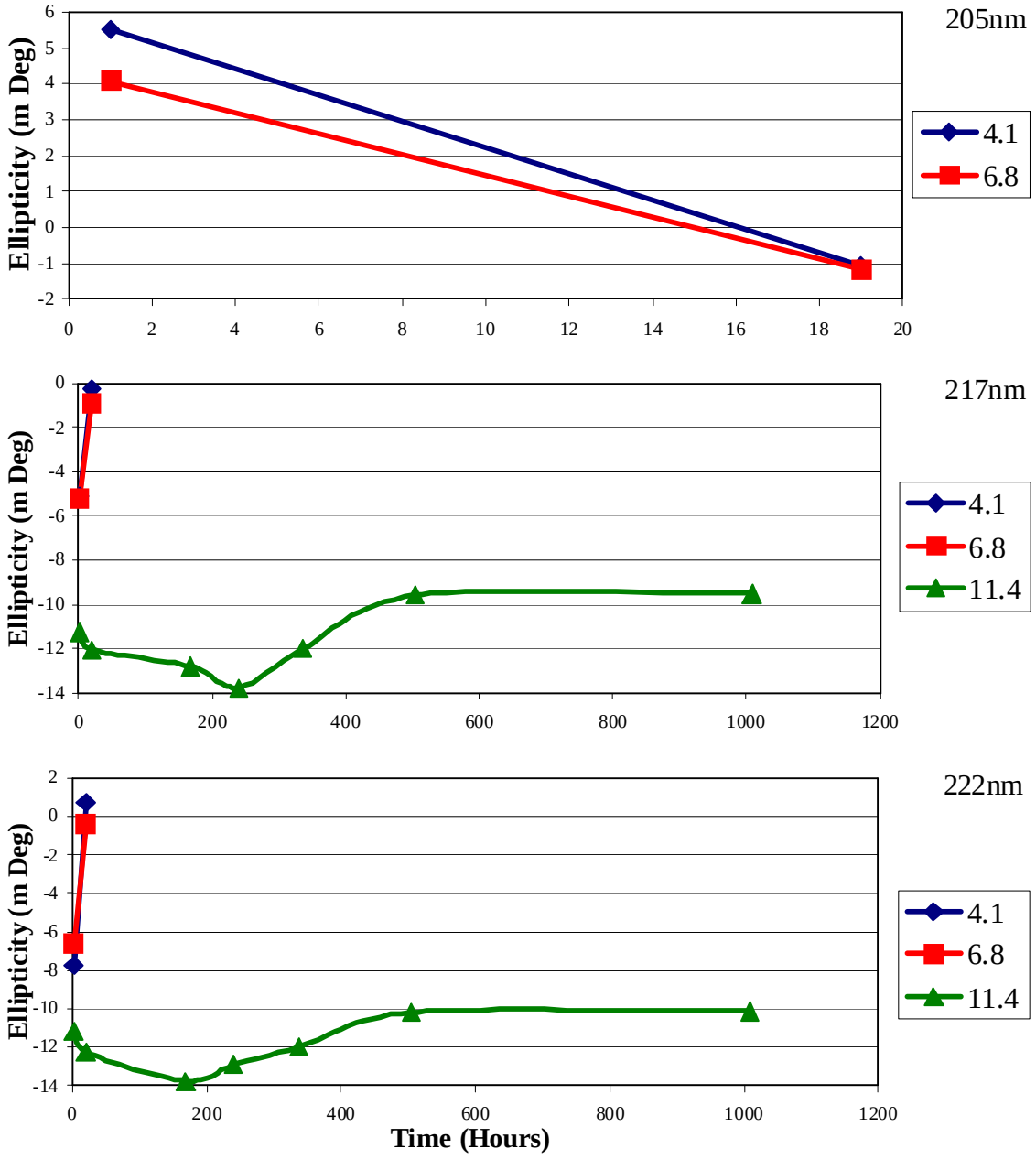

Figure 3-27. Stability of soluble Aβ in 0.90 M KPhos at pH 4.1, 6.8, and 11.4. The 205 nm spectra at top were analyzed to 19 h only.

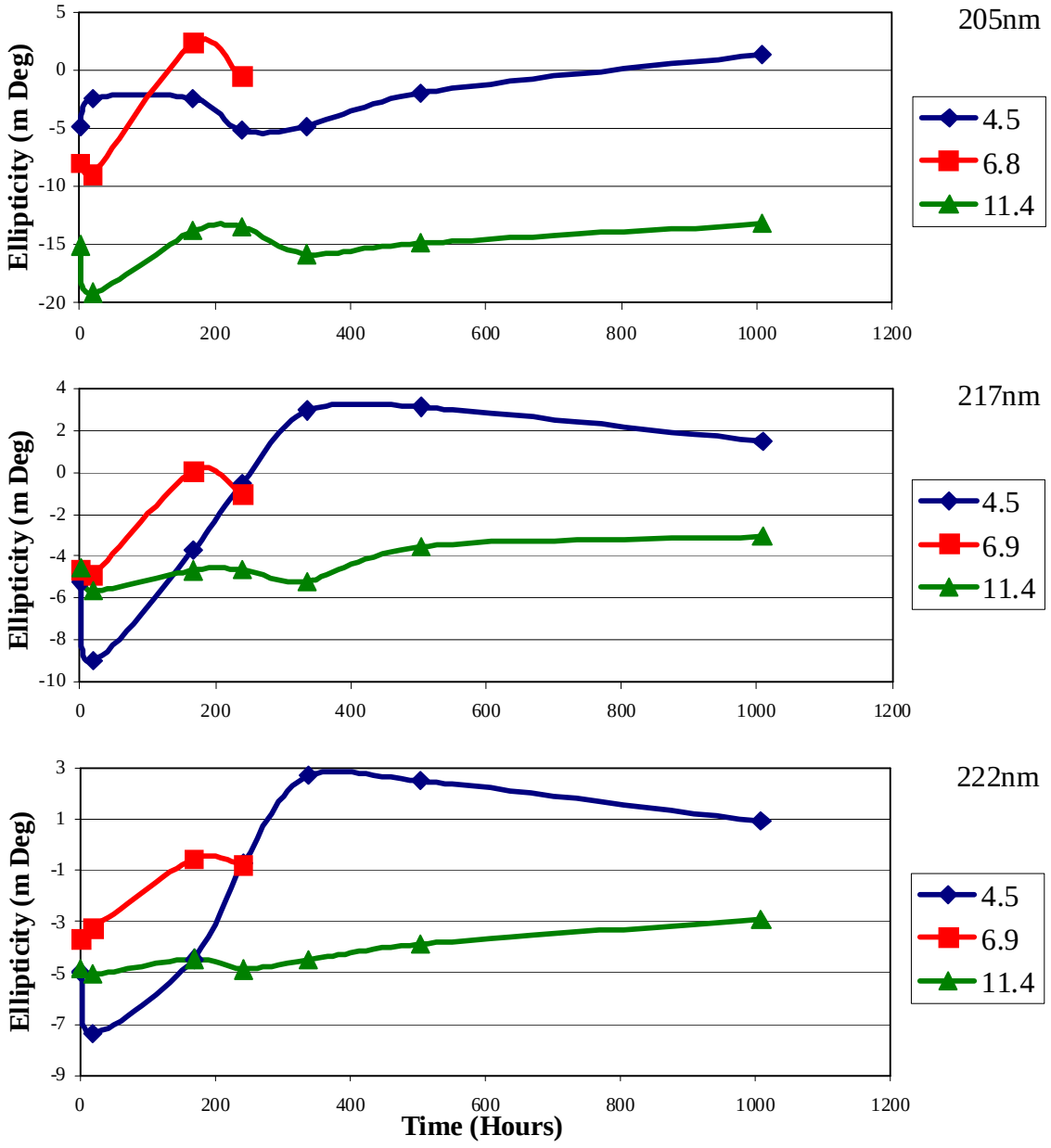

Figure 3-28. Stability of soluble Aβ in 45.0 mM KPhos at pH 4.5, 6.9, and 11.4.

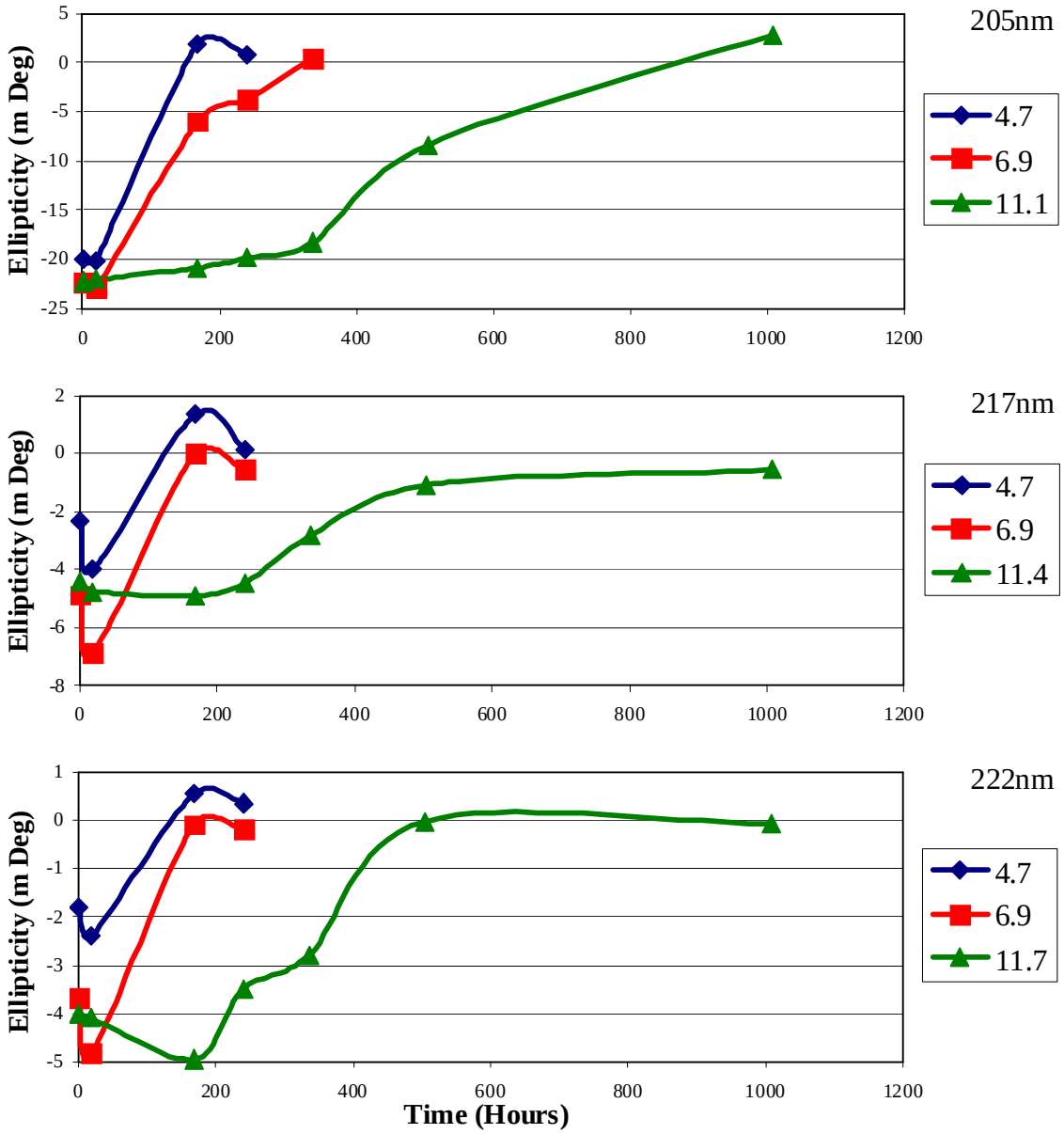

Figure 3-29. Stability of soluble Aβ in 9.0 mM KPhos at pH 4.5, 6.9, and 11.4.

In 45.0 mM KPhos, all Aβ samples gave similar random coil spectra at 1 h. At 19 h, the peptide at pH 4.5 gave a single weak minimum around 217 nm and at 168 h took on some random structure indicated by a loss of the 217 nm intensity signal and a completely negative signal below 236 nm. The 217 nm signal continued to weaken and eventually became positive after 240 h with a negative signal at 205 h. This change in spectra suggested that the peptide unfolded from a beta fold to a highly random coil fold before it aggregated out of solution. At 240 h, the pH 6.9 sample gave a flat-zero spectrum indicating aggregation. The two samples at the lower pH values developed a white film on the bottom of their centrifuge tube, most likely due to aggregation. The sample at pH 11.4 again proved to be most aggregation resistant, and this property was most likely due to a negative repulsive charge on the peptide at this pH that dominated over the hydrophobic driving force of peptide aggregation.

A random coil spectrum was observed for all samples in 9.0 mM KPhos at 1 h, and again the two samples at lower pH values quickly aggregated out of solution. This profile was retained throughout the experiment by all samples. Aggregation was observed in the pH 4.7 sample at 168 h. Again, the peptide sample at pH 11.7 showed the most resistance to aggregation. A conclusion drawn from all these spectra, and in agreement with theory, was that the peptide must be partially unfolded or adopt a random coil structure before aggregation. All samples with stable secondary structure appeared to have resisted aggregation and unfolded to a random coil structure before aggregating.

3.5. Soluble vs. Aggregated Peptide Spectra

In solution, solubilized Aβ initially yielded three different spectra depending on the solvent: random coil/molten globule, beta sheet, and an anomalous profile that yielded a minimum anywhere between 220 nm and 230 nm, likely due to diffraction. It was this third type of spectrum that is proposed to be the result of actively aggregating peptides and, therefore, that of a species whose solubility was decreasing. Spectra with red shifted minima tended to have spectra that flattened to zero faster than any other, indicating aggregation. The other two structure classifications showed increased stability with increasing secondary structure that can be measured by the 217 nm and 222 nm signal intensities. The increased strength of these signals, relative to the rest of the spectrum, returned increasingly stable spectra in time. Above, it was shown that Aβ in 10% HFIP solution initially gave a random coil spectrum that shifted to a species that yielded a stable beta sheet spectrum. Figure 3-30 shows a comparison of these two types of soluble (top) and aggregated (bottom) species. The spectra of aggregated Aβ species were taken from 0.90 M KPhos samples at pH 4.1 and 6.8. The samples were vortexed for 30 s to resuspend the fibers, and the spectra were immediately taken. Notice the similarity between these resuspended aggregates and the spectra shown in Figure 3-15 (top) for the same peptide sample before precipitation.

Looking at the stable/soluble spectra in Figure 3-30, it can be seen at 1 h (blue) that the 10% solution gave a helical structure profile but evolved into a stable beta structure (black) at 504 h. Once this beta structure formed with the characteristic minimum near 215 nm, the signal intensity began to stabilize as a function of time (see

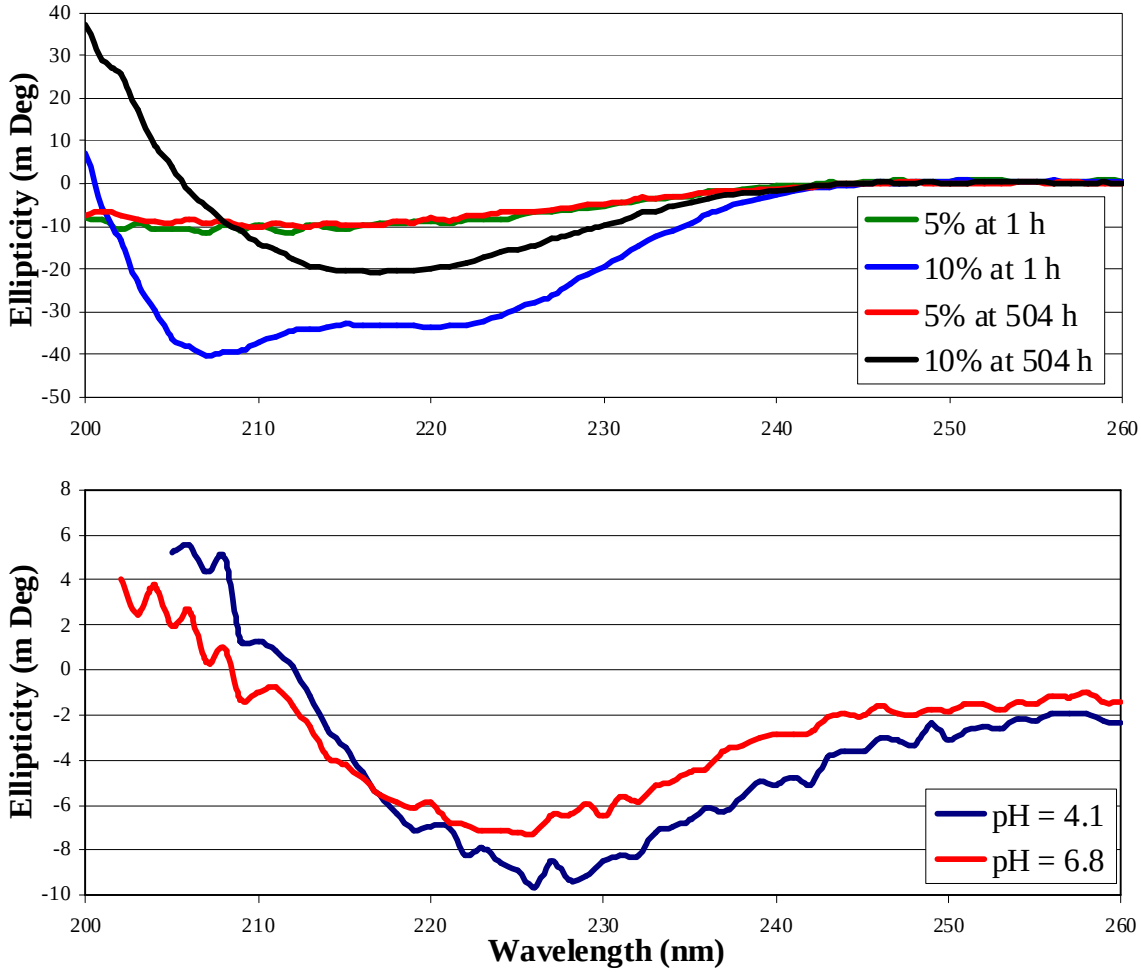

Figure 3-30. Analysis of soluble vs. aggregated species in solution. Top: Aβ in 5% and 10% HFIP solutions at 1 and 504 h. Bottom: Vortexed aggregates of Aβ in 0.90 M KPhos solution. Samples were vortexed for at least 30 s to resuspend the amyloid fibers, and the spectra were taken immediately.

Figure 3-25, 336 – 504 h). The sample at 5% HFIP (green and red) returned spectra that were both negative at 200 nm, which is characteristic of random coil structure. The inset in Figure 3-13 shows the spectrum for this sample after 1 day in solution. In this spectrum, there is a minimum near 210 nm that may indicate the peptide had begun to take on some secondary structure and would explain its resistance to aggregation. Both

aggregated spectra have a single minimum between 220 nm and 230 nm. Therefore, if a red shift in minima is observed in the other more typical spectra, this may indicate that aggregation is occurring.

3.6. Structural Changes of Encapsulated Peptides vs. Time

3.6.1. Encapsulated PolyQ

Encapsulated polyQ showed little change in structure as a function of time when it was stored in the same solution throughout the experiments. In the absence of leaching during solvent exchange, the spectra were relatively stable, and, because the peptide was only 15 glutamine residues, 19 amino acids in total, there was little driving force for the peptide to form any stable structure. The one observed change was in a partially prepared xerogel glass that was not allowed to shrink to completion; the final size was approximately 75% the total original volume. Over a period of 3 days, the sample changed from a helical spectrum to a single minimum near 220 nm (Figure 3-31). On the third day the sample had become visibly foggy, perhaps indicating a light diffraction problem. A comparison of the spectrum 3 days after to the solution spectrum in H_2O after 1008 h (inset) showed almost identical results. It's unlikely that large aggregates formed in the xerogel because: (1) even small aggregates would not easily diffuse through the xerogel matrix to form larger ones, and (2) thermodynamically, the peptides would not be driven to a central pore to form a large aggregate. Therefore, the changing spectra in Figure 3-31 arise from some other diffraction-related phenomenon, such as smaller highly ordered aggregates that are only a few peptides in size. Excluded volume

effects should favor a more compact state, and therefore, a tighter packing of the hydrophobic residues driving aggregation.

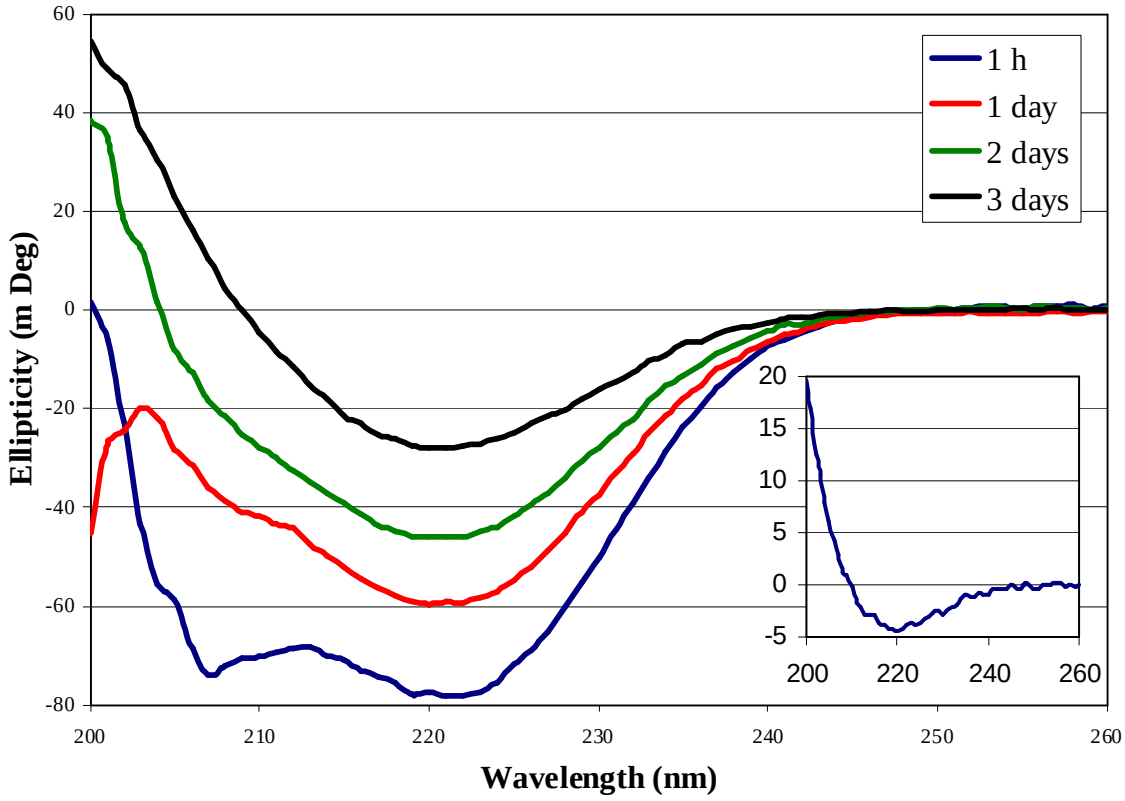

Figure 3-31. Aggregation of glass encapsulated polyQ. The partially dried glass was not allowed to shrink to completion which may have allowed the peptide to leach through the matrix and to form oligomers. The sample was kept at 25°C in 1.00 M KPhos. The glass was clear on the first day and slowly became foggy. Notice the evolution of a single minimum close to 220 nm. This is likely red shifted due to diffraction. Inset: Soluble polyQ in H_2O after 1008 h (Figure 3-20 top).

3.6.2. Encapsulated Aβ

Figure 3-32 shows spectra for the 25% HFIP sample at 1, 50 and 54 days. Here the sample initially gave a spectrum that appeared to contain both helical and beta structure. This can be seen by the rather uniform negative intensity between 207 nm and

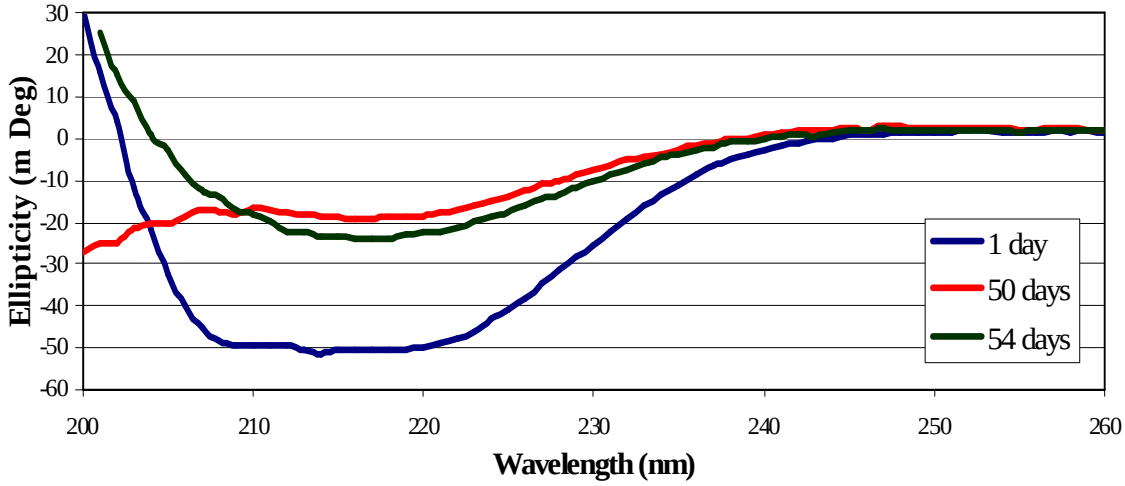

Figure 3-32. Xerogel encapsulated Aβ in 25% HFIP in H_2O (v/v) at 1, 50, and 54 days. At day 1 (blue) the spectra is that of a mixed beta and helical structure. On day 50 (red) the spectra is that of random coil indicating that the much of the secondary structure has been lost. An apparent beta spectrum with minimum at 217 nm is seen on day 54 (green).

222 nm. When the peptide unfolded at day 50, it retained some structure as seen by the signal near 217 nm. At day 54 a single minimum was observed near 217 nm that may indicate a significant amount of beta structure. This was also observed in the 10% HFIP solution, discussed in Section 3.5, and may indicate a semi-stable folding intermediate. Even if these results were due to evaporation of the HFIP, the negative signal at 200 nm in the day 50 spectrum was not observed at a HFIP concentration between those concentrations that returned similar spectra to the 1 and 54 days spectra (Figure 3-13). Since the HFIP concentration could not have increased between day 50 and 54 this data still suggests the presence of a folding intermediate.

3.7. Thermal Stability

3.7.1. Thermal Stability of Soluble Peptides

Temperature did not induce aggregation in any of the solution experiments, and all samples showed complete reversibility. Figure 3-33 shows the 222 nm signal for polyQ in H_2O upon heating. The change in ellipticity was negligible and most likely represented noise in the system. Without aggregation, the steady signal intensity was to be expected in a sample with random structure, such as this sample. Samples that started with increased secondary structure should have shown a change in signal intensity as a function of temperature, as was the case in Figure 3-34 for soluble polyQ in 25% HFIP. In the top panel, the 222 nm signal for heating and cooling can be seen, and in the bottom panel the full spectra for the starting sample at 25°C, at 75°C, and after returning to 25°C

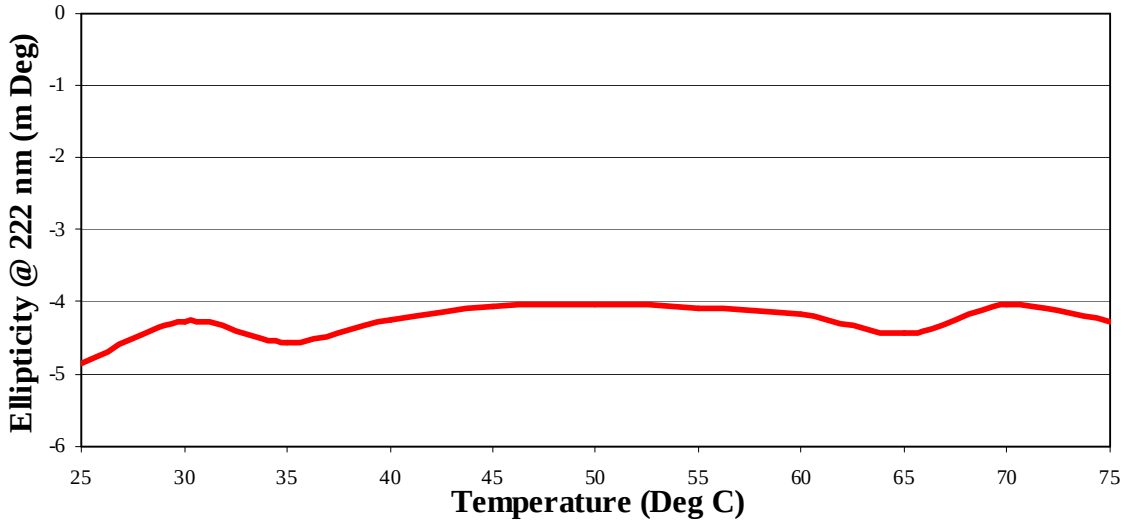

Figure 3-33. Thermal stability of polyQ in H_2O by tracking ellipticity at 222 nm. The background has not been subtracted. A temperature step of 5°C was used with an equilibration time of 30 s and 1 s averaging time. Data shown is for heating only. The initial solution structure is that seen in Figure 3-6. Since the structure was already random coil, heating had little effect, as indicated by the relatively flat line.

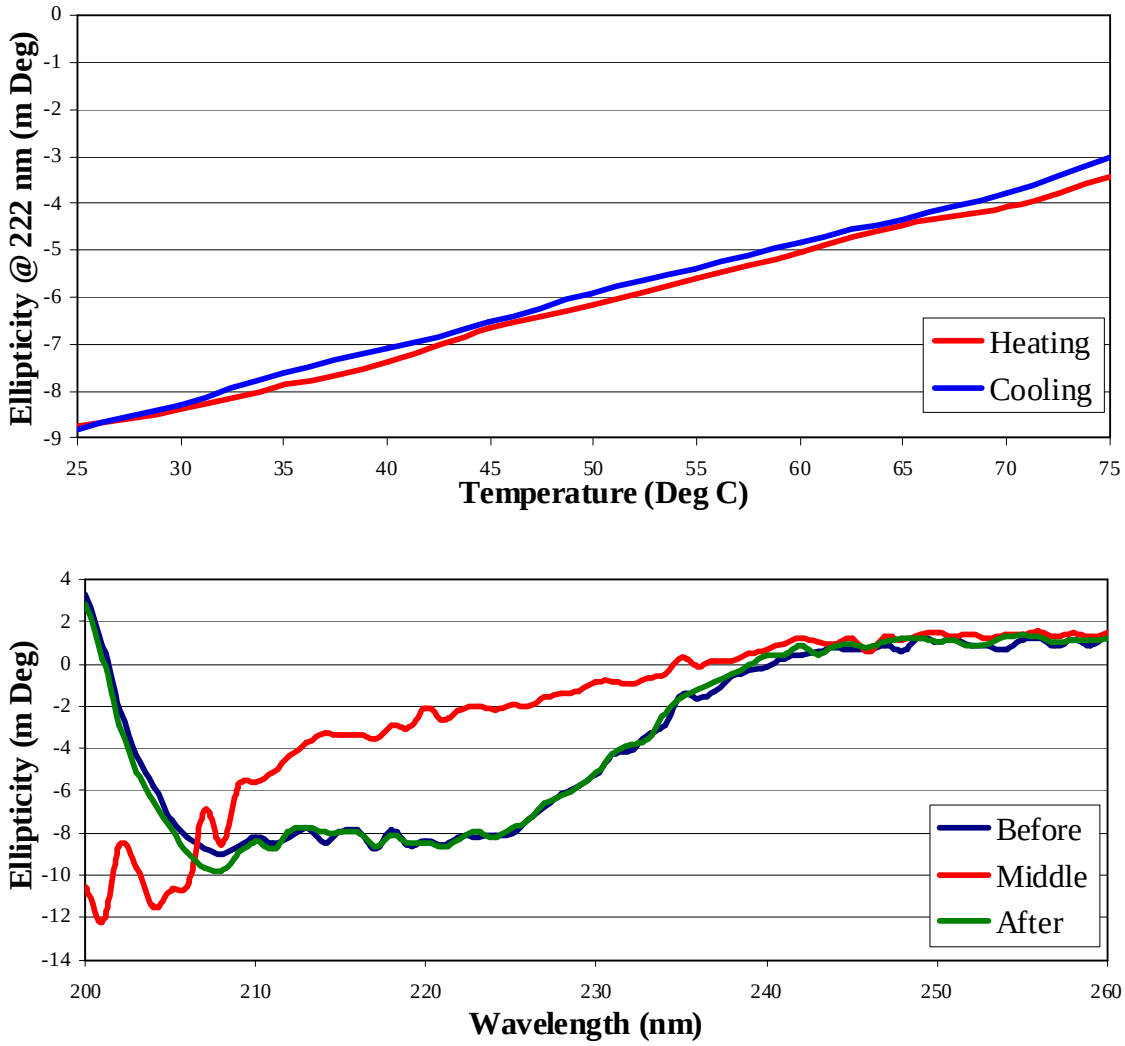

Figure 3-34. Thermal stability of soluble polyQ in 25% HFIP in H_2O (v/v). Top: 222 nm signal intensity as a function of temperature. Bottom: spectra at 25°C before heating (blue), at 75°C before cooling (red), and at 25°C after cooling (green). The background has not been subtracted for 222 nm signal intensity curves (top), but has been for the spectra (bottom). A temperature step of 5°C was used with an equilibration time of 15 s and 1 s averaging time. The solution was held at 75°C for 1 min between heating and cooling.

are displayed. Notice that, noise aside, the spectra were completely reversible and there was no evidence of aggregation. Figure 3-35 shows the result for Aβ under the same

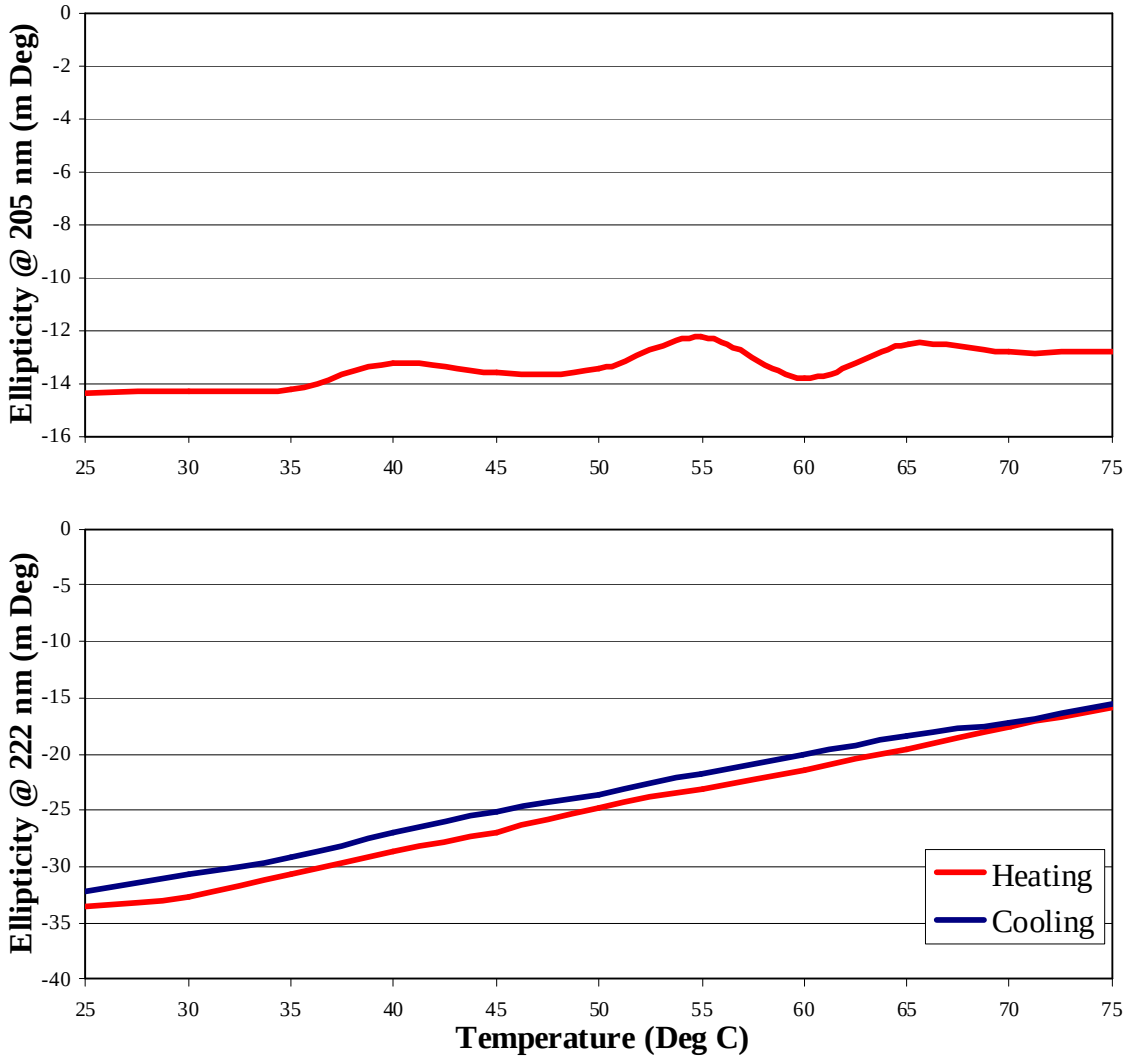

Figure 3-35. Thermal stability of soluble Aβ in H_2O and 25% HFIP 222 nm signal intensities. Top (H_2O) and bottom (HFIP). The background has not been subtracted. A temperature step of 5°C was used with an equilibration time of 30 s and 1 s averaging time. Data for the sample in water (top) is for heating only. The 25% HFIP sample was held at 75°C for 5 min between heating and cooling. The initial solution structures are those seen in Figure 3-12 and 3-13. Since the sample's structure in water was already random coil, heating had little effect, as indicated by the relatively flat line. The 25% HFIP sample shows a reversible process.

conditions as those for polyQ that returned very similar results (Figure 3-12 and 3-13 for the full spectra at 24 h).

These results were to be expected in the random coil spectra since the peptide was already mostly disordered. Samples showing secondary structure were expected to aggregate upon cooling since they would be partially disordered along this path. This lack of aggregation would indicate that the helical random coil structure with strong 222 nm and 205 nm signals were largely molten globule with some helical structure. A similar experiment was not performed on a sample showing beta character, but it would be interesting to see if the results were similar. It is possible the peptide would aggregate out of solution upon partial unfolding (slow heating) when the hydrophobic beta core is exposed, should the HFIP not help to stabilize the structure. Upon cooling after unfolding, the peptide may return a molten globule spectrum.

3.7.2. Thermal Stability of Encapsulated Peptides

In general, all structural changes that took place during thermal experiments were reversible. A slight loss of signal sometimes occurred that was most likely due to leaching of the peptides through the xerogel matrix at elevated temperatures. Leaching at room temperature was shown in Figures 3-4 and 3-5, where it was demonstrated that leaching was reduced in xerogels relative to wet-aged glasses. Figure 3-36 summarizes the data for polyQ in H_2O at temperatures both above and below 25°C. In both cases, when the temperature was returned to 25°C, the original spectrum was largely recovered.

In samples that showed highly disordered spectra, as that shown in Figure 3-37 for encapsulated Aβ in H_2O, the 222 nm value did not change as a function of temperature. This 222 nm stability implies that the spectrum was of a molten globule or

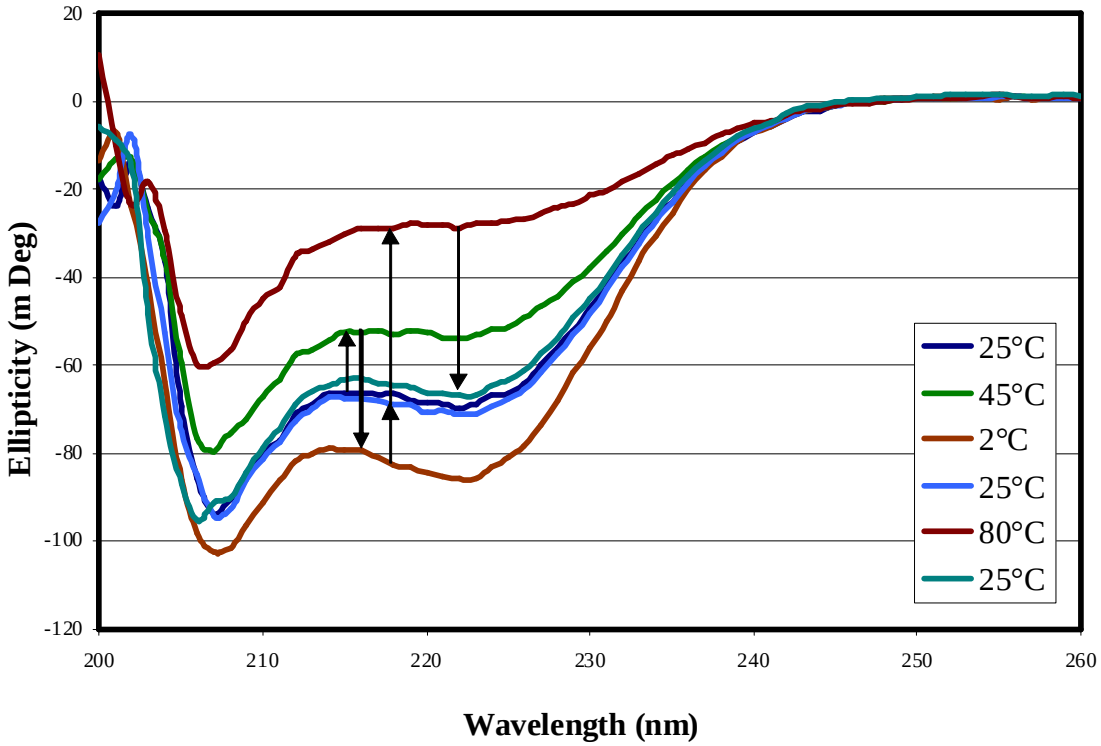

Figure 3-36. Xerogel encapsulated polyQ in H_2O gives a reversible secondary structure at high and low temperatures. The temperature was varied as indicated by the arrows from left to right, indicated by the key, beginning at the top and moving successively downward. Each spectra was taken when the ellipticity at 222 nm stabilized, approximately 2 to 5 min after the indicated temperature was reached.

of an irreversibly adsorbed protein. Only one other structure demonstrated similar thermal stability after encapsulation, the beta structure of Aβ peptide after 2 months. Figures 3-38 and 3-39 show these beta spectra at several temperatures and demonstrate the stability of the structure. Figure 3-38 shows the spectra for the sample in 25% HFIP after 54 days at the indicated temperatures. The spectral shape indicate that there was probably some random coil structure because of the spread of the signal between 210 nm and 222 nm, but over the temperature range of the experiment there was little change in

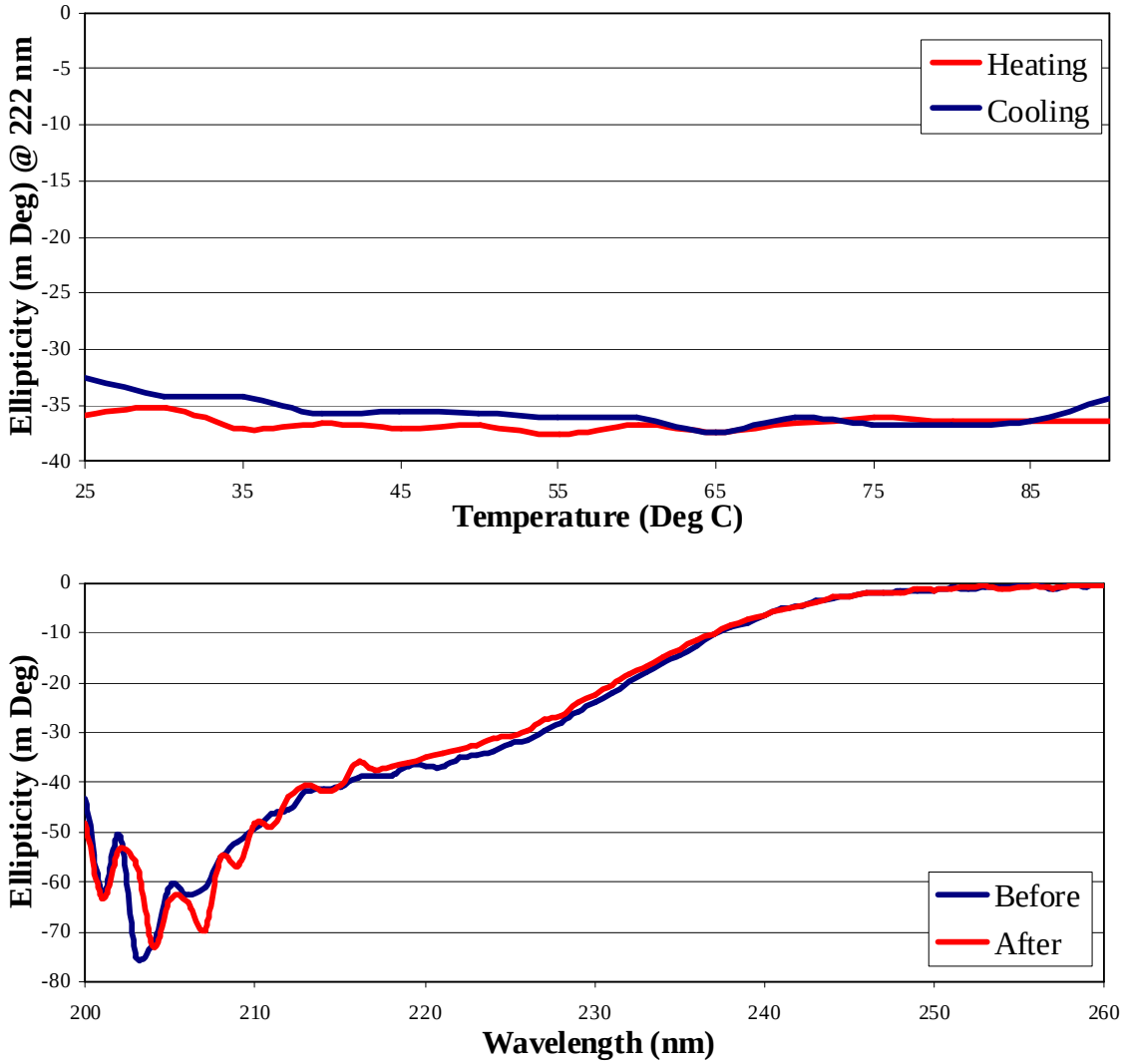

Figure 3-37. Xerogel encapsulated Aβ in H_2O as a function of temperature. Top: The 222 nm signal intensity as a function of temperature. Bottom: Spectra at 25°C before (blue) and after (red) heating and cooling. The sample was stored in a 3 ml cuvet at 25°C for 24 h.

the intensities of this region. Unfortunately, the experiment was interrupted by a sudden drop in the pressure of the gas used to cool the lamp in the CD instrument, and a larger range of temperatures could not be explored. Figure 3-39 shows the sample in water after 54 days at the indicated temperatures. There were three possibilities for the stability of

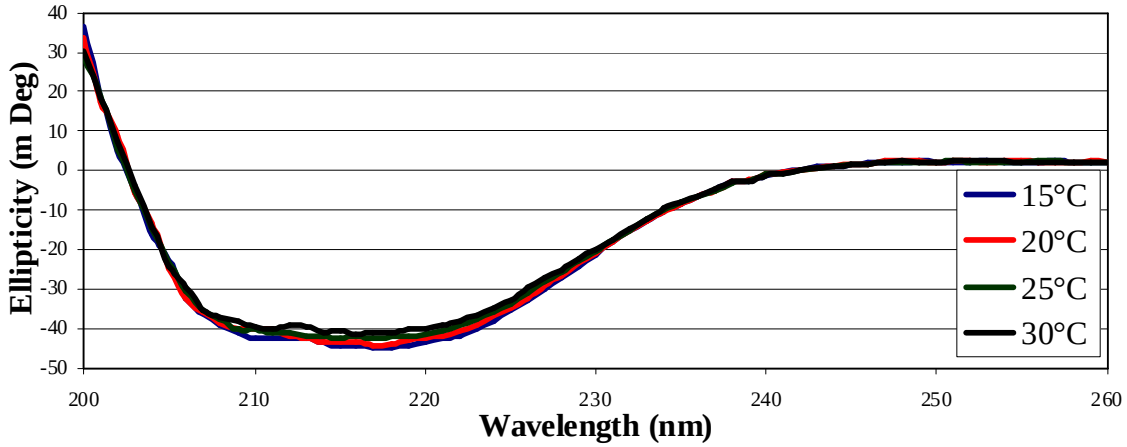

Figure 3-38. A small variation in temperature has little effect on Aβ's secondary structure in 25% HFIP. The temperatures were varied as indicated by the key from top to bottom. The spectra were taken when the ellipticity at 222 nm stabilized, approximately 2 to 5 min after the indicated temperature was reached.

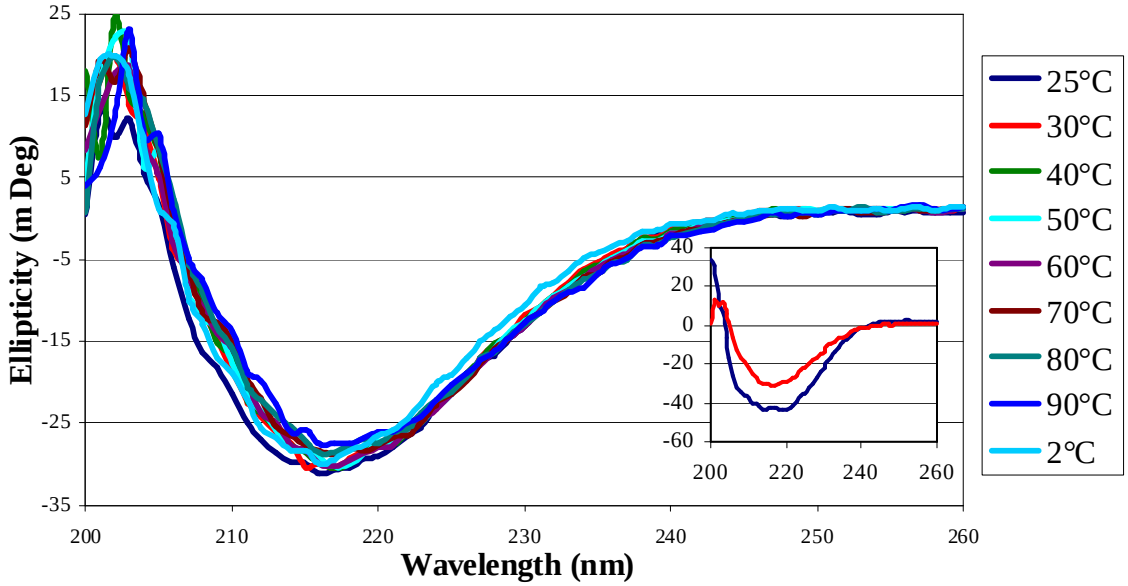

Figure 3-39. Thermally stable encapsulated Aβ in pure water for 54 days. The shape is similar to the reversible alcohol induced beta Xerogel spectrum. Once this data was collected the sample was placed in 50% HFIP for 24 h and the spectrum was taken. The 217 nm signal intensified and flattened out around 210 – 220 nm, indicating the presence of some helical content (inset; 0% HFIP in red and 25% HFIP 24 h later in blue).

this structure: (1) the structure was a semi-stable intermediate, (2) the peptide had leached through the glass and aggregated, or (3) it had become irreversibly adsorbed to the glass. After the data was taken the sample was transferred to 25% HFIP and allowed to equilibrate at room temperature over night. The inset of Figure 3-39 compares the 25°C spectrum of the main panel to the spectrum taken in 25% HFIP at 25°C. The increase in intensity was most likely due to unstructured regions of the peptide taking on helical structure.

3.8. Effects of Solvent Exchange on Encapsulated Peptide Secondary Structure

To test further the folding landscape of the two peptides in this study, and to search for stable intermediate states, xerogel samples were swapped between the different solvents used to characterize these peptides. If the spectra showed an irreversible change or the existence of multiple folds over a narrow range of solvent concentrations, then intermediates may possibly be identified. In addition, if certain spectra of soluble peptides not yet seen in xerogel samples were produced, then the thermodynamic effects of the xerogel matrix may be further characterized. And if the conditions corresponding to these spectra are known to lead to aggregation in solution then, not only do we learn about the folding path to these states and the stabilizing effects of excluded volume, but we also learn what solvent conditions may induce these states. In addition, defining such conditions would allow one to begin the investigation of how to prevent the formation of these aggregation-prone states.

During solvent exchange, because there was already solvent within the xerogel, some of the previous solvent would have been carried over to the new solvent. A generous estimation of the xerogel's volume that was solvent would be 80%. This estimation corresponds to a volume of just 0.04 ml for a typical glass sample. Each sample was incubated in 3.00 ml of the new solvent before the spectra were taken. Thus, the percent of the old solvent volume in the new solvent was about 1.3%. An example of the approximate change in concentration when moving a sample from 35% to 5% HFIP would be

((3.00 ml x 5.00%) + (0.04 ml x 35.0%))/3.04 ml = 5.39% HFIP (v/v).

Likewise, the change from water to 5% HFIP would result in an effective concentration of 4.93% HFIP, with a difference of 0.46% HFIP between the two re-equilibrated examples above. Where appropriate, these changes will be discussed in further detail.

3.8.1. PolyQ

3.8.1.1. Exchanges between HFIP and Water

An increase in helical secondary structure was seen with increasing HFIP concentration for encapsulated polyQ. To check the reversibility of these structures, xerogel samples were incubated in 1%, 5%, 10%, 25%, 35%, and 42% HFIP in H_2O (v/v) for 24 h, and the CD spectra were taken. After rinsing with H_2O, the samples where allowed to equilibrate for 1 h and then replaced with fresh H_2O. At hour 48, 24 h after the solvent was changed to H_2O, the spectra were taken, and the process was repeated to

return each sample to its original HFIP concentration. Figure 3-40 shows these three spectra for each HFIP concentration.

All experiments except the 1% and 10% samples showed complete reversibility. The 1% sample was uninteresting due to the fact there was no difference between the original spectrum and the H_2O spectrum. This general reversibility was an indication that the xerogel samples did not form any stable irreversible structures and that the peptide did not transition through a highly unstructured state. The 10% sample was the only one that showed a modest failure to completely recover its original CD profile. Since the experiment was not repeated, it is possible that the glass was not made uniformly and that the 72 h spectrum was not taken from the same region of the glass.

To further investigate the influence of these solvents on the secondary structure of polyQ, the 48 h spectra of the samples in Figure 3-40, all in H_2O, were compared, as seen in Figure 3-41. To provide a basis of comparison, the spectrum of a control sample that had only been equilibrated in H_2O has been added. This spectrum was obtained at the initial 24 h time point, and the sample was cut from the same glass. Thus, the significant differences between the control and all other sample were: (1) the control had only been in solution for 24 h, whereas the other samples were 48 h old, (2) the control had not gone through a solvent exchange, and (3) there was no residual concentration of HFIP in the control as a result of a solvent exchange. Although difficult to discern in Figure 3-41, there was an increase in ellipticity with increasing initial HFIP concentration, and all except the sample that came from 42% HFIP were slightly less intense than that of the control. This difference in ellipticity was most likely due to residual HFIP in the 0%

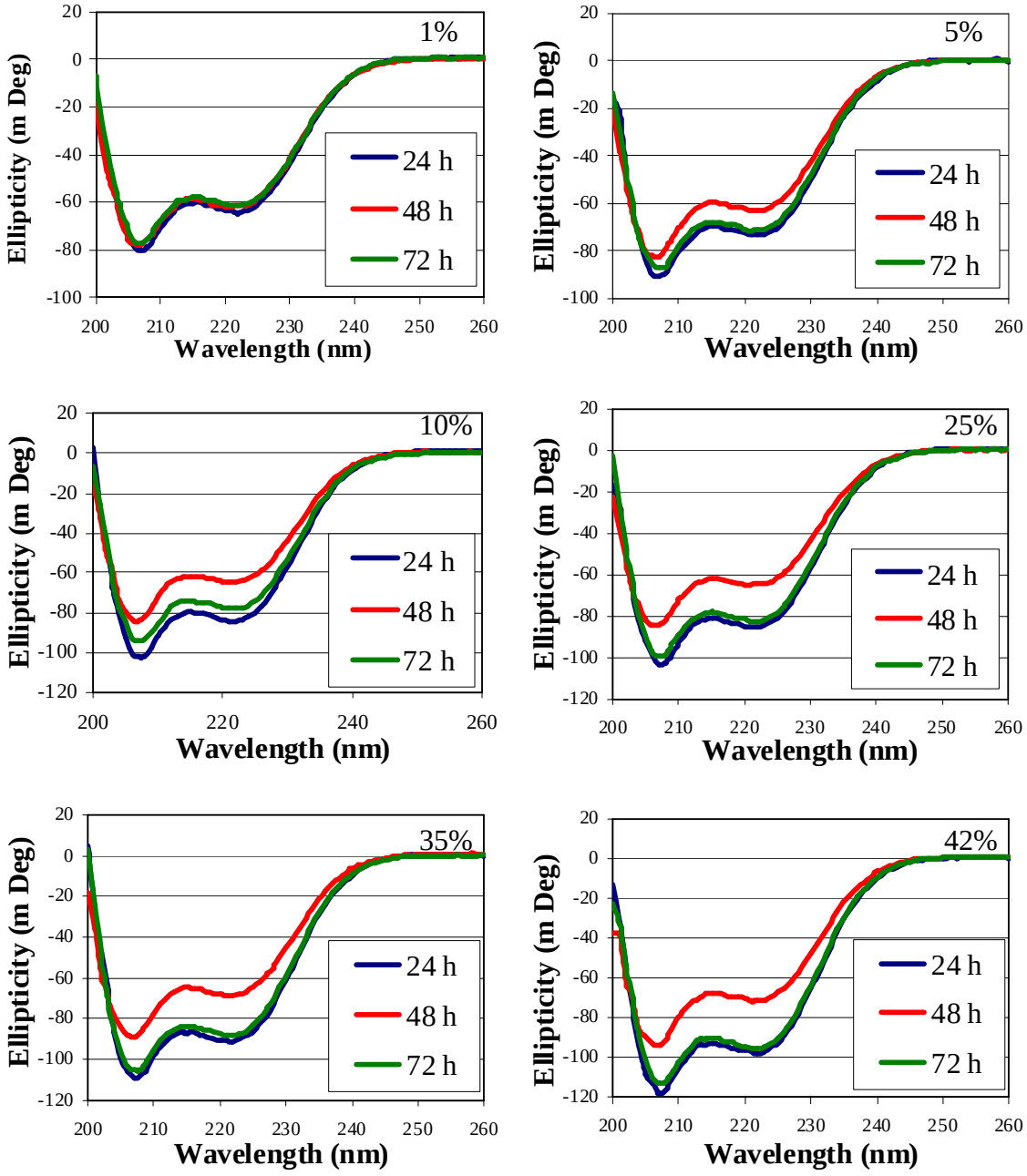

Figure 3-40. Solvent exchange effects on encapsulated polyQ from the indicated %HFIP (24 h) to water (48 h) and back (72 h). After the spectra were taken, the sample was allowed to equilibrate for 1 h in the new solvent at which time the solvent was drained and replaced with a fresh sample of the new solvent. This was done to reduce the amount of the previous solvent carried over in the xerogel matrix.

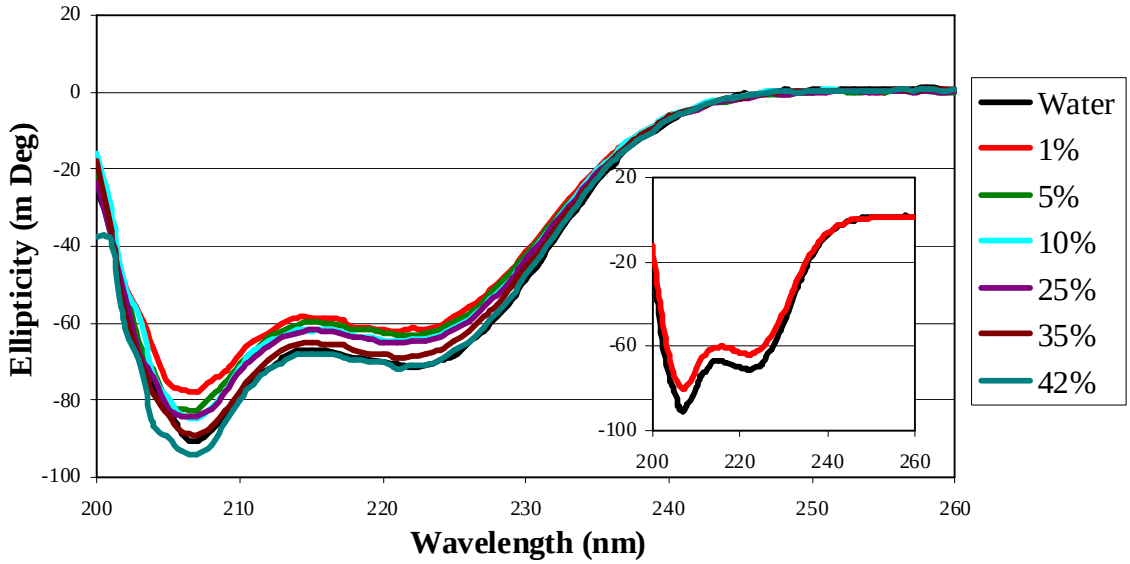

Figure 3-41. Comparison of polyQ samples in 0% HFIP for 24 h after initially incubating in the indicated %HFIP for 24 h. The same as those shown in Figure 3-40. After the spectra were taken, the sample was allowed to equilibrate for 1 h in the new solvent at which time the solvent was drained and replaced with a fresh sample of the new solvent. This was done to reduce the amount of the previous solvent carried over in the xerogel matrix. Inset: Comparison of the initial 24 h spectra of the 0% and 1% samples. Spectra colors follow the main panel's figure legend. Note that the 1% had decreased ellipticity.

HFIP samples. The inset shows the 24 h spectra for the 0% and 1% HFIP samples. It can be seen that the 1% sample had a decreased ellipticity which may indicate that very low concentrations of HFIP actually reduced secondary structure, or that, when the samples were initially placed in their respective HFIP concentrations, some amount of leaching had occurred since the samples were rehydrated with water after shrinking of the glass sample had ceased. What is more notable is the similarity of all the spectra when this initial difference in the samples in 0% and 1% HFIP is taken into account and when the residual HFIP concentrations that where carried over during the initial solvent

exchange are accounted for. The data indicated complete reversibility under the conditions of the experiment.

3.8.1.2. Exchanges between KPhos and Water

The effects of KPhos on polyQ's secondary structure were not only dependent on concentration but also on pH. Therefore, the three concentrations used previously at each of the three pH values were used in solvent exchange experiments, and a protocol identical to that described in the previous section was employed. Figure 3-8 shows that, in 1.00 M KPhos at pH 6.8, there was an increase in ellipticity and that the spectra retained the same general shape. Additionally, Figure 3-9 shows the pH dependence with pH 6.8 giving the strongest signal, pH 4.1 giving the weakest signal but with the same general shape, and pH 11.4 giving the most random structure with the signal near 207 nm being much more intense relative to that at 222 nm. Figure 3-42 shows the spectra for the solvent exchange between these samples and water. At an initial pH of 4.1, there was a small reduction in signal intensity when the spectrum was reanalyzed in water. Upon return to the original solvent, the sample recovered its original intensity with a modest increase at 222 nm. The source of this increase is unknown.

In the sample at pH 6.8, there was a significant loss in signal intensity at 48 h when the spectrum was taken in water. This extent of random coil shape was not seen in spectra of equivalent samples in water with no prior solvent incubation (Figure 3-8), but was similar to the spectrum obtained in 10.0 mM KPhos at the same pH. This similarity indicated that solvent exchange was not complete and that a small concentration of

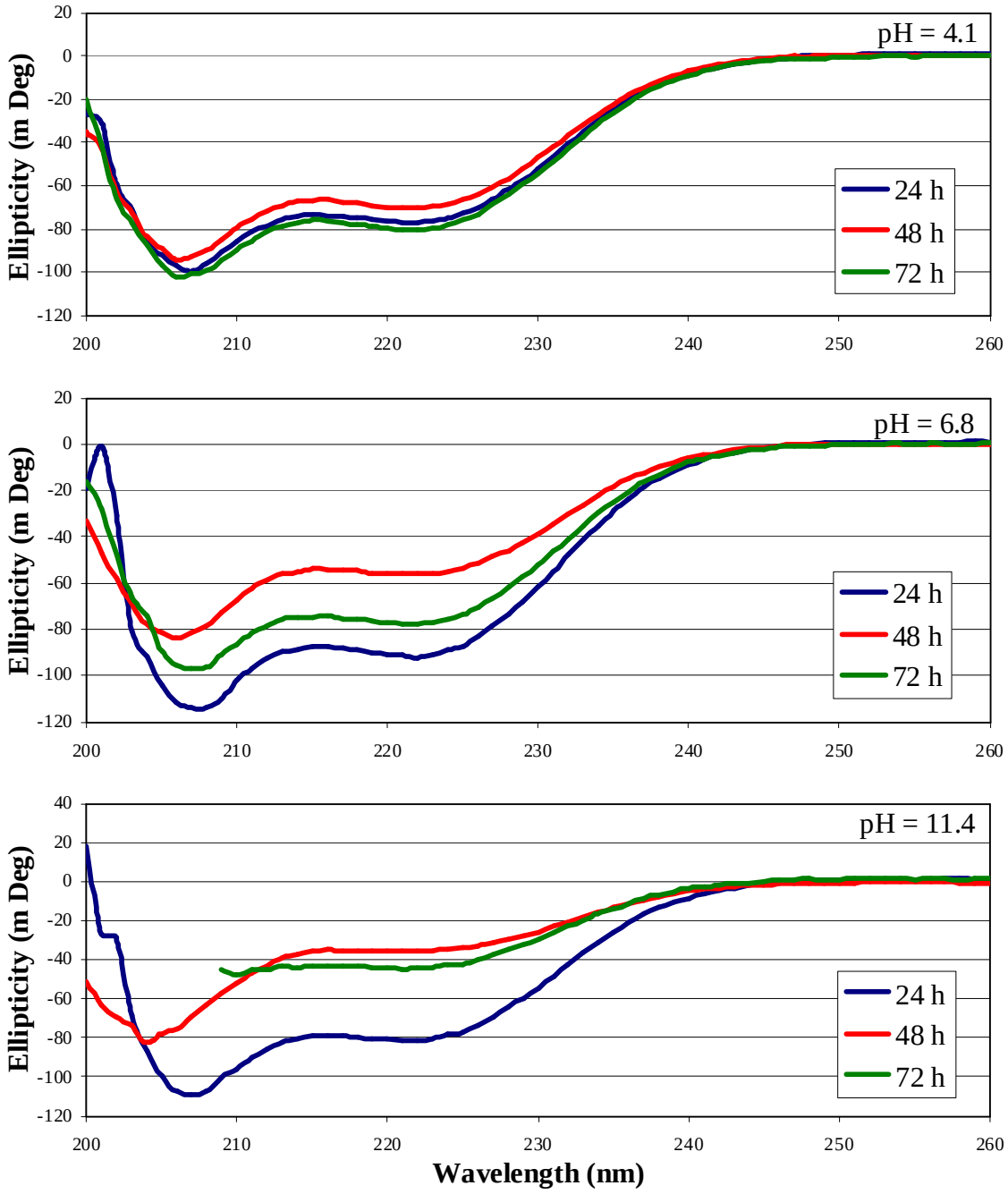

Figure 3-42. Solvent exchange effect on encapsulated polyQ from 1.00 M KPhos at pH 4.1 (top), 6.8 (middle), and 11.4 (bottom) to water (48 h) and back (72 h).

KPhos was present in the 48 h spectrum. Because this was a random coil structure, which was prone to leaching, and because the same general shape of the 24 h spectrum was regained at 72 h, just less intense, leaching must have been a factor during the experiment.

A similar result was obtained in the pH 11.4 experiment at 24 and 48 h, except both spectra were more random in character as compared to the pH 6.8 experiment. The 72 h spectrum became too noisy below 210 nm to interpret, but the 222 nm signal was greatly reduced as compared to the 24 h spectrum. Since the two previous spectra had increased random character, it was likely that leaching was much more of a factor than for the sample at pH 6.8. Here the 48 h spectrum in water indicated a slightly more random structure than that of the 10.0 mM pH 11.1 sample seen in Figure 3-11, but the 50.0 mM pH 11.4, seen in Figure 3-10, was more random in structure than the 10.0 mM sample. Therefore, the spectrum at 48 h may have been of a low concentration of KPhos, near 10.0 mM, but at a higher pH, increasing its random coil structure.

Both Figures 3-43 and 3-43 give results similar to one another and show signs of leaching, as observed in 1.00 M KPhos. The effects of leaching were reduced in Figure 3-44, which was to be expected since 10.0 mM KPhos is less concentrated than the 50.0 mM used in Figure 3-43. The changes in the spectra at the lower and neutral pH values in both of these figures, across the individual experiments, were negligible, but gave similar results as Figures 3-10 and 3-11 where the lower pH values were more helical than the neutral. Figure 3-8 shows that the spectrum of the control sample in water was more helical than both of these samples. Since the samples at 48 h in Figures

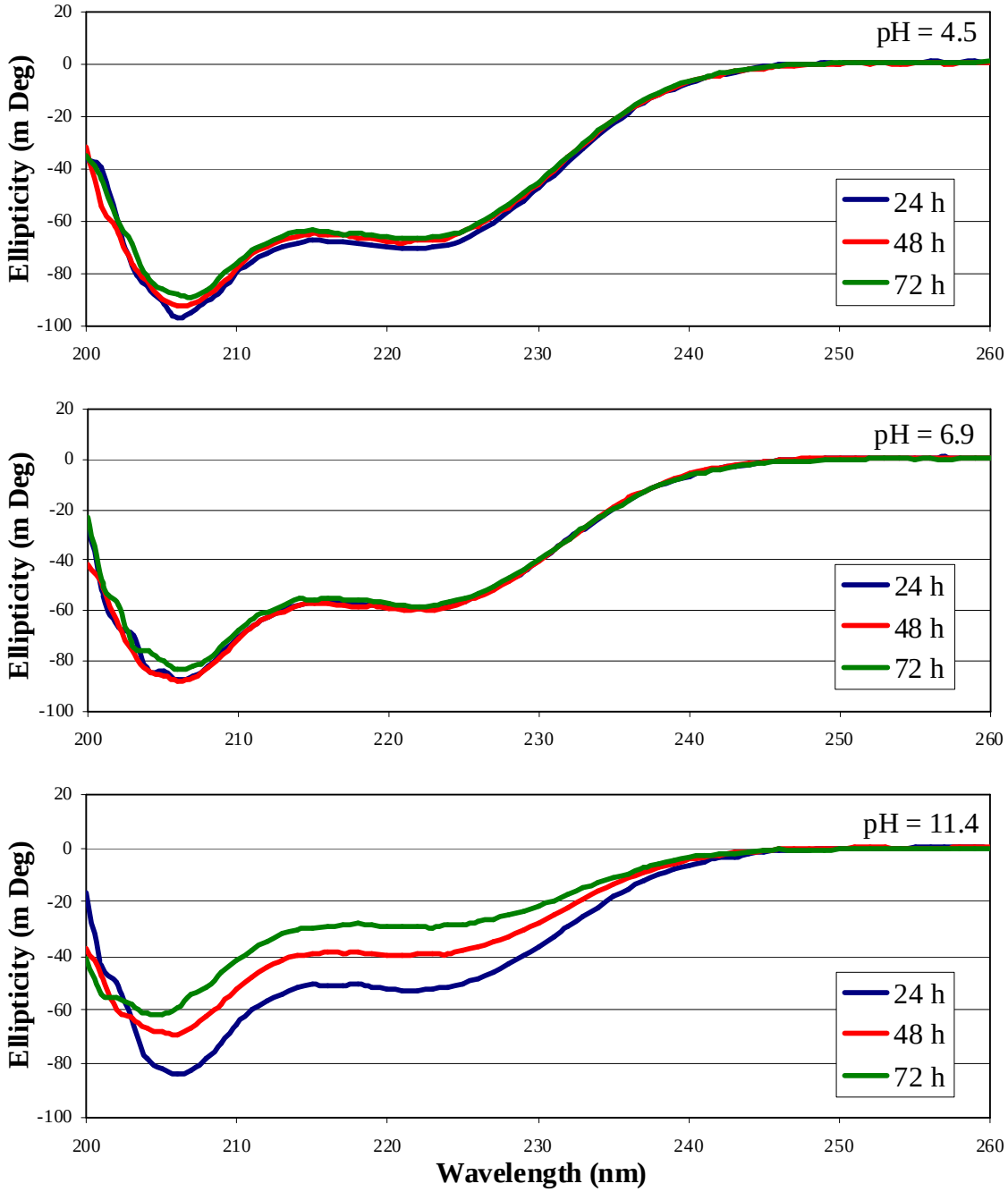

Figure 3-43. Solvent exchange effect on encapsulated polyQ from 50.0 mM KPhos at pH 4.5 (top), 6.9 (middle), and 11.4 (bottom) to water (48 h) and back (72 h).

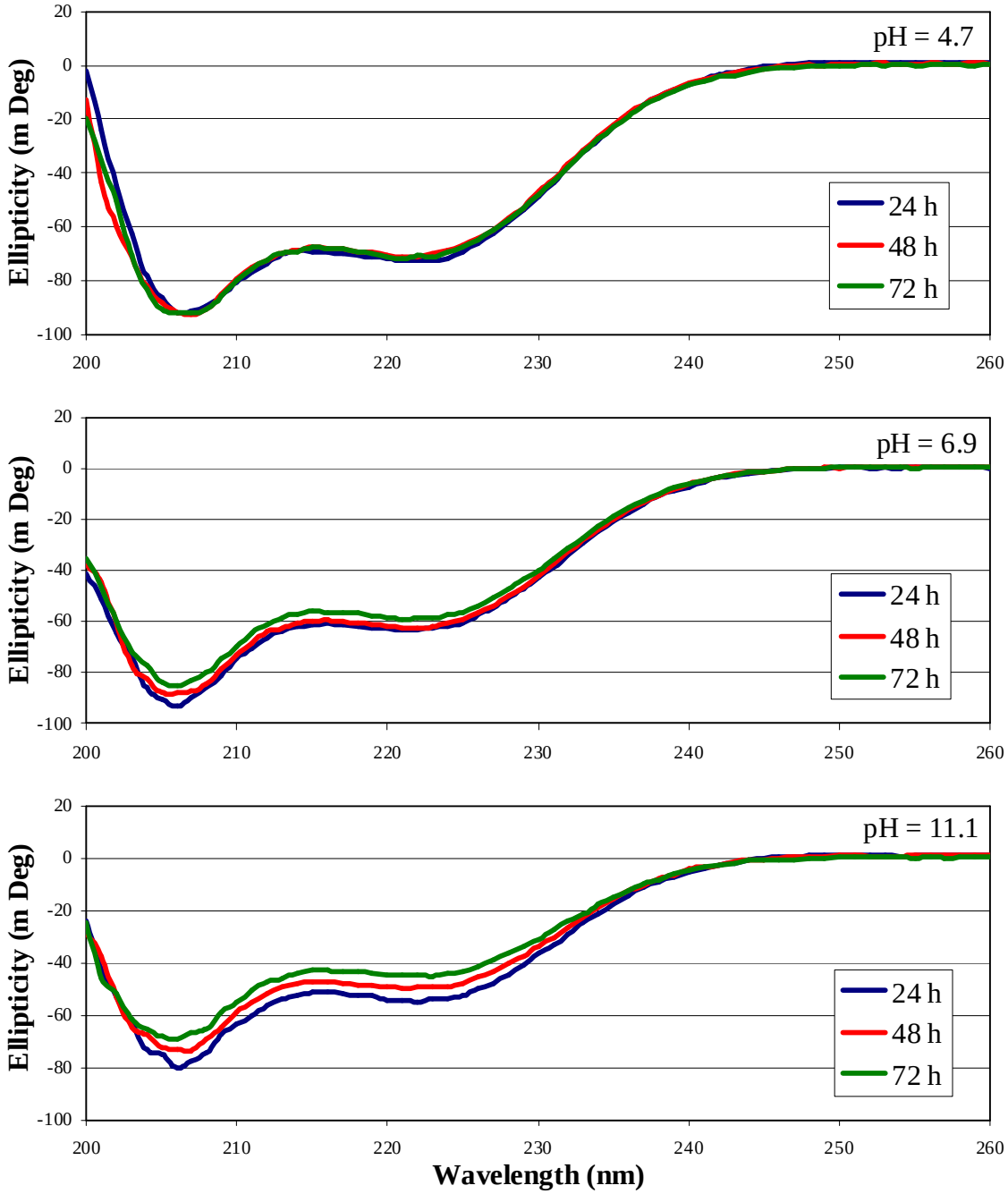

Figure 3-44. Solvent exchange effect on encapsulated polyQ from 10.0 mM KPhos at pH 4.7 (top), 6.9 (middle), and 11.1 (bottom) to water (48 h) and back (72 h).

3-43 and 3-44 did not recover this structure, some rearrangement must have taken place in the original solution that was not energetically forbidden in water. The concentration of KPhos in these samples at 48 h must have been miniscule. The higher pH samples provide support for this last statement. Both showed signs of leaching, and this leaching could only be driven by solvent exchange. Each successive solvent exchange lowered the intensity of the spectra with little effect on the spectral shape. At these lower concentrations of 10.0 mM and 50.0 mM any residual buffer carried over would result in a negligible concentration in the spectra at 48 h after the solvent had equilibrated.

Figure 3-45 shows the results from the reverse experiment where the sample was incubated first in water and changed to 50.0 mM KPhos at pH 11.4, and then back, using the same protocol. It is again seen that each successive solvent exchange caused a

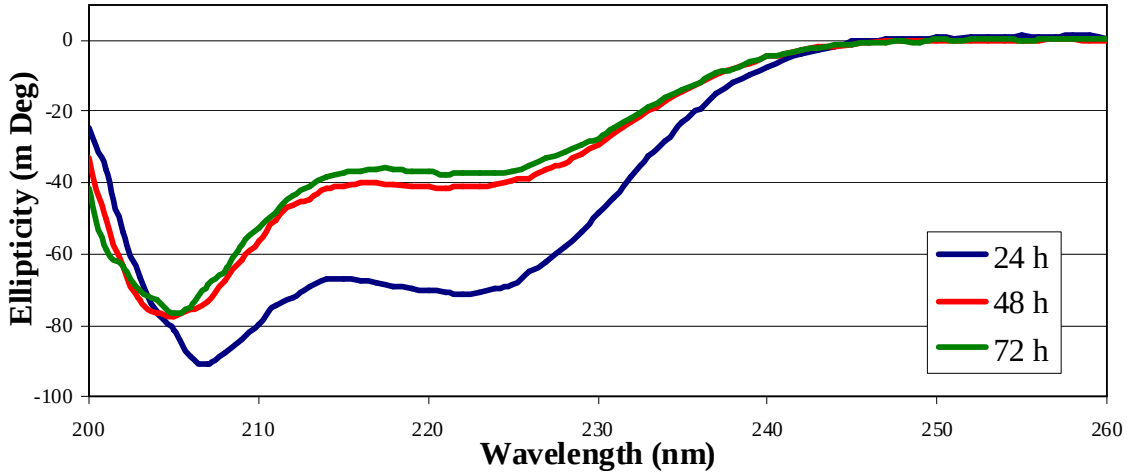

Figure 3-45. Solvent exchange effect on encapsulated polyQ from H_2O to 50.0 mM KPhos at pH 11.4 (48 h) and back (72 h).

reduction in intensity, indicating leaching, and that the 48 h spectrum shows a loss of secondary structure that was not recovered when the sample was returned to water. This

difference between the two experiments provided further support that leaching was a factor for KPhos buffers of high pH. Because both the peptide and the silica surface of the glass would be negatively charged at high pH, enhanced leaching may be due to charge repulsion.

3.8.2. Solvent Exchange Studies with Aβ Peptide

The experiments in section 3.8.1 for polyQ were simultaneously performed in an identical manner with Aβ peptide. This includes peptide solubilization, glass preparation, and choice of all solutions. Therefore, the only significant difference between the experiments was the peptide.

3.8.2.1. Exchanges between HFIP and Water

The results from Aβ peptide xerogel samples exchanged between HFIP solutions and H_2O are shown in Figure 3-46 below. Figure 3-13 showed that after 24 h of incubatiing there was an increase in ellipticity with increasing HFIP concentration, starting with a random coil spectrum and showing a significant amount of helical structure at the higher HFIP concentrations. As in Figure 3-13, there was noise at the shorter wavelengths in Figure 3-46 making the spectra difficult to interpret. Each set of spectra demonstrates the ability to take on the same random coil profile in water upon solvent exchange (Figure 3-47 top). Upon return to the original solvent, the 10% sample showed a loss in ellipticity intensity that may indicate a slight loss of structure as compared to the original 24 h structure. What's more significant is that the higher HFIP

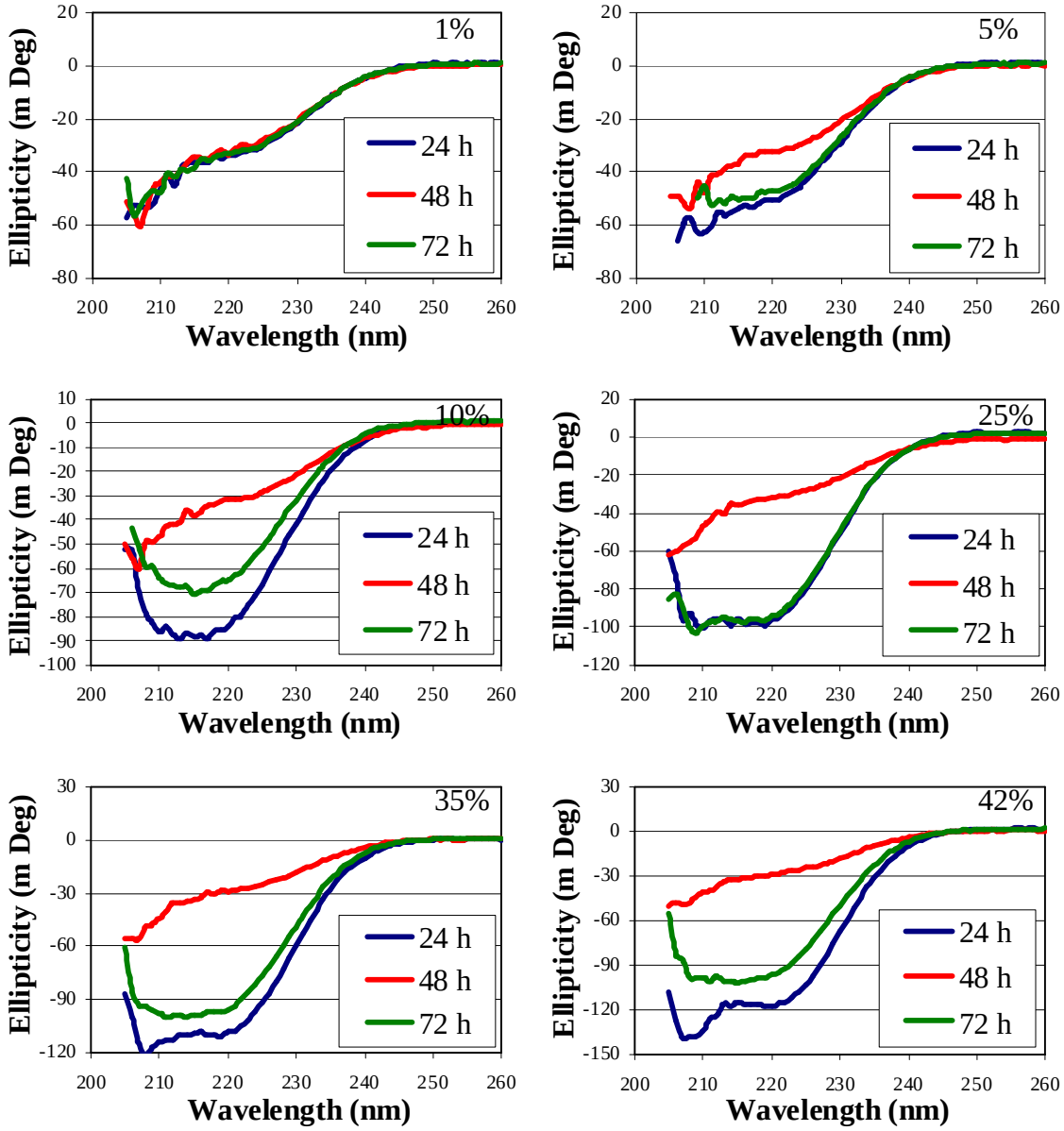

Figure 3-46. Solvent exchange effect on encapsulated Aβ from the indicated %HFIP (24 h) to water (48 h) and back (72 h).

concentrations of 25%, 35%, and 42% all returned the same spectra, in the discernible region, upon return to their original solution (Figure 3-47 bottom). These spectra appear to have had some helical characteristic as indicated by the flattened region between 210

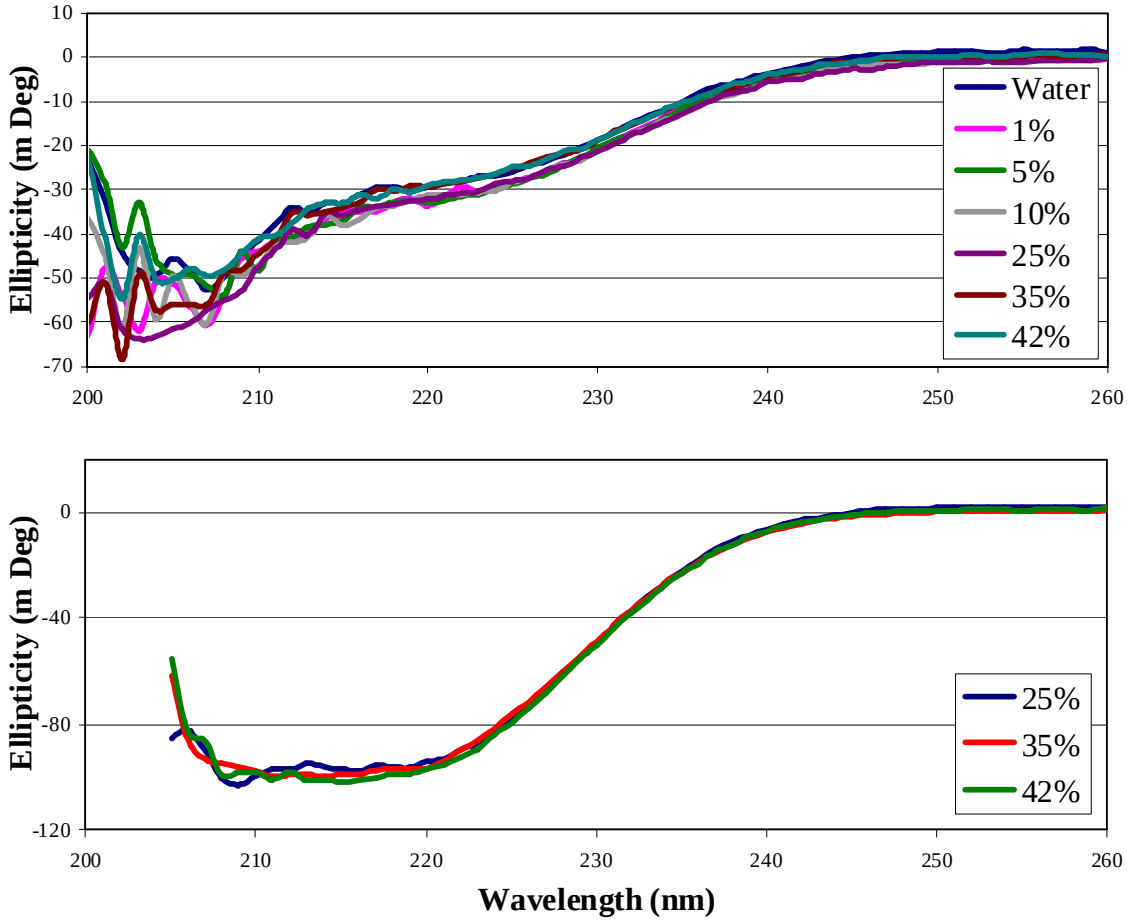

Figure 3-47. Comparison of Aβ samples at 48 (top) and 72 (bottom) hours during solvent exchange between HFIP and water for the indicated concentrations. The same as those shown in Figure 3-46.

nm and 220 nm. The fact that the ellipticity did not increase with increasing HFIP concentration above 25%, as seen at the first time point, may indicate the formation of some semi-stable secondary structure. In addition, these spectra overlap with the original spectrum for the sample in 25% HFIP that was capable of unfolding to the same endpoint in water at 48 h.

Figure 3-25 shows that just a slight increase in secondary structure decreased the rate of aggregation. The reversibility of the conformational states shown in Figure 3-46 is further demonstrated in Figure 3-47. Here it is seen that, no matter the initial HFIP concentration, all samples adopt the same conformation in water at 48 h. This is similar to the spectrum of the 0% HFIP sample in Figure 4-25 that precipitated out of solution (Figure 3-12). Since Aβ is believed to aggregate from a disordered state, this finding is significant because it demonstrates that the peptide's secondary structure is highly sensitive to its environment.

3.8.2.2. Exchanges between KPhos and Water

In Figure 3-14 it was shown that encapsulated Aβ increased in ellipticity with increasing KPhos concentration. Both 10.0 mM and 50.0 mM KPhos showed similar random structure as observed in water and were just slightly increased in intensity, whereas the 1.00 M spectrum appears to be more helical and was the strongest signal. The corresponding time stability data in Figures 3-27 to 3-29 show that Aβ quickly aggregated out of solution at the two lower KPhos concentrations. It was also shown in these experiments that the samples at lower pH aggregated out of solution at approximately the same time. Only the samples at the higher pH values showed any amount of time stability in solution, and this stability increased with increasing phosphate concentration. It has been mentioned that the peptides at the higher pH values have a net negative charge causing a repulsive force, which would have prevented aggregation. In addition, the silica surface should also have had a negative charge in basic pH. Figures 3-

48 to 3-50 below give the spectra for solvent swap experiments between KPhos, to water, and back to the original solvent. Most of the data is uninteresting because no significant

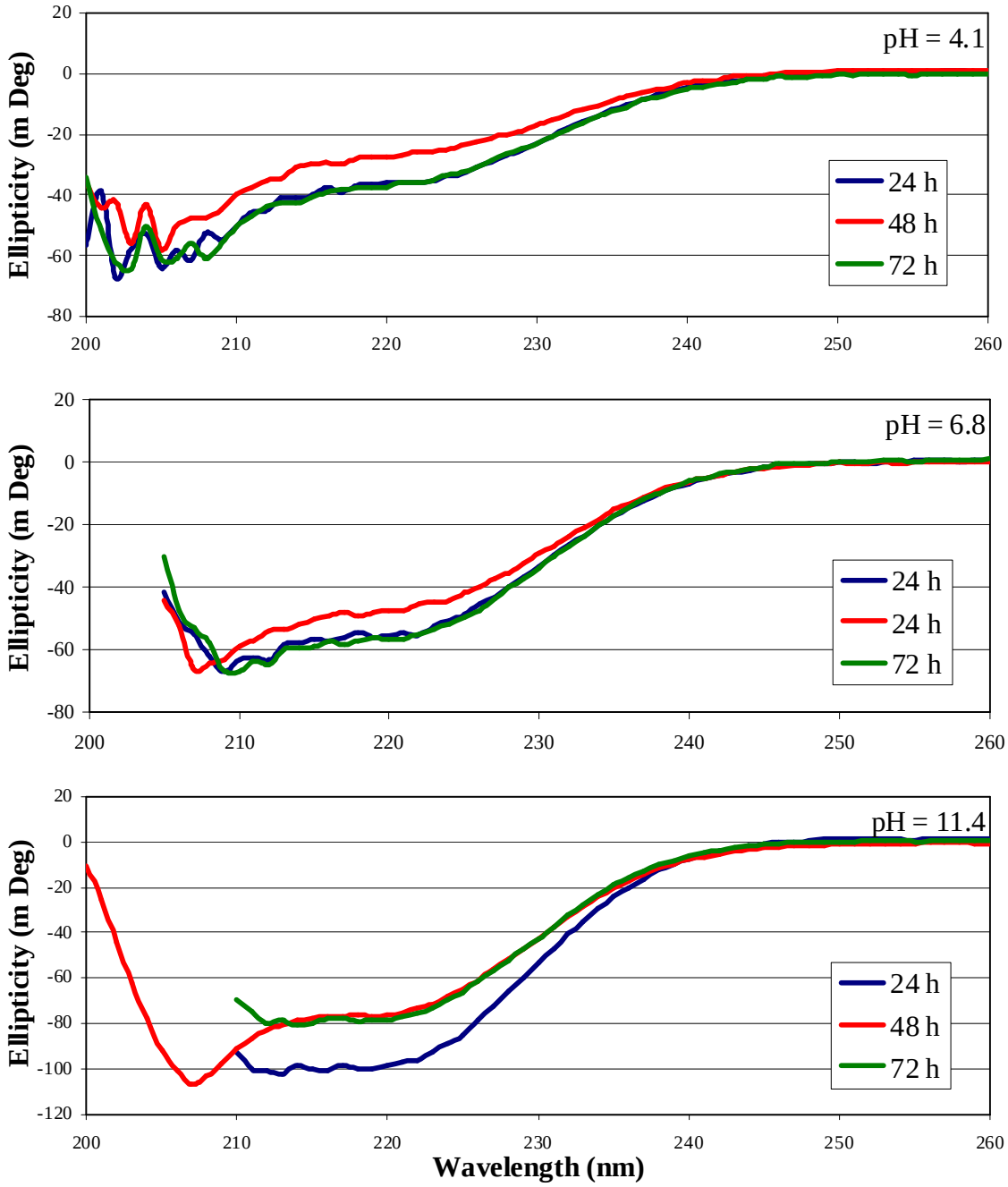

Figure 3-48. Solvent exchange effect on encapsulated Aβ from 1.00 M KPhos at pH 4.1 (top), 6.8 (middle), and 11.4 (bottom) to water (48 h) and back (72 h).

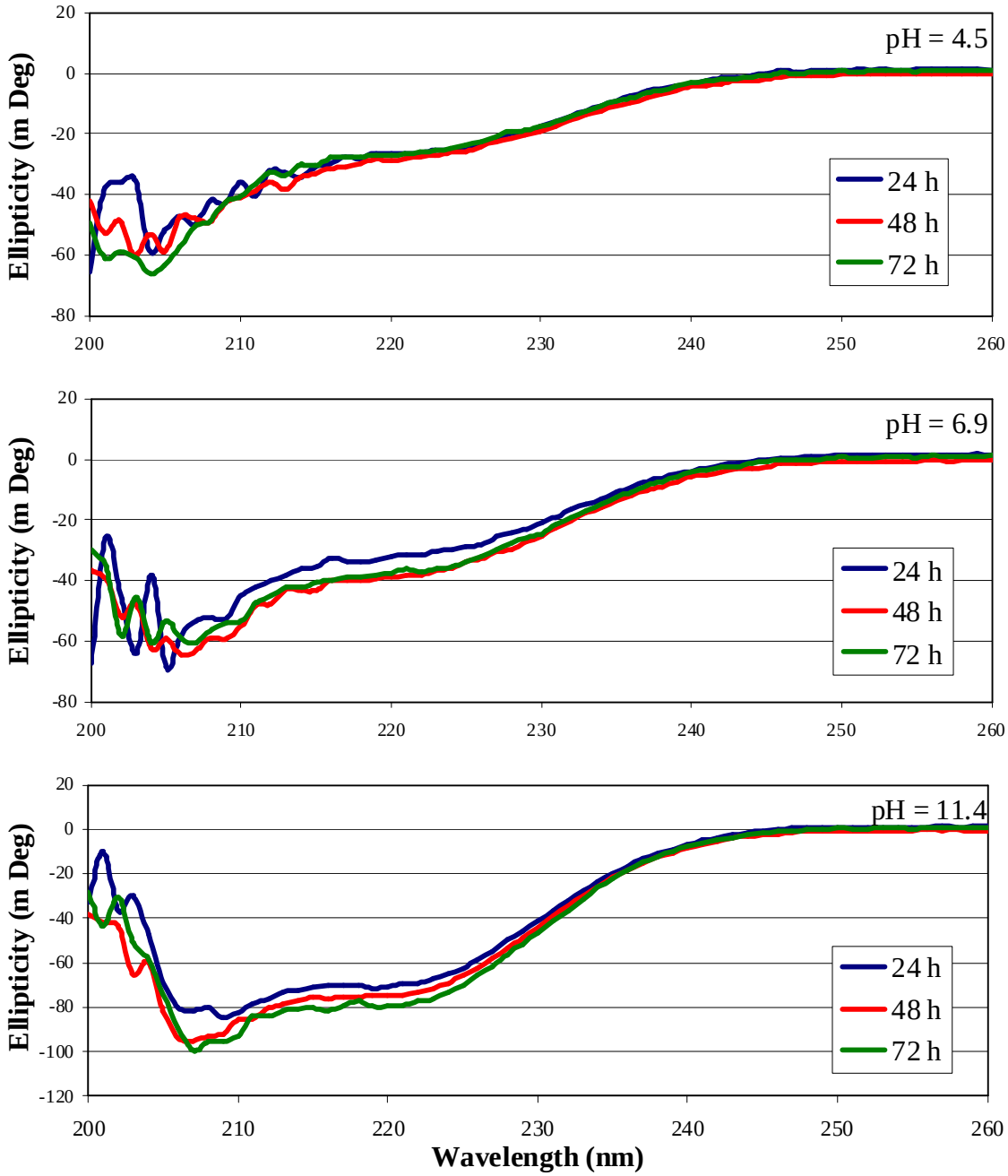

Figure 3-49. Solvent exchange effect on encapsulated Aβ from 50.0 mM KPhos at pH 4.5 (top), 6.9 (middle), and 11.4 (bottom) to water (48 h) and back (72 h).

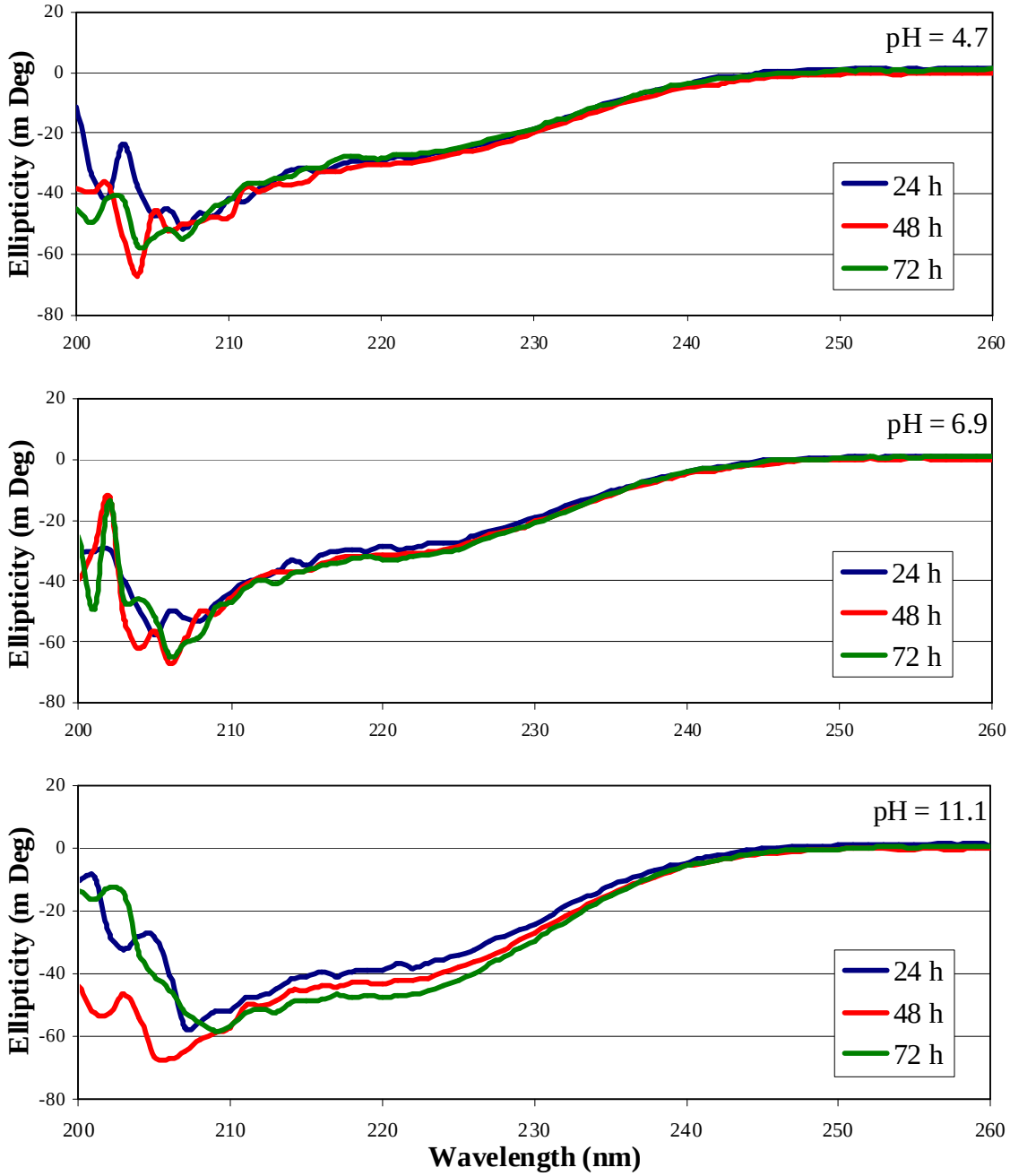

Figure 3-50. Solvent exchange effect on encapsulated Aβ from 10.0 mM KPhos at pH 4.7 (top), 6.9 (middle), and 11.1 (bottom) to water (48 h) and back (72 h).

changes in the spectra were observed.

One experiment that returned interesting data is seen in Figure 3-48 (bottom) for the 1.0 M KPhos sample at pH 11.4. A major problem with this pH at this concentration was that the CD signal became too noisy at the shorter wavelengths and the spectra could not be interpreted. After the sample was moved to water for 24 h, a complete spectrum was obtained indicating significant helicity. As mentioned previously, the high absorbance and noise problem was due to [PO_4^{3-}] at pH 11. Though special care was taken to reduce the amount of solvent carried over, it was likely that some amount of the 1.0 M KPhos at pH 11.4 buffer remained in the water sample, raised the pH, and stabilized the peptide in a helical structure. It is interesting that upon return to the original KPhos buffer, the sample did not return to its original intensity, but instead the 48 (water) and 72 (buffer) hours samples were the same in the discernible region. PolyQ under the same conditions (Figure 3-42) similarly did not regain its original structure.

Figure 3-51 gives data for a sample that is initially incubated in water for 24 h

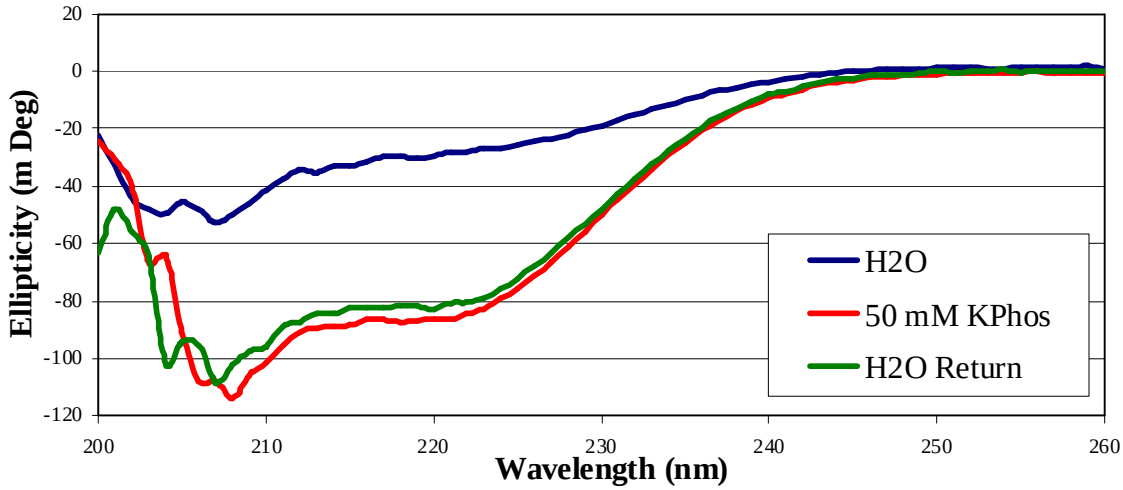

Figure 3-51. Solvent exchange effect on encapsulated Aβ from H_2O to 50.0 mM KPhos at pH 11.4 and back. The blue spectrum was taken first, then red, and then green.

before the first spectrum was taken. The same exchange protocol was utilized in treating the xerogel. The sample was transferred to 50 mM KPhos at pH 11.4 for another 24 h, and the spectrum was retaken before returning it to water. It can be seen that the sample did not return to its original spectrum at 72 h. A similar situation was seen for polyQ (Figure 3-45) where the signal intensity decreased at 48 h, instead of increasing, and the 72 h spectrum remained similar to the 48 h spectrum. This may indicate that the 48 h structures were stabilized by the lower pH that was carried over upon return to the original solvent.

Results from Figures 3-46, 3-47, 3-48, and 3-51 are contradictory because the irreversibility in the spectra did not depend on the starting solvent. All show a change between the 24 h and 48 h spectra, but from 48 h to 72 h the change was irreversible. What the figures do demonstrate is that when high pH was involved the spectra were not reversible.

3.9. Unique Results of Other Investigations

Several additional experiments were carried out to further characterize the peptides and the xerogel environment. These included the use of different solvents for solvent exchange, exploration of a narrower range of HFIP concentrations to characterize Aβ's transition out of the random coil spectra, use of different solvents to compare polyQ and Aβ, and the use of buffer in glass formation to expedite xerogel preparation.

3.9.1. Influence of 80% Ethanol on PolyQ's Secondary Structure

The general influence of alcohols on protein secondary structure has been well characterized, and so the following experiment was carried out on polyQ. The peptide was first incubated in 80% ethanol overnight, and the spectrum was taken, as shown in Figure 3-52 (blue). The spectrum is similar to the helical conformation obtained in ≥ 25% HFIP. The sample was then moved to 10.0 mM KPhos at pH 6.9, at which time a separate second sample was prepared using fresh 10.0 mM KPhos at pH 6.9. These solutions were allowed to equilibrate overnight before both spectra were taken. The sample transferred from 80% ethanol (red) showed an increase at the 222 nm signal and a decrease at the signal near 207 nm, as compared to the sample exposed only to 10 mM KPhos. This was most likely due to some ethanol being retained in the glass, inducing a slightly higher content of helical structure.

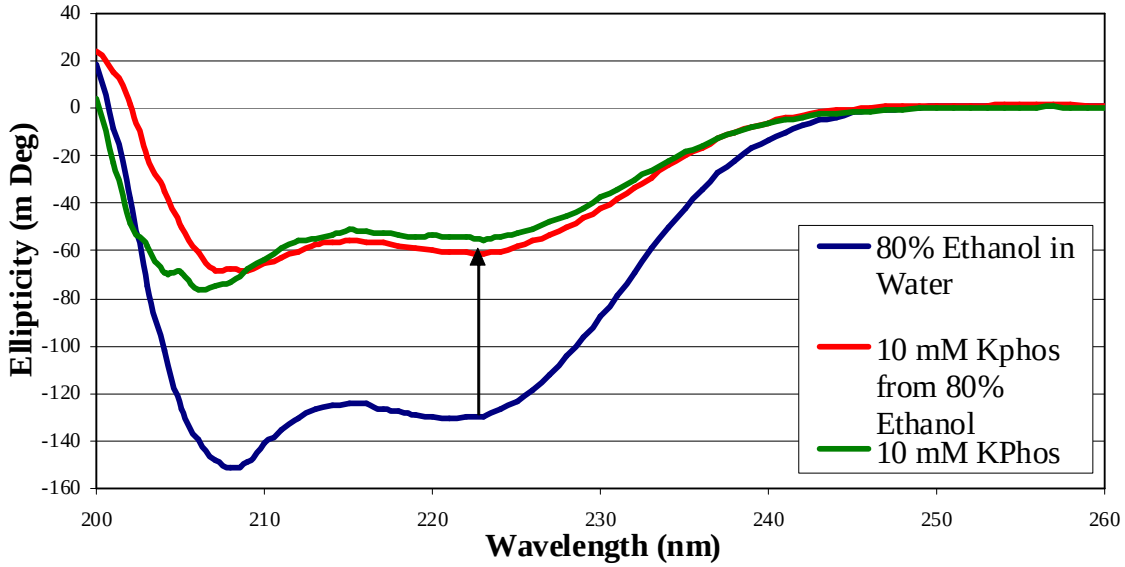

Figure 3-52. Encapsulated polyQ shows an irreversible gain in helical structure upon solvent exchange from 80% ethanol to 10 mM KPhos, pH 6.9. The arrow points from the 80% ethanol spectrum to the spectrum of the same sample in 10 mM KPhos afterwards.

3.9.2. Aβ's Folding Transition

The Aβ peptide demonstrated that it could take on different amounts of secondary structure when returned to the original HFIP concentration during solvent exchange, Figures 3-46 and 3-47. To further investigate this transition, the following experiments were performed: a solvent exchange between water and 50:50 TFE in water and an exchange from higher to lower concentrations of HFIP using a new sample. In the first exchange, TFE was chosen because of its helical inducing properties, similar to HFIP. Figure 3-53 gives the resulting spectra. Following the same solvent exchange protocol given in Section 3.8, a glass sample was first equilibrated in water, moved to TFE, and then returned to water. As expected, the peptide changed between the weak helical structure found in water, to an apparent beta conformation in TFE, and then returned to a weak helical structure when returned to water. Due to noise at the shorter wavelengths,

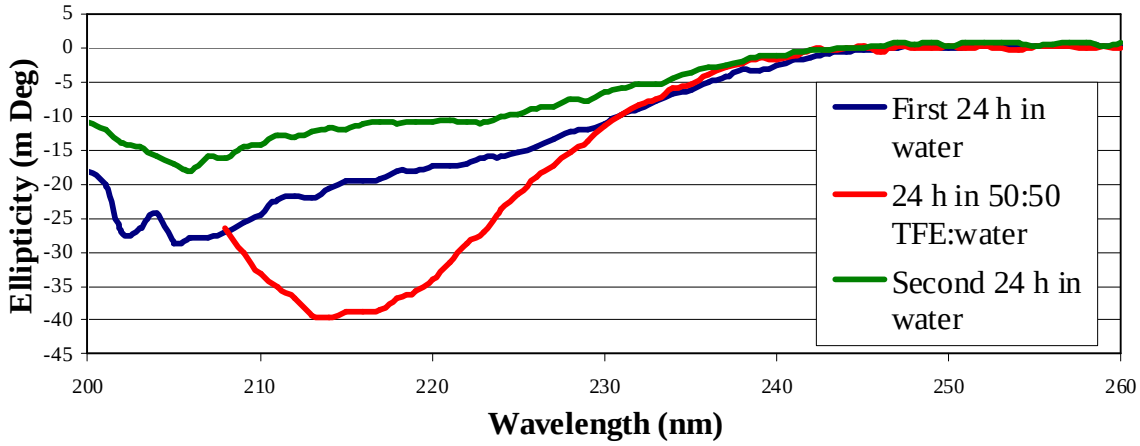

Figure 3-53. Encapsulated Aβ stored at 25°C for 24 h in H_2O, then moved to 50% TFE/H_2O for 24 h, and returned to H_2O. The spectra were taken at the end of the 24 h periods. Both the structures in water are random-coil while in TFE solution they are beta. The same experiment has been repeated in shorter times, and in different alcohols (fluorinated and unfluorinated). The loss of signal is most likely due to leaching of the peptide during solvent exchange.

the TFE spectrum could not be fully interpreted; the CD instrument crossed its suggested absorbance threshold at 208 nm. The second spectrum in water was reduced in intensity but had the same spectral shape, indicating that leaching took place. This leaching was more extensive than was seen in experiments with HFIP. Because the fluorinated alcohols were not buffered, some of the inconsistency may be due to a difference in pH, and therefore charge of the peptide. The shapes of the spectra suggest complete reversibility of the transition.

Figure 3-46 and 3-47 showed that all the Aβ samples in HFIP were able to return to an identical random coil conformation when in water. The second experiment was performed to investigate the transition between the random coil spectra and the enhanced spectra of the HFIP solutions to see if a stable intermediate was detectable. This was done by taking samples that previously gave the apparent beta spectra in high HFIP concentrations and incubating them in 2.5%, 5%, and 7.5% HFIP solutions. These samples were moved to water and then returned to their respective HFIP solutions. After 24 h in each solution at 25°C, the spectra were taken. Initially, the HFIP exchanges were prepared in the following manner: 10% → 2.5%, 35% → 5%, and 50% → 7.5%. Because each sample came from a different original HFIP concentration, the new starting concentrations (v/v) were estimated using the calculation from Section 3.8 for the sample in 5% HFIP. For the other two combinations, the new initial and final concentrations would have been:

$$2.5\%\ \text{initial} = 100\%((3.00\ \text{ml} \times 2.5\%) + (0.04\ \text{ml} \times 10\%))/3.04\ \text{ml} = 2.60\%$$

$$2.5\%\ \text{final} = 100\%(3.00\ \text{ml} \times 2.5\%)/3.04\ \text{ml} = 2.47\%$$

7.5% initial = 100% ((3.00 ml x 7.5%) + (0.04 ml x 50%))/3.04 ml = 8.06%

7.5% final = 100% (3.00 ml x 7.5%)/3.04 ml = 7.40%.

The percent HFIP carried over to the water from the 8.06% sample works out to be 0.01%, and so, in terms of significant figures, may be neglected.

Figure 3-54 shows the results for this experiment. It can be seen that the 2.5% sample remained random coil throughout the experiment, the 5% sample gave an apparent beta signal when brought down from a higher concentration but was random when brought up from water, and the 7.5% sample yielded an apparent beta structure both times, though reduced when brought back up from water.

In solution, the beta structure of Aβ was apparently aggregation resistant (Figures 3-25 and 3-30), but the results in Figure 3-54 indicate that it was sensitive to [HFIP]. In addition, it has been seen that, with increasing HFIP concentration, there was an increase in helical structure. The existence of stable soluble oligomers has been well documented [11, 100, 101, 103], but monomeric beta structure is not. In section 3.3.2.1, it was suggested that this spectrum could in fact represent beta structure (Figure 3-13 bottom panel inset). Since it is believed that encapsulated Aβ is monomeric, it may be that the solution beta spectrum was that of stable soluble oligomers, whereas the encapsulated peptide was monomeric and contains significant helical structure in addition to beta structure.

Figure 3-54 suggests that there was a very small thermodynamic barrier between the random coil conformation and the structure with enhanced ellipticity, Figure 3-55 for an energy level representation of these two states. It may be that this thermodynamic

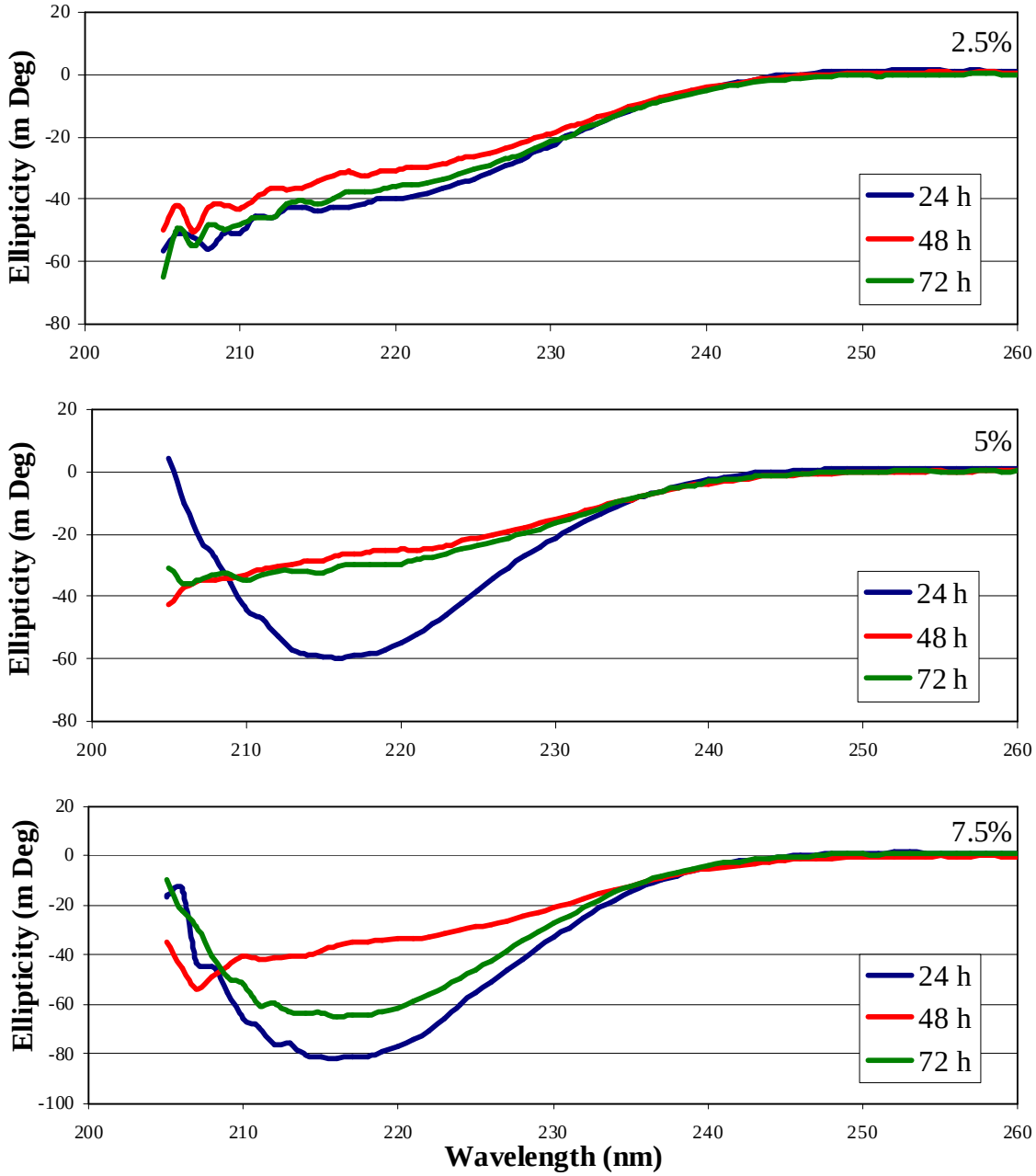

Figure 3-54. Encapsulated Aβ folding transition. Encapsulated Aβ gives different spectra in the same solution, depending on its solution history. All samples were stored in >10% HFIP solution for 24 h before being placed in 2.5% HFIP (top), 5% HFIP (middle), and 7.5% HFIP (bottom), moved to water (48 h) and back (72 h).

barrier is also the barrier to aggregation. It was shown in Figure 3-13 (top) that the 5% HFIP sample was the lowest concentration to give any sign of secondary structure, and Figure 3-30 (top) shows that this sample was stable with time.

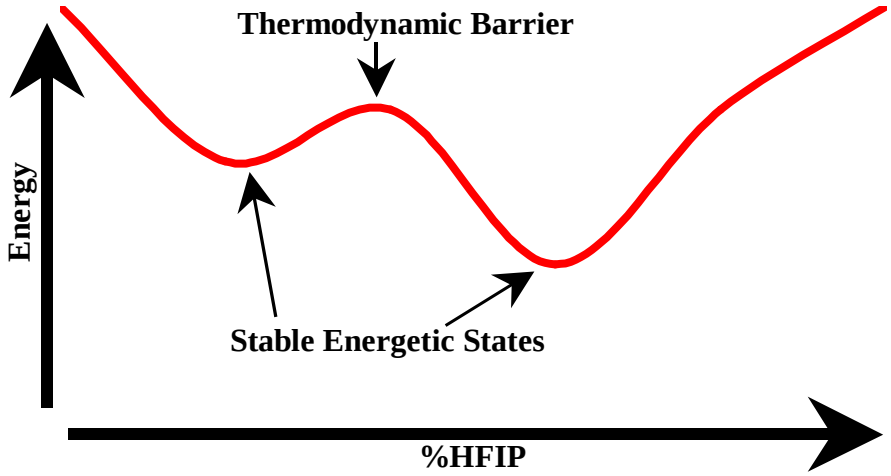

Figure 3-55. A representation of the two possible energetically close stable states for the transition seen in Figure 3-54.

3.9.3. Comparison of Encapsulated PolyQ and Aβ in Various Solvents

Several well-characterized solvents were used in an attempt to find commonalities between the two peptides in this study and to possibly develop a unifying mechanism behind protein aggregation. Because both peptides demonstrated a resistance to aggregation in KPhos at high pH, 50.0 mM KPhos pH 11.4 was included in the comparison (Figure 3-56). A notable commonality is the general shape of the spectra that was likely due to the influence of the F_3-propyl modifier. All samples except those in 80% ethanol were characterized by weak helical structure. For polyQ, the 80% ethanol sample gave an enhanced helical ellipticity, whereas for Aβ the signal became too noisy

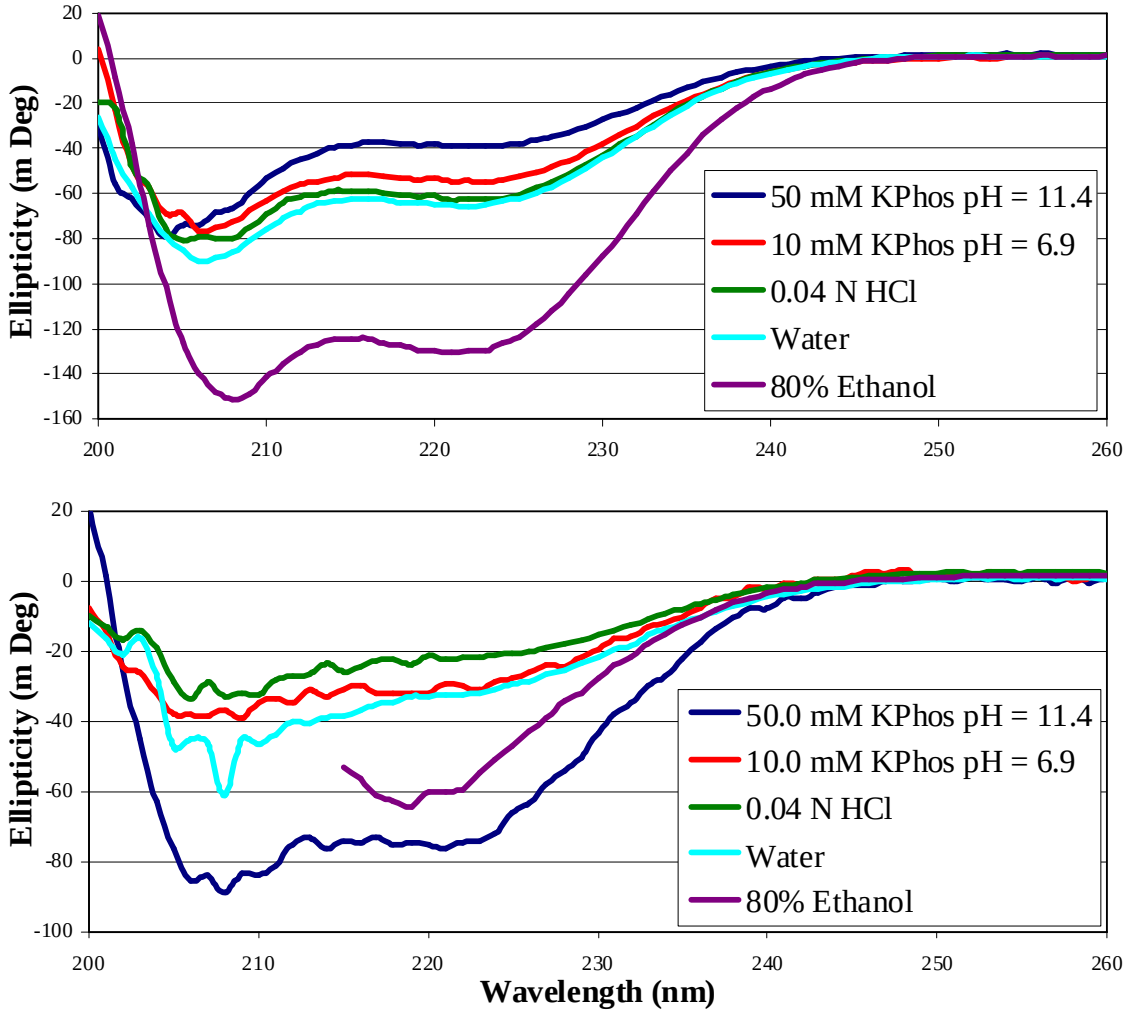

Figure 3-56. Comparison of encapsulated polyQ and Aβ in various solvents. Top (polyQ) and bottom (Aβ). Xerogel samples of polyQ show a loss of structure with an increase in pH, while Aβ shows the opposite. The Aβ samples in 50.0 mM and 10.0 mM KPhos did not come from the same glass, so their spectra were adjusted to compensate for the difference in concentration.

to interpret. As discussed in the previous section, this spectrum was most likely similar in shape to the other helical spectra in Figure 3-56. They were similar in the fact that they both return intense signal strength. Another notable difference is that polyQ samples demonstrated increased helicity in acidic solution whereas Aβ was more random. This

can be explained by the relative charge distribution on each peptide. PolyQ had its termini oppositely charged, so the monomeric peptide was soluble. Aβ had positive and negative charges distributed intermittently along its backbone and also contained a hydrophobic region. Uversky and Dunker (2010) [14] describe polar amino acids as residues that promote disorder within a polypeptide. Therefore the peptide may have been adsorbed to the hydrophobic silica surface and/or may have remained largely unstructured. This is seen by comparing the signal intensities to that of the samples in water. The most notable difference is the intensities of the samples in 50.0 mM KPhos pH 11.4 samples. PolyQ showed a weak helical structure at pH 11.4 that should not be due to adsorption since both it and the silica surface were negatively charged at this pH, but was more likely due to a lack of structure. On the other hand, Aβ showed an enhanced helical structure at pH 11. This may have been due to the fact that it was negatively charged like polyQ, keeping it from adsorbing to the silica surface, but Aβ also had a hydrophobic region, driving folding. Most important was the similarity between the two most aggregation-prone structures, water and 10.0 mM KPhos at pH 6.9. These spectra return weak intensity and mainly random coil structures. This indicated a lack of intermolecular hydrogen bonds for stabilizing secondary structure, verifying that the unfolded state is an aggregation prerequisite.

3.9.4. Use of Buffer in Xerogel Preparation

Because it took several days for both peptides to aggregate out of solution in 50.0 mM KPhos at pH 4.5 and because a buffered sol will harden into a sol-gel in a

matter of minutes, an attempt to create a sol-gel for each peptide was made with potassium acetate as a buffer at pH 4.6. Unexpectedly, both glasses took 2 days to harden and contained visible "patches" of aggregated peptide. The glass itself was clear, but it contained multiple 4-9 mm^2 opaque regions. Figure 3-57 gives the spectra of each glass, suggesting again that the analysis was compromised by diffraction due to aggregated peptides.

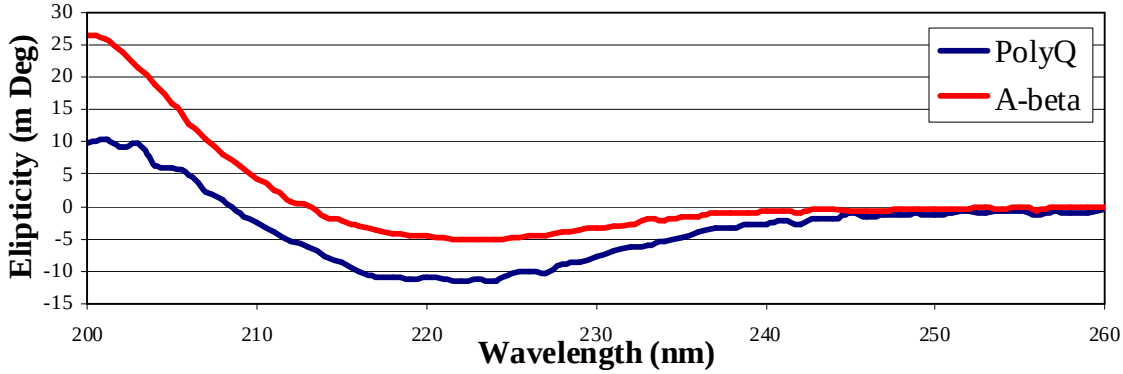

Figure 3-57. PolyQ and Aβ glass encapsulated peptides made with acetate buffer. Both glasses contained regions of opaqueness indicating that aggregation had occurred.

4. CONCLUSIONS

The purpose of this work was to study two aggregate prone peptides, Aβ and polyQ, by encapsulating the peptides in a sol-gel matrix to prevent aggregation. The first challenge was to solubilize the peptides so that they may be brought up in a solution and have the glass matrix form around them before aggregation occured. As stated in Section 3.1, two steps were identified as being most crucial to successful encapsulation of the monomer: (1) when solubilizing the peptide, the clarified solution must be allowed to sit overnight at room temperature (~14 h) in order to obtain consistent results, and (2) after the solubilized peptide had been dried, resuspension in TFA solution requires clarification by performing a series of repetitive pipettings over the course of ~1 h. It then must have been allowed to rest for no less than an additional 30 min prior to use. Following these two peptide preparation steps gave consistent results in subsequent experiments.

For first attempts at encapsulation, leaching of the peptide was identified as a detrimental problem because, like aggregation, leaching cannot be controlled and leads to an unknown change in the peptide's concentration making interpretation of the data difficult. To minimize leaching, a protocol for making a xerogel was developed that still yielded optically transparent glasses for CD analysis. In Section 3.2.2.1 it was shown that xerogels reduced leaching with an increase in signal due to a higher peptide concentration. This was observed in Figures 3-1 to 3-4 where the only differences in the spectra were the intensities, not the general shape, and where leaching was studied as a function of peptide structure, ionic strength, time, temperature, and solvent exchange. As

in the wet-aged glasses, xerogel samples showed increased helicity or enhanced secondary structure compared to solution samples. This was most likely due to the F_3-propyl modifier and to excluded volume effects as discussed in Section 3.3.1.1.

It has been demonstrated that polyQ and Aβ peptides are stabilized against aggregation when immobilized in their monomeric form within a 10% trifluoropropyl silica glass xerogel. The molecular confinement of the peptide prevented aggregation and minimized intermolecular interactions. This idea is supported by results in Sections 3.3.1.2 and 3.3.1.3 where Figures 3-8 to 3-11 suggest that the polyQ peptides were monomeric after encapsulation. These results showed that soluble polyQ spectra directly overlap each other for different KPhos concentrations and pH values, pH 11 excluded. Under these same solvent conditions, the encapsulated peptide's spectra separated out into distinct intensities that were dependent on both KPhos concentration and pH value. This is significant because the failure of the peptide to produce distinct solvent-dependent spectra in solution may suggest that polyQ forms intermolecular bonds, making the study of the monomeric form difficult by standard methods.

Since the peptide was initially isolated in a monomeric form in the glass, there is also no question as to whether the spectra correspond to the monomeric or oligomeric forms. In Section 3.3.2.1, it was demonstrated that Aβ transitioned from a random coil through an apparent beta structure to a mostly helical conformation (Figure 3-13). These forms are seen often in the literature, but the sample usually contained soluble aggregates making it difficult to interpret. Additionally, two of the papers discussed in Section 1.6 have reported CD spectra with a single minimum near 222 nm as beta structure for polyQ

[93] and for Aβ [101]. Here it was demonstrated that these red shifted beta-like signals most likely arose from a diffraction phenomenon and may be indicative of aggregating or aggregated peptides. For examples see Figures 3-15 (diffraction spectrum), 3-16 (zero spectrum corresponding to 3-15), 3-31 (vortexed fibers), and 3-32 (aggregated polyQ in an under-prepared xerogel).

This work agrees with most authors in that the peptides in this study aggregated most quickly in solution when near their isoelectric point. Both peptides showed increased solubility at high pH where they contained a net negative charge. These high pH samples have unresolved spectra because of high absorbance near 200 nm. However it is clear that the peptides had an increase in ellipticity, supporting the hypothesis that increased secondary structure resists aggregation. In addition, both peptides show increased solubility in time with increasing secondary structure (Figures 3-23 to 3-25 for polyQ, and 3-27 to 3-29 for Aβ).

In solution, polyQ and Aβ showed a tendency to transition from a soluble helical structure to a beta structure, but under different peptide-specific conditions. PolyQ had an isodichroic point, seen in Figure 3-20, which indicated a two-state transition between a random coil and beta structure in water. Likewise, Aβ followed a similar transition in 10% HFIP solution. The difference is that polyQ showed a loss of signal indicating aggregation in water, whereas Aβ seemed to be stable in 10% HFIP (Figure 3-20 for polyQ, and Figures 3-26 and 3-30 for Aβ). The stability of this beta fold was also demonstrated by Aβ's resistance to thermal denaturization when encapsulated (Figure 3-39). The question is, would the peptide demonstrate the same stability in solution or

would it precipitate out? In Section 3.7.2, it was shown that all thermal experiments in solution for both peptides were reversible, and, with the exception of minor leaching at high temperatures, so were the xerogel experiments.

The majority of the solvent exchange experiments also demonstrated complete reversibility. In Section 3.8, all exchanges with polyQ xerogels showed reversibility, and it was seen that low concentrations of HFIP actually reduced secondary structure (Figure 3-41). Encapsulated Aβ did not show reversibility in HFIP/water exchange experiments. Figure 3-47 shows that, upon return to the starting concentrations of 25%, 35%, and 50% HFIP, from water, all samples had the same spectral intensities. This could be due to the formation of a stable intermediate or to irreversible adsorption to the glass. Aβ also shows a folding intermediate over a narrow range of low HFIP concentrations. Encapsulated Aβ appeared to be able to take on two different structures at 5% HFIP, depending on whether the solvent conditions were approached from a higher HFIP concentration or from water (Figure 3-54). In this case, the form with increased secondary structure also showed increased solubility in time. Furthermore, both peptides showed the most random coil structure in the solutions in which they were most prone to aggregation (Figure 3-56).

In summary, this work is in agreement with current theory on protein aggregation studies that implicate partially unstructured peptides as aggregation precursors. Furthermore, sol-gel encapsulated peptides separated into distinct solvent dependent spectra not seen in solution suggesting that the peptide was monomeric in the glass, whereas the oligomeric state was uncertain in solution. The peptides have also been

studied under solvent conditions in which aggregation occurred for the soluble peptide, such as near the isoelectric point. Therefore, this work demonstrates the ability to examine aggregation-prone peptides in solvent conditions that would be impossible by standard solution methods.

5. FUTURE WORK

Commonly, researchers use solvents that are well understood for their effects on proteins. These solvents include salts and buffers (Hofmeister series), alcohols, crowding agents, *etc*. In this study, KPhos buffers were used as a solvent variable, and, as a consequence, certain spectra could not be interpreted because of absorption and noise due to the high PO_4^{3-} concentration at high pH. It was also the high pH samples that proved to be aggregation resistant in time. By the use of different salts and buffers, it may be beneficial to further investigate this structure since the results in Sections 3.3.1.3 and 3.3.2.3 suggested that the enhanced ellipticity was most influenced by high pH. In addition, since the high PO_4^{3-} concentration should have also been a factor because it is a strong kosmotrope, careful consideration of the Hofmeister series may allow a comparable anion to be chosen, such as sulfate, which may not cause the same absorption and noise interference. Furthermore, a more thorough investigation of the Hofmeister series is suggested to further characterize the peptide at all pH values.

The F_3-propyl modifier used in this study was likely to have increased the amount of helicity of the encapsulated peptide as compared to solution (Figure 3-6). Successful encapsulation of the peptide in glasses using different metal alkaloid precursors may reveal important properties unique to disordered peptides, not only because of the influences of the silica surface on solvent properties, but also because the peptide remains soluble during network formation as the environment becomes more crowded. Since it has been shown that the hydrophobicity of the precursor can influence the encapsulated polypeptide's structure [92], the use of different silica precursors may allow different

structures to be seen in encapsulation, such as that seen in solution. A range of precursors with different hydrophobicity should be tried, perhaps including a slightly less hydrophobic precursor such as propyltrimethoxysilane, the unfluorinated version of that used in this research.

The concentration of the F_3-propyl modifier, or other precursors, could be varied to characterize the influences of the modifiers alone. A new glass modifier may also allow for a lower modifier concentration to be used, better reproducing the solution behavior of the peptides in the encapsulated environment. Such experiments would also determine whether leaching in the xerogel was reduced due to the F_3-propyl modifier chemistry or due to a reduced channel size in the glass.

A more thorough investigation of the encapsulation peptide's stability in time and how its structure changes, or does not change, is suggested. In this study, the solvent was not changed, so, in samples that were analyzed over long periods up to two months, there is the possibility that some HFIP evaporated. A change in HFIP concentration could have influenced some of the results and may be overcome by regularly replenishing the solvent every couple of days. During these long-term experiments, some encapsulated samples showed changes in secondary structure: namely Aβ's transition to an apparent beta structure. It would be interesting to see if, over a period of time greater than that used in this study, all samples transitioned to this beta structure. And, can any changes be reversed by either solvent or temperature to a helical or random coil structure? If irreversible changes are found, are they seen in solution? If not, that may indicate an aggregate-prone state. Such a study may be the starting point for finding a small

molecule to introduce that would stabilize the peptide and keep it from forming the irreversible state.

One such experiment would be a thermal experiment on soluble Aβ that has taken on the apparent beta structure in solution. The current study only investigated the thermal folding and unfolding of helical and random coil structures that all showed complete reversibility, Section 3.7. In solution, Aβ in 10% HFIP transitioned to an apparent beta structure. Performing a thermal experiment on a sample showing this beta structure, at a very slow rate, may prove to be irreversible. If the peptide aggregates out of solution, this would suggest that the thermally stable beta structure seen after encapsulation is on the aggregation pathway. Should the soluble beta structure aggregate, then testing the transition to the beta fold may lead to the discovery of a small molecule that prevents its formation. Studying this transition may be accomplished by standard solution methods, but in the glass, valuable information about aggregation-prone structures may be revealed by failed attempts because the peptide cannot aggregate. A failed attempt would mean the peptide either transitions to the beta structure or the peptide aggregates out of solution. In the glass, the peptide cannot aggregate out of solution so the structure can still be analyzed, and testing can be done to see if the structure is reversible. Also, there is a strong possibility that multiple aggregation-prone states exist because there are multiple forms of aggregates. Differentiating between these two scenarios is impossible by standard methods due to the simple fact that they aggregate out of solution. After encapsulation, these different states may be identified, and, should each state require a different stabilizing agent against aggregation, this state-

dependent characteristic may be identified, and a more in depth understanding of the aggregation-prone state may be developed.

A second experiment would be to repeat the Aβ folding transition seen in Figure 3-54 where the 5% HFIP sample showed two different structures depending on the prior solvent. Closer investigation of this experiment, with more concentration values or slight variations in temperature, may reveal a destabilized state that is aggregation-prone. Repeating the experiment in solution by titration with HFIP or slight temperature variations would reveal whether the state is on the aggregation pathway. If the peptide does aggregate, then the glass sample could be used to investigate different solutes for one that stabilizes the peptide against taking on the aggregation-prone state. Again, it cannot be understated that these suggested experiments are only possible with the unique approach of silica entrapment, as demonstrated in this work.

REFERENCES

1. Buda, O., Arsene, D., Ceausu, M., Dermengiu, D., and Curca, G.C., *Georges Marinesco and the early research in neuropathology.* Neurology, 2009. **72**(1): p. 88-91.

2. Alzheimer, A., *Über eine eigenartige eskrankung der nirnrinde.* Allg. Z. Psychiatr. Psych.-Gerichtl., 1907. **64**: p. 146-148.

3. Prusiner, S.B., *Novel proteinaceous infectious particles cause scrapie.* Science, 1982. **216**: p. 136-144.

4. Garrett, R.H., Grisham, C. M. Chapter 4: Amino Acids. *Biochemistry*. 3 ed.; S. Kiselica; Thomson Brooks/Cole: Belmont, CA, 2005; p. 77-84.

5. Wang, W., Nema, S., and Teagarden, D., *Protein aggregation--pathways and influencing factors.* Int. J. Pharm., 2010. **390**(2): p. 89-99.

6. Calamai, M., Taddei, N., Stefani, M., Ramponi, G., and Chiti, F., *Relative influence of hydrophobicity and net charge in the aggregation of two homologous proteins.* Biochemistry, 2003. **42**(51): p. 15078-15083.

7. Patro, S.Y., Przybycien, T.M., *Simulations of kinetically irreversible protein aggregate structure.* Biophys. J., 1994. **66**: p. 1274-1289.

8. Istrail, S., Schwartz, R., *Lattice simulations of aggregation funnels for protein folding.* Comp. Biol., 1999. **6**: p. 143-162.

9. Fink, A.L., *Protein aggregation: Folding aggregates, inclusion bodies and amyloid.* Fold. Des., 1998. **3**(1): p. R9-R23.

10. Querol, E., Perez-Pons, J.A., and Mozo-Villarias, A., *Analysis of protein conformational characteristics related to thermostability.* Protein Eng., 1996. **9**(3): p. 265-271.

11. Soto, C., Castano, E.M., Frangione, B., and Inestrosa, N.C., *The -helical to - strand transition in the amino-terminal fragment of the amyloid -peptide modulates amyloid formation.* J. Biol. Chem., 1995. **270**(7): p. 3063-3067.

12. Soto, C. and Castano, E.M., *The conformation of Alzheimer's beta peptide determines the rate of amyloid formation and its resistance to proteolysis.* Biochem. J., 1996. **314**(2): p. 701-707.

13. Wang, W., *Protein aggregation and its inhibition in biopharmaceutics.* Int. J. Pharm., 2005. **289**(1-2): p. 1-30.

14. Uversky, V.N. and Dunker, A.K., *Understanding protein non-folding.* Biochim. Biophys. Acta, 2010. **1804**(6): p. 1231-1264.

15. Prusiner, S.B., *Shattuck lecture - neurodegenerative diseases and prions.* New J. Med., 2001. **344**(20): p. 1516-1526.

16. Walsh, D.M.A.-S., Dennis J., *Deciphering the molecular basis of memory failure in Alzheimer's disease.* Neuron, 2004. **44**(1): p. 181-193.

17. Rossor, M.N., Revesz, T., Lantos, P.L., and Warrington, E.K., *Semantic dementia with ubiquitin-positive tau-negative inclusion bodies.* Brain, 2000. **123**(2): p. 267-276.

18. Kerr, M.L. and Small, D.H., *Cytoplasmic domain of the beta-amyloid protein precursor of Alzheimer's disease: Function, regulation of proteolysis, and implications for drug development.* J. Neurosci. Res., 2005. **80**(2): p. 151-159.

19. Koudinov A. R., B.T.T., *Alzheimer's amyloid-beta is an essential synaptic protein, not neurotoxic junk.* Acta Neurobiol. Exp., 2004. **64**(1): p. 71-79.

20. Huber, G., Bailly, Y., Martin, J.R., Mariani, J., and Brugg, B., *Synaptic beta-amyloid precursor proteins increase with learning capacity in rats.* Neuroscience, 1997. **80**(2): p. 313-320.

21. Cummings, C.J. and Zoghbi, H.Y., *Fourteen and counting: Unraveling trinucleotide repeat diseases.* Hum. Mol. Genet., 2000. **9**(6): p. 909-916.

22. Kamenetz, F., Tomita, T., Hsieh, H., Seabrook, G., Borchelt, D., Iwatsubo, T., Sisodia, S., and Malinow, R., *APP processing and synaptic function.* Neuron, 2003. **37**(6): p. 925-937.

23. Zuccato, C., Ciammola, A., Rigamonti, D., Leavitt, B.R., Goffredo, D., Conti, L., Macdonald, M.E., Friedlander, R.M., Silani, V., Hayden, M.R., *et al.*, *Loss of huntingtin-mediated BDNF gene transcription in Huntington's disease.* Science, 2001. **293**(5529): p. 493-498.

24. He, X.-H., Lin, F., and Qin, Z.-H., *Current understanding on the pathogenesis of polyglutamine diseases,* in *Neuroscience Bulletin*. Shanghai Inst. Biol. Sci. C.A.S., 2010, p. 247-256.

25. Dill, K.A. and Chan, H.S., *From Levinthal to pathways to funnels.* Nat. Struct. Biol., 1997. **4**(1): p. 10-19.

26. Morgan, C., Colombres, M., Nuñez, M.T., and Inestrosa, N.C., *Structure and function of amyloid in Alzheimer's disease.* Progr. Neurobiol., 2004. **74**(6): p. 323-349.

27. Cleland, J.L. and Wang, D.I.C., *Refolding and aggregation of bovine carbonic anhydrase B: Quasi-elastic light scattering analysis.* Biochemistry, 1990. **29**(50): p. 11072-11078.

28. Tomski, S.J. and Murphy, R.M., *Kinetics of aggregation of synthetic beta-amyloid peptide.* Arch. Biochem. Biophys., 1992. **294**(2): p. 630-638.

29. Uversky, V.N., Fink, A.L., Khurana, R., Karnoup, A.S., Segel, D.J., and Doniach, S., *Association of partially-folded intermediates of staphylococcal nuclease induces structure and stability.* Protein Sci., 1999. **8**(1): p. 161-173.

30. Lomakin, A., Teplow, D.B., Kirschner, D.A., and Benedek, G.B., *Kinetic theory of fibrillogenesis of amyloid-beta protein.* Proc. Natl. Acad. Sci. U.S.A., 1997. **94**(15): p. 7942-7947.

31. Speed, M.A., King, J., and Wang, D.I.C., *Polymerization mechanism of polypeptide chain aggregation.* Biotechnol. Bioeng., 1997. **54**(4): p. 333-343.

32. Weiss, W.F., Young, T.M., and Roberts, C.J., *Principles, approaches, and challenges for predicting protein aggregation rates and shelf life.* J. Pharm. Sci., 2009. **98**(4): p. 1246-1277.

33. *Protein misfolding, aggregation, and conformational diseases*; Uversky, V.N. and Fink, A.L., M.Z. Atassi. eds.; Protein Rev.Vol. 4; Springer Science: New York, 2006.

34. Walsh, D.M., Klyubin, I., Fadeeva, J.V., Cullen, W.K., Anwyl, R., Wolfe, M.S., Rowan, M.J., and Selkoe, D.J., *Naturally secreted oligomers of amyloid beta protein potently inhibit hippocampal long-term potentiation in vivo.* Nature, 2002. **416**(6880): p. 535-539.

35. Selkoe, D.J., *Folding proteins in fatal ways.* Nature, 2003. **426**(6968): p. 900-904.

36. Lashuel, H.A., Hartley, D., Petre, B.M., Walz, T., and Lansbury, P.T., *Neurodegenerative disease: Amyloid pores from pathogenic mutations.* Nature, 2002. **418**(6895): p. 291.

37. Zhang, Y., Mclaughlin, R., Goodyer, C., and Leblanc, A., *Selective cytotoxicity of intracellular amyloid beta peptide1-42 through p53 and bax in cultured primary human neurons.* J. Cell Biol., 2002. **156**(3): p. 519-529.

38. Haass, C. and Steiner, H., *Protofibrils, the unifying toxic molecule of neurodegenerative disorders?* Nat. Neurosci., 2001. **4**(9): p. 859.

39. Kirkitadze, M.D., Bitan, G., and Teplow, D.B., *Paradigm shifts in Alzheimer's disease and other neurodegenerative disorders: The emerging role of oligomeric assemblies.* J. Neurosci. Res., 2002. **69**(5): p. 567-577.

40. Lansbury, P.T., Jr., *Evolution of amyloid: What normal protein folding may tell us about fibrillogenesis and disease.* Proc. Natl. Acad. Sci U.S.A., 1999. **96**(7): p. 3342-3344 CR - Copyright © 1999 National Academy of Sciences.

41. Dobson, C.M., *Protein misfolding, evolution and disease.* Trends Biochem. Sci., 1999. **24**(9): p. 329-332.

42. Caughey, B. and Lansbury, P.T., *Protofibrils, pores, fibrils, and neurodegeneration: Separating the responsible protein aggregates from the innocent bystanders.* Ann. Rev. Neurosci., 2003. **26**(1): p. 267-298.

43. Goldberg, M.S. and Lansbury Jr, P.T., *Is there a cause-and-effect relationship between alpha-synuclein fibrillization and Parkinson's disease?* Nat. Cell Biol., 2000. **2**(7): p. E115-E119.

44. Chiti, F. and Dobson, C.M., *Protein misfolding, functional amyloid, and human disease.* Ann. Rev. Biochem., 2006. **75**(1): p. 333-366.

45. Pepys, M.B., *Pathogenesis, diagnosis and treatment of systemic amyloidosis.* Philos. Transact.: Biol. Sci., 2001. **356**(1406): p. 203-211.

46. Barton, S., Jacak, R., Khare, S.D., Ding, F., and Dokholyan, N.V., *The length dependence of the polyQ-mediated protein aggregation.* J. Biol. Chem., 2007. **282**(35): p. 25487-25492.

47. Ross, C.A., Poirier, M.A., Wanker, E.E., and Amzel, M., *Polyglutamine fibrillogenesis: The pathway unfolds.* Proc. Natl. Acad. Sci. U.S.A., 2003. **100**(1): p. 1-3.

48. Duennwald, M.L., Jagadish, S., Muchowski, P.J., and Lindquist, S., *Flanking sequences profoundly alter polyglutamine toxicity in yeast.* Proc. Natl. Acad. Sci. U.S.A., 2006. **103**(29): p. 11045-11050.

49. Cha, J.-H.J., *Transcriptional dysregulation in Huntington's disease.* Trends Neurosci., 2000. **23**(9): p. 387-392.

50. Reinhard, C., Hebert, S.S., and De Strooper, B., *The amyloid-beta precursor protein: Integrating structure with biological function.* EMBO J., 2005. **24**(23): p. 3996-4006.

51. Kamal, A., Almenar-Queralt, A., Leblanc, J.F., Roberts, E.A., and Goldstein, L.S.B., *Kinesin-mediated axonal transport of a membrane compartment containing beta-secretase and presenilin-1 requires APP.* Nature, 2001. **414**(6864): p. 643.

52. Serpell, L.C., *Alzheimer's amyloid fibrils: Structure and assembly.* Biochim. Biophys. Acta, 2000. **1502**(1): p. 16-30.

53. Steiner, H. and Haass, C., *Intramembrane proteolysis by presenilins.* Nat. Rev. Mol. Cell Biol., 2000. **1**(3): p. 217-224.

54. Skovronsky, D.M., Moore, D.B., Milla, M.E., Doms, R.W., and Lee, V.M.-Y., *Protein kinase c-dependent alpha-secretase competes with gamma-secretase for cleavage of amyloid-beta precursor protein in the trans-golgi network.* J. Biol. Chem., 2000. **275**(4): p. 2568-2575.

55. Hardy, J. and Selkoe, D.J., *The amyloid hypothesis of Alzheimer's disease: Progress and problems on the road to therapeutics.* Science, 2002. **297**(5580): p. 353-356.

56. Fatouros, A., Ã–Sterberg, T., and Mikaelsson, M., *Recombinant Factor VIII sq-influence of oxygen, metal ions, pH and ionic strength on its stability in aqueous solution.* Int. J. Pharm., 1997. **155**(1): p. 121-131.

57. Richards, J.P., Stickelmeyer, M.P., *et al.*, *Self-association properties of monomeric insulin analogs under formulation conditions.* Pharm. Res., 1998. **15**: p. 1434-1441.

58. Bush, L., Webb, C., Bartlett, L., Burnett, B, *The formulation of recombinant Factor IX: Stability, robustness, and convenience.* Sem. Hema., 1998. **35**(2): p. 18-21.

59. Pikal, M.J., Dellerman, K.M., Roy, M.L., and Riggin, R.M., *The effects of formulation variables on the stability of freeze-dried human growth hormone.* Pharm. Res., 1991. **8**(4): p. 427-436.

60. Shahrokh, Z., Eberlein, G., Buckley, D., Paranandi, M.V., Aswad, D.W., Stratton, P., Mischak, R., and Wang, Y.J., *Major degradation products of basic fibroblast growth factor: Detection of succinimide and iso-aspartate in place of aspartate.* Pharm. Res., 1994. **11**(7): p. 936-944.

61. Shahrokh, Z., Stratton, P.R., Eberlein, G.A., and Wang, Y.J., *Approaches to analysis of aggregates and demonstrating mass balance in pharmaceutical protein (basic fibroblast growth factor) formulations.* J. Pharm. Sci., 1994. **83**(12): p. 1645-1650.

62. Min Won, C., Molnar, T.E., Mckean, R.E., and Spenlehauer, G.A., *Stabilizers against heat-induced aggregation of rpr 114849, an acidic fibroblast growth factor (AFGF).* Int. J. Pharm., 1998. **167**(1-2): p. 25-36.

63. Curatolo, L., Valsasina, B., Caccia, C., Raimondi, G.L., Orsini, G., and Bianchetti, A., *Recombinant human il-2 is cytotoxic to oligodendrocytes after in vitro self aggregation.* Cytokine+, 1997. **9**(10): p. 734-739.

64. Tomski, S.J. and Murphy, R.M., *Kinetics of aggregation of synthetic β-amyloid peptide.* Arch. Biochem. Biophys., 1992. **294**(2): p. 630-638.

65. Sluzky, V., Tamada, J.A., Klibanov, A.M., and Langer, R., *Kinetics of insulin aggregation in aqueous solutions upon agitation in the presence of hydrophobic surfaces.* Proc. Natl. Acad. Sci. U.S.A., 1991 **88** (21): p. 9377-9381.

66. Kerwin, B.A., Akers, M.J, *et al*., *Acute and long-term stability studies of deoxy hemoglobin and characterization of ascorbate-induced modifications.* J. Pharm. Sci., 1999. **88**: p. 78-88.

67. Tobitani, A. and Ross-Murphy, S.B., *Heat-induced gelation of globular proteins. 2. Effect of environmental factors on single-component and mixed-protein gels.* Macromolecules, 1997. **30**(17): p. 4855-4862.

68. Kendrick, B.S., Carpenter, J.F., Cleland, J.L., and Randolph, T.W., *A transient expansion of the native state precedes aggregation of recombinant human interferon-3.* Proc. Natl. Acad. Sci. U.S.A., 1998. **95**(24): p. 14142-14146.

69. Kendrick, B.S., Cleland, J.L., Lam, X., Nguyen, T., Randolph, T.W., Manning, M.C., and Carpenter, J.F., *Aggregation of recombinant human interferon gamma: Kinetics and structural transitions.* J. Pharm. Sci., 1998. **87**(9): p. 1069-1076.

70. James, E.L. and Bottomley, S.P., *The mechanism of alpha1-antitrypsin polymerization probed by fluorescence spectroscopy.* Arch. Biochem. Biophys., 1998. **356**(2): p. 296-300.

71. Dong, A., Prestrelski, S.J., Allison, S.D., and Carpenter, J.F., *Infrared spectroscopic studies of lyophilization- and temperature-induced protein aggregation.* J. Pharm. Sci., 1995. **84**(4): p. 415-424.

72. Alexandrescu, A.T. and Rathgeb-Szabo, K., *An NMR investigation of solution aggregation reactions preceding the misassembly of acid-denatured cold shock protein A into fibrils.* J. Mol. Biol., 1999. **291**(5): p. 1191-1206.

73. Tsai, P.K., Volkin, D.B., Dabora, J.M., Thompson, K.C., Bruner, M.W., Gress, J.O., Matuszewska, B., Keogan, M., Bondi, J.V., and Middaugh, C.R., *Formulation design of acidic fibroblast growth factor.* Pharm. Res., 1993. **10**(5): p. 649-659.

74. Helms, L.R. and Wetzel, R., *Specificity of abnormal assembly in immunoglobulin light chain deposition disease and amyloidosis.* J. Mol. Biol., 1996. **257**(1): p. 77-86.

75. Parbhu, A., Lin, H., Thimm, J., and Lal, R., *Imaging real-time aggregation of amyloid beta protein (1-42) by atomic force microscopy.* Peptides, 2002. **23**(7): p. 1265-1270.

76. van Holde, K.E., Johnson, W.C., and Ho, P.S. Linear and Circular Dichroism. In *Principles of physical biochemistry*. 2 ed, G. Carlson.; Pearson Education Inc.: Upper Saddle River, 2006; p. 471-497

77. Eggers, D.K. and Valentine, J.S., *Molecular confinement influences protein structure and enhances thermal protein stability.* Protein Sci., 2001. **10**(2): p. 250-261.

78. Otzen, D.E., Miron, S., Akke, M., and Oliveberg, M., *Transient aggregation and stable dimerization induced by introducing an Alzheimer sequence into a water-soluble protein.* Biochemistry, 2004. **43**(41): p. 12964-12978.

79. Konno, T., *Amyloid-induced aggregation and precipitation of soluble proteins: An electrostatic contribution of the Alzheimer's beta(25-35) amyloid fibril.* Biochemistry, 2001. **40**(7): p. 2148-2154.

80. Masino, L., Kelly, G., Leonard, K., Trottier, Y., and Pastore, A., *Solution structure of polyglutamine tracts in gst-polyglutamine fusion proteins.* FEBS Lett., 2002. **513**(2-3): p. 267-272.

81. Ellis, R.J., *Macromolecular crowding: An important but neglected aspect of the intracellular environment.* Curr. Opin. Struct. Biol., 2001. **11**(1): p. 114-119.

82. Stefani, M. and Dobson, C., *Protein aggregation and aggregate toxicity: New insights into protein folding, misfolding diseases and biological evolution*. J. Mol. Med., 2003, Springer Berlin / Heidelberg. p. 678-699.

83. Pappu, R.V., Wang, X., Vitalis, A., and Crick, S.L., *A polymer physics perspective on driving forces and mechanisms for protein aggregation.* Arch. Biochem. Biophys., 2008. **469**(1): p. 132-141.

84. Rocha, V.A. and Eggers, D.K., *Hydrophobic, organically-modified silica gels enhance the secondary structure of encapsulated apomyoglobin.* Chem. Comm., 2007(12): p. 1266-1268.

85. Gill, I. and Ballesteros, A., *Bioencapsulation within synthetic polymers (part 1): Sol-gel encapsulated biologicals.* Trends Biotech., 2000. **18**(7): p. 282-296.

86. Brennan, J.D., *Cheminform abstract: Using intrinsic fluorescence to investigate proteins entrapped in sol-gel derived materials.* ChemInform, 1999. **30**(30): p. 106A-121A

87. Dave, B.C., Dunn, B., Valentine, J.S., and Zink, J.I., *Sol-gel encapsulation methods for biosensors.* Anal. Chem., 1994. **66**(22): p. 1120A-1127A.

88. The Besley Group Home Page. http://besley.chem.nottingham.ac.uk/research/research-prospec.html (accessed November 6th, 2011). *Cd curves*, Besley Group: Nottingham.

89. Eggers, D.K. and Valentine, J.S., *Crowding and hydration effects on protein conformation: A study with sol-gel encapsulated proteins.* J. Mol. Biol., 2001. **314**(4): p. 911-922.

90. Ellis, R.J., *Macromolecular crowding: Obvious but underappreciated.* Trends Biochem. Sci., 2001. **26**(10): p. 597-604.

91. Menaa, B., Torres, C., Herrero, M., Rives, V., Gilbert, A.R.W., and Eggers, D.K., *Protein adsorption onto organically modified silica glass leads to a different structure than sol-gel encapsulation.* Biophys. J., 2008. **95**(8): p. L51-L53.

92. Menaa, B., Herrero, M., Rives, V., Lavrenko, M., and Eggers, D.K., *Favourable influence of hydrophobic surfaces on protein structure in porous organically-modified silica glasses.* Biomaterials, 2008. **29**(18): p. 2710-2718.

93. D Darnell, G., Orgel, J., Pahl, R., and Meredith, S.C., *Flanking polyproline sequences inhibit beta-sheet structure in polyglutamine segments by inducing PPII-like helix structure.* J. Mol. Biol., 2007. **374**(3): p. 688-704.

94. Walters, R.H. and Murphy, R.M., *Aggregation kinetics of interrupted polyglutamine peptides.* J. Mol. Biol., 2011. **412**(3): p. 505-519.

95. Altschuler, E.L., Hud, N.V., Mazrimas, J.A., and Rupp, B., *Random coil conformation for extended polyglutamine stretches in aqueous soluble monomeric peptides.* J. Pept. Res., 1997. **50**(1): p. 73-75.

96. Perutz, M.F., Johnson, T., Suzuki, M., and Finch, J.T., *Glutamine repeats as polar zippers: Their possible role in inherited neurodegenerative diseases.* Proc. Natl. Acad. Sci. U.S.A., 1994 **91** (12): p. 5355-5358.

97. Sharma, D., Sharma, S., Pasha, S., and Brahmachari, S.K., *Peptide models for inherited neurodegenerative disorders: Conformation and aggregation properties of long polyglutamine peptides with and without interruptions.* FEBS Lett., 1999. **456**(1): p. 181-185.

98. Perutz, M.F., Staden, R., Moens, L., and De Baere, I., *Polar zippers.* Curr. Biol., 1993. **3**(5): p. 249-253.

99. Fraser, P.E., Nguyen, J.T., Surewicz, W.K., and Kirschner, D.A., *PH-dependent structural transitions of Alzheimer amyloid peptides.* Biophys. J., 1991. **60**(5): p. 1190-1201.

100. Wood, S.J., Maleeff, B., Hart, T., and Wetzel, R., *Physical, morphological and functional differences between pH 5.8 and 7.4 aggregates of the Alzheimer's amyloid peptide.* J. Mol. Biol., 1996. **256**(5): p. 870-877.

101. Barrow, C.J., Yasuda, A., Kenny, P.T.M., and Zagorski, M.G., *Solution conformations and aggregational properties of synthetic amyloid beta-peptides of Alzheimer's disease: Analysis of circular dichroism spectra.* J. Mol. Biol., 1992. **225**(4): p. 1075-1093.

102. Fezoui, Y., Hartley, D., Jd, H., R, K., Walsh, D.M., Condron, M.M., Selkoe, D.J., Lansbury Jr, P.T., Fink, A.L., and Teplow, D.B., *An improved method of preparing the amyloid beta-protein for fibrillogenesis and neurotoxicity experiments.* Int. J. Exp. Clin. Invent., 2000. **7**(3): p. 166-178.

103. Hou, L., Kang, I., Marchant, R.E., and Zagorski, M.G., *Methionine 35 oxidation reduces fibril assembly of the amyloid beta-(1-42) peptide of Alzheimer's disease.* J. Biol. Chem., 2002. **277**(43): p. 40173-40176.

104. Chen, S. and Wetzel, R., *Solubilization and disaggregation of polyglutamine peptides.* Protein Sci., 2001. **10**(4): p. 887-891.

105. Ellerby, L.M., Nishida, C.R., Nishida, F., Yamanaka, S.A., Dunn, B., Valentine, J.S., and Zink, J.I., *Encapsulation of proteins in transparent porous silicate glasses prepared by the sol-gel method.* Science, 1992. **255**(5048): p. 1113-1115.

106. Cacace, M.G., Landau, E.M., and Ramsden, J.J., *The Hofmeister series: Salt and solvent effects on interfacial phenomena.* Q. Rev. Biophys., 1997. **30**(03): p. 241-277.

107. Buck, M., *Trifluoroethanol and colleagues: Cosolvents come of age. Recent studies with peptides and proteins.* Q. Rev. Biophys., 1998. **31**(3): p. 297-355.

108. Böhm, G., *CDNN, CD spectra deconvolution*. 1997: Univ. of Halle-Wittenberg, Halle, Germany.

109. Monera, O.D., Sereda, T.J., Zhou, N.E., Kay, C.M., and Hodges, R.S., *Relationship of sidechain hydrophobicity and alpha-helical propensity on the stability of the single-stranded amphipathic alpha-helix.* J. Pept. Sci., 1995. **1**(5): p. 319-329.

110. Sereda, T.J., Mant, C.T., Sannichsen, F.D., and Hodges, R.S., *Reversed-phase chromatography of synthetic amphipathic alpha-helical peptides as a model for ligand/receptor interactions effect of changing hydrophobic environment on the relative hydrophilicity/hydrophobicity of amino acid side-chains.* J. Chromatogr., A, 1994. **676**(1): p. 139-153.

111. Bollen, Y.J.M., Sanchez, I.E., and Van Mierlo, C.P.M., *Formation of on- and off-pathway intermediates in the folding kinetics of azotobacter vinelandii apoflavodoxin*. Biochemistry, 2004. **43**(32): p. 10475-10489.